UNIVERSITÀ
DI TORINO

DIPARTIMENTO DI NEUROSCIENZE

"Rita Levi Montalcini"

DOTTORATO DI RICERCA IN

NEUROSCIENZE

CICLO XXXIV

"Investigating the impact of CDKL5 on grey matter myelination through mouse models analysis"

TESI PRESENTATA DA: Sunaina Devi

TUTOR: Prof. Maurizio Giustetto

COORDINATORE DEL

DOTTORATO: Prof. Andrea Calvo

ANNI ACCADEMICI: 2018-2022

SETTORE SCIENTIFICO-DISCIPLINARE DI AFFERENZA: BIO/16

CONTENTS

Abstract……..…….5-6
1. INTRODUCTION…….……..……7-42
1.1 Myelination……..…….……7
1.1.1 Myelin sheath structure and composition.....7-9
1.1.2 CNS myelin proteins.....9-13
1.1.3 CNS myelinating glia and axo-glial interaction.....13-16
1.1.4 Myelin Assembly.....16-18
1.1.5 Myelin disorders…….…..…..……18-19
1.2 Neurodevelopmental disorders……..…….20-21
1.3 CDKL5 deficiency disorder…….…….……...…..21-24
1.4 CDKL5 gene and protein…….....24-27
1.4.1 *Cdkl5* gene: mutations and genotype-phenotype correlation……...…27-28
1.4.2 Tissue expression and subcellular localization…….....28-29
1.4.3 Role of CDKL5 in the nucleus…….……..29-30
1.4.4 Role of CDKL5 in the cytoplasm…….……..…30-32
1.4.5 Role of CDKL5 in glial cells…….…….32-33
1.5 Validation of pharmacological therapeutic approaches for CDD.....33-34
1.6 CDD mouse model……..……..…35-42
1.6.1 Generation and validation of *Cdkl5*-KO mice……...35-37
1.6.2 Analysis of *Cdkl5*-KO mice's behavior…….37-40
1.6.3 Anatomical and cellular signaling abnormalities have shown by *Cdkl5*-KO mice……..40-42
2. AIMS……..…….……...43-44
3. MATERIALS AND METHODS……..…….45-50
4. RESULTS……...51-63
4.1 Altered mGluR5/Homer1bc organization in the cerebral cortex of *Cdkl5*$^{-/y}$ mice……...……...51-52
4.2 Excitatory neurotransmission and mGluR5-mediated signaling are severely disrupted in *Cdkl5*$^{-/y}$ cortical neurons…….52-54
4.3 CDPPB potentiates NMDAR current in cortical neurons lacking CDKL5……...54
4.4 CDPPB treatment ameliorates visual, sensorimotor, and memory functions in *Cdkl5*$^{-/y}$ mice……...……..…….....54-56

4.5 mGluR5 PAMs rescue both synaptic and activity defects in *Cdkl5*$^{-/y}$ cerebral cortex...……..…57-59
4.6 A protracted treatment with CDPPB effectively restores *Cdkl5*$^{-/y}$ mice deficit……...…….59-61
4.7 The BA17 cortex of CDD patients recapitulates the synaptic defects shown by *Cdkl5*$^{-/y}$ mice.....62-63
5.1 Expression of CDKL5 in MACs isolated OPCs……...……64
5.2 Lack of *Cdkl5* results in the decreased intensity of Sudan black B staining in most brain regions……...…….64-65
5.3 Lack of *Cdkl5* leads to a reduction of mature OLs density, leaving OPCs unaffected……...…….....65-66
5.4 Myelin basic protein expression is reduced in the primary cortices of both young and adult *Cdkl5*$^{-/y}$ mice……..……..…..66-68
5.5 The neurofilaments are greatly compromised in the cortices of *Cdkl5*$^{-/y}$ mice……...……...69-72
5.6 Lack of *Cdkl5* affects myelin sheath thickness……...….72-73
5.7 *Cdkl5* loss is associated with alterations in the axo-myelinic arrangement at nodal/paranodal structures…….....73-75
5.8 Neuronal, but not oligodendroglial, expression of *Cdkl5* is required for typical MBP expression……..……..75-76
5.9 The primary visual cortex of CDD patients exhibits disorganized myeloarchitecture…….……76-77
5.10 Modulation of mGluR5 activity rescues the expression of MBP in *Cdkl5*$^{-/y}$ mice……...……...77-78
6. DISCUSSION……...……79-85
7. BIBLIOGRAPHY……..……86-101
ANNEXURE……..……102-118

Abstract

Myelination is a complex process that involves the wrapping of axonal segments by a multi-layered, insulating structure called the myelin sheath. The process of myelination improves the speed and efficiency of nerve signals, protects axons from damage, and plays a crucial role in brain function. Several neurodevelopmental disorders (NDDs), like autism spectrum disorder (ASD) and cerebral palsy, include aberrant myelination within their pathophysiology. NDDs are a group of variegated conditions that influence about 1-2% of the newborn population, characterized by intellectual disability, behavioral abnormalities, cognitive impairments, sensory and motor changes, speech and language deficits leading to impaired brain growth, and neurological dysfunction. This work is focused on a monogenic NDD, CDKL5 deficiency disorder (CDD). CDD is an X-linked NDD still without a cure caused by mutations in the cyclin-dependent kinase-like 5 (*CDKL5*) gene that affects mainly girls with an incidence of 1:40,000-60,000 live births. CDKL5 is a serine/threonine kinase highly expressed in forebrain neurons where it participates in the regulation of epigenetic factors, dendritic morphology, and synaptogenesis. Interestingly, along with neurons, CDKL5 is also expressed by oligodendroglial cells where it could play an important role in the myelination process as indicated by MRI imaging of human CDD subjects showing white matter alterations. However, whether and how the loss of CDKL5 can affect myelin organization has not yet been investigated. The general aim of my thesis is to address this issue. I evaluated the post-natal developmental trajectory of myelination in the cerebral cortex of Cdkl5-mutant mice by analyzing myelin directly and the expression of molecules involved in myelin deposition or axonal injury. This analysis showed a reduction of both myelin basic protein and phospho-neurofilaments expression in both V1 and S1 cortices of mutant mice. Moreover, g-ratio analysis of myelinated axons showed reduced myelin sheath thickness in mutants, while nodes of Ranvier length and density were also severely affected in Cdkl5-KO mice. In addition, I found that CDKL5 is required for oligodendrocytes (OL) maturation as the density of mature myelinating OL was reduced in mutant mice whereas OL precursor cells were not affected. Although CDKL5 was found expressed by the OL lineage, the conditional deletion of CDKL5 further showed that this protein must play a pivotal role in neuronal-glial communication underlying myelination. Finally, the

early treatment with a positive allosteric modulator of the metabotropic glutamate receptors type 5 was able to rescue the myelin defects in Cdkl5 mutants. In conclusion, with this thesis, I provide evidence indicating that primary cortical areas in CDD mice and human subjects exhibit a severe reduction/distortion of myelination and related processes and disclose a novel role of CDKL5 activity, likely of pivotal importance for CDD.

1. INTRODUCTION

1.1 Myelination

Neuronal signal propagation of the action potential is required for motor, sensory, and cognitive functions of the nervous system, which in vertebrates is facilitated by myelination. Myelination is a complex process that involves the wrapping of axonal segments by a multi-layered, insulating structure called the myelin sheath. The ensheathment of axons throughout their length by myelin provides them electrical insulation along with an increase in their diameter. This evolutionary organization allows energy-efficient saltatory action potential propagation which accelerates nerve conduction 20–100 fold compared with non-myelinated axons of the same diameter (Nave and Werner, 2014). In homo-sapiens myelination starts around the last trimester of gestation and continues until 20 and 30 years of age (Snaidero and Simons, 2014). In rodents, myelination begins around postnatal day 10 (P10), with the highest rate of myelin formation happening around P20. Nevertheless, myelin accumulation does continue throughout maturity, although at a slower rate.

Myelin has long been considered an inert membrane that, due to its low capacitance and high resistance, facilitates efficient and fast conduction of action potentials. With progressive understanding, myelin has been acknowledged as a dynamic participant in CNS physiology. Various signaling molecules embedded in the myelin sheath regulate the maturation, survival, and regenerative capacity of the axon through the neurotrophic support system. Several myelin-related proteins play a role in the modification of the axonal cytoskeleton which affects sprouting, stability of existing synapses, and neurite outgrowth (Morelli et al., 2011; Pirko, 2012). Loss of myelin's normal fine structure can result in late-age axonal degeneration and even mortality, as demonstrated by mice mutants lacking particular myelin-specific proteins. For example, axonal spheroids, which cause axonal degeneration to become prominent in the white matter tracts of animals lacking the myelin proteins PLP or CNP (Edgar et al., 2009; Werner et al., 2013)

1.1.1 Myelin sheath structure and composition

Myelin is a multi-layered, concentric, and uniformly thick membrane in which the major dense line and the intraperiod line alternate each other to form a spiral structure as shown by the electron microscopic image (Fig 1A)(Hartline, 2008). On one hand, the major dense line represents closely condensed cytoplasmic myelin membranes, whereas the interperiod line consists of the tightly apposed outer membrane Fig 1B. All the layers of myelin are tightly compact and stable resulting in a periodicity of about 12 nm. The myelinated segments of the axons i.e., internodes are around 1.5 mm in length and are only interrupted by small gaps, the nodes of Ranvier as represented in Fig 1C. The node of Ranvier contains sodium channels at a high density and is flanked on both sides by a domain called paranode, which is a site of contact between the myelinating glial cell and axon (Hedrick, 2008). This complicated architecture allows energy-efficient saltatory propagation of action potentials. The division of axonal diameter on the total myelinated fiber diameter gives a value called g-ratio, which is used to assess myelin thickness as shown in Fig 1B. This value usually stands between 0.6-0.7 with some variance according to the size of axons, i.e., bigger axons have thicker myelin, and vice versa (Sherman and Brophy, 2005). The structure and molecular composition of the myelin sheath are very unique which confers its insulating property. Unlike other plasma membranes, myelin is made up of 70% lipids (highly enriched in glycosphingolipids and cholesterol) and 30% of myelin-specific proteins (Jahn et al., 2009). None of the lipids is unique for myelin, but certain lipids are clearly enriched. Among these lipids are cholesterol, cerebrosides, sulfatides, and galactolipids in general, while the overall amount of lecithin and ethanolamine is reduced.

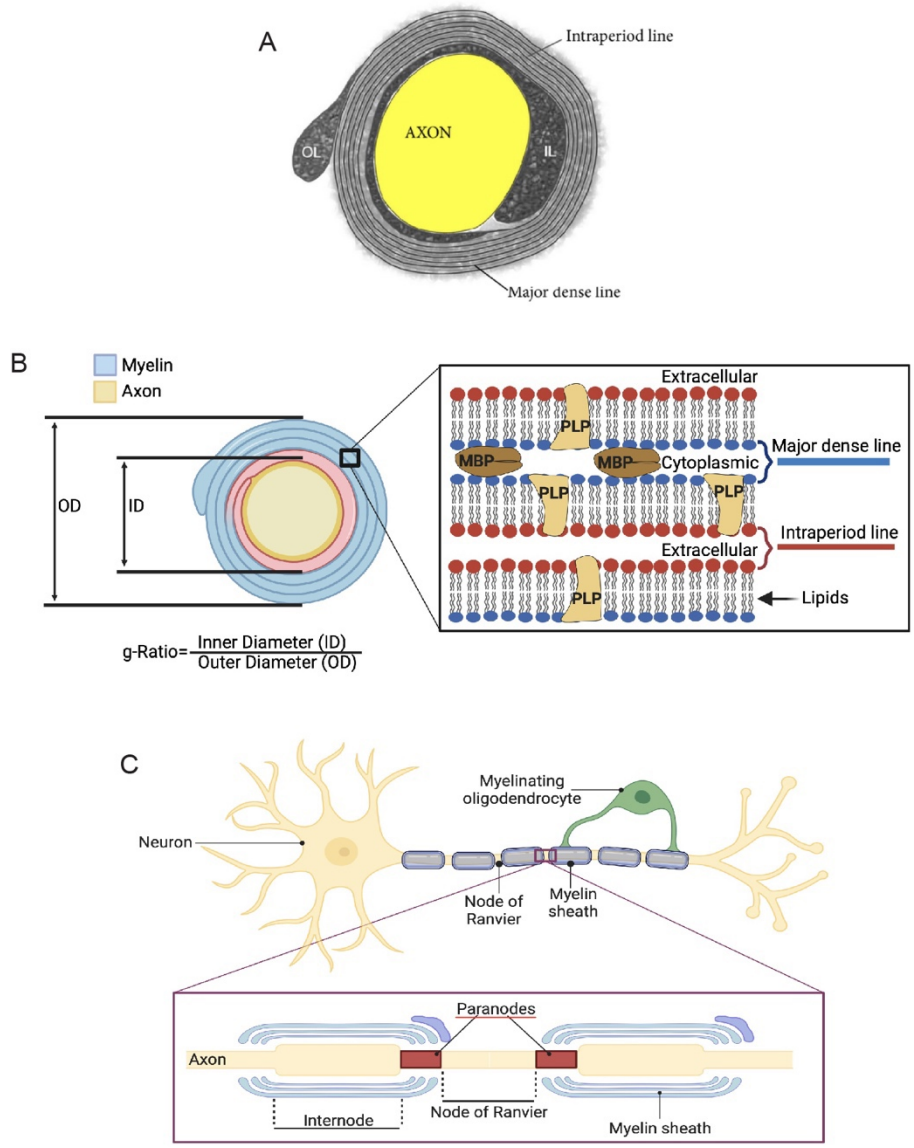

Figure 1: ***Structure of the myelin sheath.*** ***(A)*** *Electron microscopic image showing compact myelin formed by the apposition of the external and internal surfaces of the myelin bilayer that constitute intraperiode line and major dense line. Except for a few tiny pockets at the membrane's edge, which can be seen as the inner loop (IL) right next to the axon and the outer loop (OL) at the membrane's outer edge, the cytoplasm is largely compact.* ***(B)*** *Transverse sectioning of axon showing multilayered myelin sheath and g-ratio calculation. The inset represents compaction between two layers of the cell (major dense line in blue, and interperoid line in red) with major myelin proteins i.e., myelin basic protein (MBP) and preoteolipid pretein (PLP)* ***(C)*** *Schematic representation of neuron with myelinated axon. Inset shows nodal paranodal and internodal domain of the axon. Image modified from (Greer, 2013; Min et al., 2009).*

1.1.2 CNS myelin proteins

The major myelin-specific proteins are myelin basic protein (MBP), proteolipid protein (PLP), and 2′,3′-Cyclic nucleotide 3′-phosphodiesterase (CNP) as indicated in Fig 2 (Simons and Lyons, 2013). As indicated by the name, MBP is highly basic at physiological pH, which permits it to bind with negatively charged

lipids and makes it important for the compaction of the myelin sheath. Various prenatal and postnatal isoforms of MBP exist differently in number based on a species' dependent manner, e.g.: 4 postnatal isoforms in humans and rats, 6 in mice. These isoforms interact with each other to form a meshwork, zip together two membranes, and squeeze out the cytoplasm (Harauz and Boggs, 2013). The importance of MBP is highlighted by the naturally occurring Shiverer mutant mice. These animals carry a mutation in the MBP gene and lack most MBP isoforms. As a result, myelin in homozygous shiverer mice cannot be compacted properly and these mice suffer from convulsions and die at a very young age (Chernoff, 1981; Massa et al., 2004).

The second major myelin protein PLP has two isoforms: DM20, highly expressed prenatally, and PLP1 expressed postnatally and during development. PLP reaches myelin after MBP and its major function is to stabilize the intraperiod line, (i.e., the opposing outer face of each wrap of the myelin membrane), and so contributes to myelin compaction (Bakhti et al., 2013). Along with myelin sheath formation, PLP is also present in non-myelinating cells where it is known to be involved in several functions such as cell migration, ion exchange, and apoptosis (Skoff et al., 2004). It forms a complex with avβ5 integrin in oligodendrocytes (OL) and oligodendrocyte progenitor cells (OPCs) The PLP-avβ5 complex formation is modulated by the activation of neurotransmitters which increases OLs binding to extracellular matrix protein fibronectin (Gudz et al., 2006; Harlow et al., 2015). This suggests a role that how neuronal activity regulates OLs maturation and subsequent myelination. Moreover, studies have shown that the amount of PLP in glial cells corresponds with the degree of apoptosis (Skoff et al., 2004). Mutations in the PLP1 gene are found in patients suffering from Pelizaeus-Merzbacher disease which starts in early childhood and is characterized by developmental retardation, tremor, general weakness, and ataxia (Raskind et al., 1991). Given the severity of this disease, it is surprising that PLP1 KO mice are well myelinated with only reduced cholesterol levels in the myelin sheath. On the other hand, double knockout mice lacking both PLP1 and the PLP-related glycoprotein M6B are severely hypo-myelinated while PLP1 overexpressing mice show dysmyelination. Apart from myelination, PLP mutations are also linked to OLs

survival as PLP products accumulate in the ER of OLs, leading to their apoptosis. Studies have shown opposing effects on the survival of OLs: when PLP expression is enhanced it leads to a reduction in survival, when is reduced leads to an increased survival (Bongarzone et al., 2001).

The 2', 3‟-cyclic-nucleotide 3’-phosphodiesterase (CNP), is expressed earlier than any other myelin protein, making up 4% of the protein content of the CNS myelin and exhibiting enzymatic activity. The two isoforms of CNP are CNP1 and CNP2, (Wang et al., 2021) that are present in OLs and noncompact myelin sheath, i.e.: the inner and outer tongue along with paranodal loops. CNP plays a major role in the extension of OLs by promoting microtubule (MT) assembly and is essential for glial trophic support to axons since is positioned next to the axons (Bansal et al., 2014). Recent studies indicate that along with many other players it is also involved in maintaining the integrity of axons and their survival (Olga et al., 2020; Raasakka and Kursula, 2014). CNP1-deficient mice appear healthy and myelin structure seems normal, but upon aging, these animals develop an axonal degeneration (Bansal et al., 2014). Moreover, they also show defective paranodal loop formation with cytoplasm-filled extensions of OLs on either side of the node. Overexpression of CNPase leads to abnormal myelin formation with aberrant OLs membrane expansion (Fulton et al., 2010).

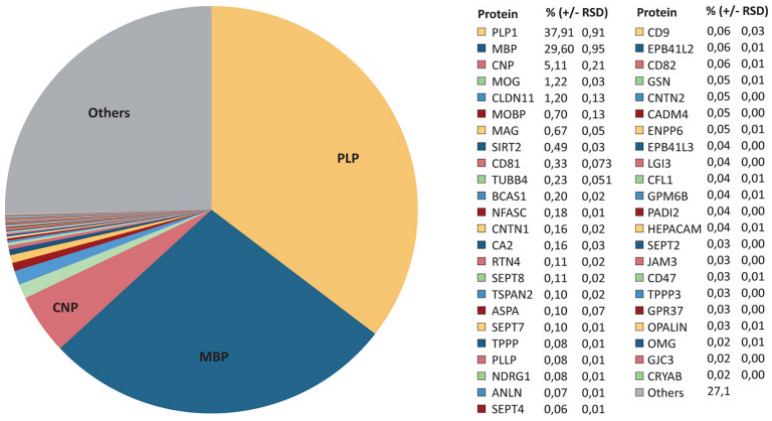

Protein	% (+/- RSD)		Protein	% (+/- RSD)	
PLP1	37,91	0,91	CD9	0,06	0,03
MBP	29,60	0,95	EPB41L2	0,06	0,01
CNP	5,11	0,21	CD82	0,06	0,01
MOG	1,22	0,03	GSN	0,05	0,01
CLDN11	1,20	0,13	CNTN2	0,05	0,00
MOBP	0,70	0,13	CADM4	0,05	0,00
MAG	0,67	0,05	ENPP6	0,05	0,01
SIRT2	0,49	0,03	EPB41L3	0,04	0,00
CD81	0,33	0,073	LGI3	0,04	0,00
TUBB4	0,23	0,051	CFL1	0,04	0,01
BCAS1	0,20	0,02	GPM6B	0,04	0,01
NFASC	0,18	0,01	PADI2	0,04	0,00
CNTN1	0,16	0,02	HEPACAM	0,04	0,01
CA2	0,16	0,03	SEPT2	0,03	0,00
RTN4	0,11	0,02	JAM3	0,03	0,00
SEPT8	0,11	0,02	CD47	0,03	0,01
TSPAN2	0,10	0,02	TPPP3	0,03	0,00
ASPA	0,10	0,07	GPR37	0,03	0,00
SEPT7	0,10	0,01	OPALIN	0,03	0,01
TPPP	0,08	0,01	OMG	0,02	0,01
PLLP	0,08	0,01	GJC3	0,02	0,00
NDRG1	0,08	0,01	CRYAB	0,02	0,00
ANLN	0,07	0,01	Others	27,1	
SEPT4	0,06	0,01			

Figure 2: ***Relative abundance of proteins involved in CNS myelination.*** *Pie chart displaying the relative abundance of proteins found in myelin isolated from human white matter and identified by Mass spectroscopy mode. Known myelin proteins' relative abundance is expressed as a percentage with a relative standard deviation (% RSD). The overall amount of myelin protein is comprised of about 73% known myelin proteins and 27% proteins that have not yet been independently verified as myelin proteins. The image is taken from* (Jahn et al., 2020).

Along with these three major proteins, other myelin-related proteins are: myelin-associated glycoprotein (MAG), myelin oligodendrocyte glycoprotein (MOG), myelin-associated oligodendrocyte basic protein (MOBP), and opalin (Montague et al., 2006). MAG is an early-expressed transmembrane protein and acts as a neural cell-adhesion molecule. It has two isoforms, i.e.: small S-MAG and L-MAG. It acts as a bidirectional signaling molecule, engaging both axon-to-myelin as well as myelin-to-axon communication. It is localized on the innermost surface of myelin along the internode where it makes contact with the axon. It is responsible for the maintenance of myelin-axon spacing i.e., periaxonal diameter, and also inhibits neurite growth (Pronker et al., 2016). MAG null mice show delayed onset of CNS myelination without alterations in myelin compaction leading to neurological deficits. They display structural abnormalities in the periaxonal areas of the myelin sheath, more specifically in the periaxonal cytoplasmic collar (Schnaar and Lopez, 2009).

Similar to MAG, MOG is also a cell adhesion molecule and a transmembrane protein. It is located on the outermost lamellae of the myelin sheath where it is involved in myelin maintenance by making cell-cell communication between OLs and neurons. It is particularly expressed on the surface of OLs in their later differentiation stage and is used as a marker of the OLs maturation (Marignier et al., 2021). MOG-deficient mice appear healthy and show no pathological abnormalities (Delarasse et al., 2003). MOBP is the third most abundant protein in CNS myelination and like MOG, is expressed in mature OLs. MOBP is located on the major dense line of compact myelin and it works in an MBP-dependent manner. It is primarily involved in the compaction and maintenance of the radial volume of the myelin sheath (Montague et al., 2006). However, Mobp homozygous null mice display no apparent clinical phenotype and no defect in the process of myelination. MOBP can induce experimental allergic encephalomyelitis in mice and has been proposed to have a role in the pathogenesis of multiple sclerosis (Yool et al., 2002). Along with these, there are several other proteins highly enriched in myelin but have lower abundance such as opalin. Opalin, also indicated as Tmem10, is a transmembrane protein that is highly expressed by OLs and paranodal loops of the axon. This protein's

physiological function is not yet been determined and Tmem10-knockout mice do not exhibit any obvious phenotype (Hardt et al., 2020; Yoshikawa et al., 2016).

The transcriptional control of central myelin-related genes is highly complex and dynamic. Hes5, is one of the stage-specific factors important for the growth of oligodendroglia. Myelin gene expression regulatory factor (MRF) is another newly activated transcription factor in the oligodendroglial lineage just before differentiation. In order to enhance the development of oligodendroglial cells, it is induced by a number of transcription factors, including Sox10, Olig2, and Zfp24 (Sock and Wegner, 2019). MRF is specifically expressed in the nucleus of post-mitotic OLs and its expression peaks during the myelination (Emery et al., 2009). In addition, MRF overexpression or deletion in vitro increases or decreases myelin gene expression levels, respectively. MRF^{null} mice form pre-myelinating OLs but die at postnatal week three due to a lack of myelin formation caused by failure to accumulate myelin-specific gene products. however, MRF has established a critical role in OLs maturation and CNS myelination, but its ability to execute a similar role in non-glial cell lines has yet to be determined (Koenning et al., 2012).

1.1.3 CNS myelinating glia and axo-glial interaction

In vertebrates, the majority of myelination occurs postnatally and is thought to continue throughout life. Myelin sheaths around axons are produced by OLs in the CNS, which are small non-neuronal cells with fewer branches. Unlike Schwann cells, which myelinate a single axon at a time in the PNS, a single OLs can simultaneously myelinate 30-40 axons (Pérez-cerdá et al., 2015). In addition to myelinate axons, OLs also support axonal energy metabolism and long-term integrity. They form synaptic connections with neurons and contribute actively and directly to the neural signaling (Sherman and Brophy, 2005). Myelination requires a sequential progression of OLs lineages to maintain the stability and integrity of myelin sheath on the axons (Hughes and Appel, 2016). In the late gestational and early postnatal periods, OLs arise from OPCs within restricted regions of the brain and spinal cord. OPCs are glial cells also known as NG2-glia or polydendrocytes as distinguished by the coexpression of NG2 (a chondroitin sulfate proteoglycan encoded by CSPG4 in humans) and platelet-derived growth

factor receptor alpha (encoded by PDGFRA) (Li et al., 2017). OPCs arise from neural precursors in the ventral spinal cord and migrate long distances in order to populate the entire CNS. In the forebrain, multiple waves of OPCs production occur from embryonic to postnatal stages starting from E12.5, and when they undergo proliferation can be identified by a higher expression of platelet-derived growth factor receptor A (PDGFRα). PDGFRα receptors are abundantly expressed by OPCs, and become down-regulated as they differentiate to form immature OLs and then finally mature myelinating OLs (Castelo-branco and Liu, 2020). Both migration and proliferation of OPCs are regulated by several signals released from neurons and astrocytes followed by their differentiation into premyelinating OLs (Sherafat et al., 2021). These signals include growth factors, protein kinases, and extracellular matrix molecules, all of which influence epigenetic modifications, transcriptional and translational regulation, and the actin cytoskeleton. In addition, only OPCs that make the appropriate contact with axons are thought to survive and initiate myelination, suggesting that axon-derived signals are crucially important for OLs survival (Duncan et al., 2021).

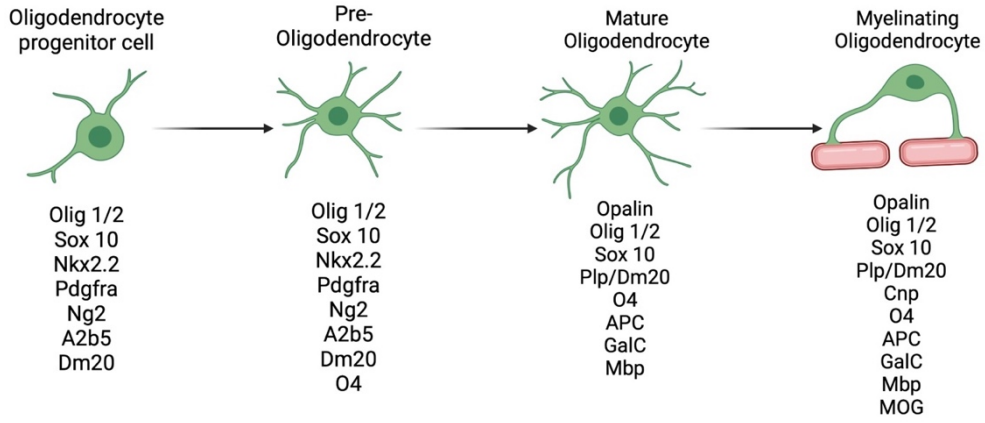

Figure 3: ***Developmental stages of oligodendrocytes lineage.*** *Morphological and antigenic expression of OPCs to myelinating OLs. Image modified from* (Traiffort et al., 2016).

Each stage of OLs development is marked by the expression of stage-specific cell surface antigens as shown in Fig 3. Their differentiation involves dramatic changes in their gene expression and morphology from bipolar OPCs to an extensive network of branches forming mature OLs (Harlow et al., 2015). These mature OLs synthesize OL-specific proteins, including PLP, MBP, neurofascin155 (NF155), MAG, and MOG. The OLs make myelin sheath and the

growing edge of the myelin membrane, called the 'inner tongue', makes contact with the axons to wrap myelin membranes in a multilamellar fashion. Starting from the inner tongue and going through the outer tongue, the completion of enwrapping myelin depends on the axonal diameter and its compaction which leads to the formation of compact internodes and non-compact paranodes (Bansal et al., 2014). Morphologically, axonal segments underlying myelinated internodes have larger calibers due to increased expression and phosphorylation of neurofilaments (NFs) (Yuan et al., 2017). It is another biomarker, the phosphorylation of which depends on the myelination pattern (Gafson et al., 2020). They are key structures of the axonal cytoskeleton and are composed of four subunits: NFH, NFM, NFL, and α-internexin based on their molecular weight. It is known from the literature that NFH and NFM consist of KSP repeats, the phosphorylation of which is induced by myelination to allow expansion of axonal radial volume. NFs are organized in parallel structures inside the axon and are expressed more highly in large myelinated axons. However, the relative amount of NF can widely differ along the course of even a single axon, e.g., their amounts are 3-fold greater in myelinated regions of axons than at the nodes of Ranvier (Yuan et al., 2017). At paranodal loop ion channel, compartmentalization is mediated by a heterotrimeric protein complex of axonal Contactin, Contactin-associated protein (Caspr), and glial NF155. In contrast, in unmyelinated axons, Caspr is diffusely organized throughout the length of the fiber along with Na_v and K_v^+ channels as shown in Fig 4 (Duncan et al., 2021).

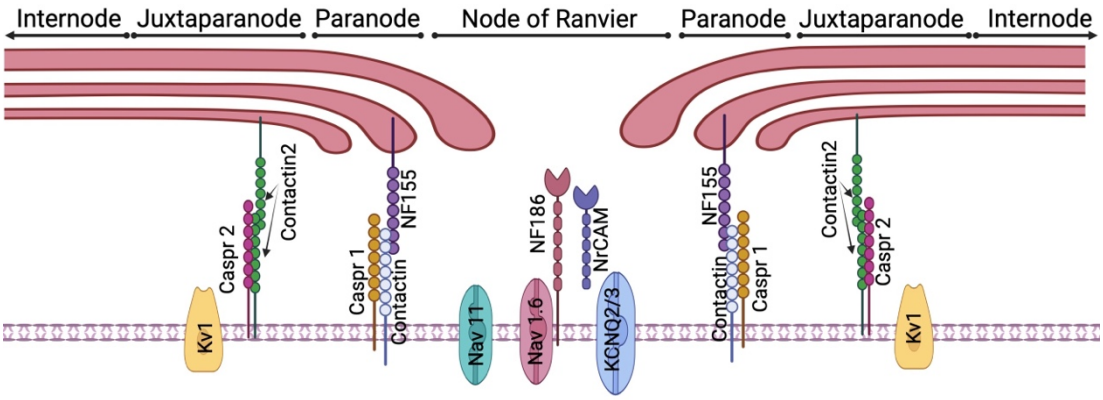

Figure 4: ***Diagrammatic representation of the several regions of a myelinated axon.*** *Node of Ranvier, which expresses voltage-gated Na+ channels clustered and anchored at the nodes via interactions with NF186 and NrCAM, the paranode, which serves as the site of myelin attachment, and the juxtaparanode, which houses the majority of voltage-gated K+ channels. The complex*

formation of Nfasc155, contactin, and CASPR1 to form the septate-like junctions at the paranode, as well as caspr2, and contactin 2 at juxtaparanode. Image modified from (Arancibia-Carcamo and Attwell, 2014).

1.1.4 Myelin assembly

Myelination is a complex process, the assembly of which includes a sequence of events such as (1) proliferation and migration of OPCs in white matter tracts, (2) differentiation of OPCs into myelinating OLs, (3) recognition of target axons and axon–glial signaling, (4) membrane outgrowth and axonal wrapping, (5) trafficking of membrane components, (6) myelin compaction, and (7) node formation (Nave and Werner, 2016). First, OPCs migrate away from the neuroepithelium of the ventricular/subventricular zone of the brain into the developing white matter, in which they proliferate and form an evenly spaced network of processes-bearing cells. Some OPCs remain in the proliferating stage as an excess of OPCs are produced to ensure that the number of OLs matches the number of axons to be myelinated, which are later eliminated by apoptosis. OPCs can remain for a long time in an immature state and once the terminal differentiation starts it takes place very rapidly (Edgar et al., 2009). The second step of myelination is the differentiation of OPCs, which depends on various known and unknown mechanisms. It is known that the neuronal signals control the transformation of OPCs into myelin-forming OLs by activation of various transcriptional regulators, such as Sox 5/6, Hes5, and Id2/4. Many of these transcription factors are also controlled by microRNAs, histone deacetylases, and signaling pathways. Once the decision has been made to initiate myelination, morphological differentiation of OPCs takes place by the activity of critical transcription factors and signaling pathways, such as Sox5/6, Hes5, PDGFRα, myogenic regulatory factors, Nxk2.2, Olig1, Sox10, YY1, and Zfp191 (Nave and Werner, 2013).

On one side we know much about oligodendrocyte lineage progression but on the other side, very little is known about how OLs choose axons for myelination, the third step of this process. Two factors are known to be involved in this decision-making. One is the caliber of axons, so fibers with a caliber of more than 400 nm are contacted by OLs to start myelination. Second is the presence of particular adhesion molecules expressed on the surface of axons identified by OLs.

However, also axons of caliber size around 200-300 nm are myelinated in some brain regions. Small-caliber axons seem to release specific signals received by OLs which likely initiates myelination. It is known from a study that nonreceptor tyrosine kinase Fyn is one of these signals because the loss of Fyn causes hypomyelination of small-sized axons without affecting larger axons (Umemori et al., 1994). In addition, neurons are reported to change their patterns of expression of axonal proteins before the onset of, and during the early stages of myelination. In particular, polysialylated neural cell adhesion molecule (PSA-NCAM) and the adhesion molecule L1 CAM promote myelination as they are expressed on the axonal surface at the beginning of myelination, but soon disappear as axons become myelinated (Barbin and Charles, 2005).

Once the contact between OLs and axon is established, the wrapping of the myelin sheath around axon (4^{th} step) starts with both Pi3K/Akt/mTOR and ERK1/2- dependant signaling pathways playing a pivotal role to produce fully mature myelin sheath with optimal g-ratio. Myelin grows by two distinct but coordinated motions: the wrapping of the leading edge at the inner tongue around the axon underneath the previously deposited membrane, and the lateral extension of myelin membrane layers toward the nodal regions (Duncan et al., 2021). Thus, the lateral cytoplasmic-rich edges of each myelin layer always stay in close contact with the axonal surface and move in a continuous helical manner toward the future node in which they align and form the paranodal loops. The different myelin components are synthesized in OLs at several subcellular localizations and are transported by various mechanisms to the growing myelin sheath. Once these proteins bound and interact with each other, the two adjacent cytoplasmic membrane surfaces appear to polymerize thereby driving membrane zippering at the cytoplasmic surfaces of the myelin bilayer (Poitelon et al., 2020).

The last step of the myelination process requires the formation of small gaps in the myelin sheath, referred to as the nodes of Ranvier. These are highly complex structures, 0.5-1 μm in length, which allow ion influx into the axon to regenerate the action potential. Early in the process of myelination, an axo-glial junction forms between the distal, uncompacted loops of myelin and the axolemma, this gives rise to the paranode that separates the node from the juxtaparanode as

shown in Fig 4(Simons and Lyons, 2013). The juxtaparanodes lie just under the compact myelin sheath immediately adjacent to the paranodes and have high densities of voltage-gated K^+ channels and neuron-glial-related NrCAMs, Caspr2, and TAG-1. These cell adhesion molecules form a complex and interact with TAG-1, which is expressed by the oligodendrocyte cell membrane (Stadelmann et al., 2022). The nodes of Ranvier are the sites for action potential regeneration and are therefore highly enriched in voltage-gated Na^+ channels. The Na^+ channels are clustered and anchored at the nodes via interactions with several cytoskeletal/scaffolding proteins, including transmembrane neurofascin-186 and NrCAM (which interact with extracellular matrix proteins), and many others. The concentration of Na^+ channels at the nodes allows for the action potential to be regenerated at each node, as it propagates from one node to the next by saltatory conduction. The process of myelination and node formation can be coordinated by axons, myelinating glia, or a mixture of both. Substantial evidence suggests that interactions with myelinating glia are vital for the assembly of nodal domains in the axon. (Barbin and Charles, 2005).

1.1.5 Myelin disorders

Several neurological disorders lead to defects in the myelin sheath resulting in abnormal functioning of the nervous system. Some of these disorders are classically characterized by the destruction of myelin with or without affecting the axons lying beneath. Demyelinating disorders are diagnosed using a combination of CSF examination, neuroimaging, and neurological analysis. Primary demyelinating diseases typically affect glial cells or myelin-related gene mutation leading to an inability of myelin formation or repair eventually leading to axonal loss. The most common primary demyelinating disease of CNS is multiple sclerosis, the etiology of which is yet not known. Other genetic demyelinating diseases are Pelizaeus-Merzbacher disease (resulting from a recessive X-linked mutation in the PLP gene), Progressive Multifocal leukoencephalopathy (caused by a destructive infection of OLs by polyomavirus JC), and Acute disseminated encephalomyelitis (usually develops after a viral infection such as HIV, influenza, hepatitis A, B, measles, chickenpox, etc.) (Wolf, 2021). Contrarily, secondary demyelinating diseases are caused due to neuronal or axonal defects leading to subsequent myelin breakdown and white matter abnormalities in various patterns.

They are known to be caused due to heterogeneous mix of conditions, including infections, nutritional deficiencies, vascular diseases, chemical agents, and genetic disorders (Ryan et al., 2014).

The significance of myelination in normal cognitive function has been highlighted from novel knowledge on the pathological signs associated with brain disorders that were previously thought to spare myelination. For example, in Down's syndrome and Alzheimer's disease, the expression levels of CNPase are significantly decreased causing both oligodendroglial and myelin alterations (Vlkolinsky et al., 2001). Furthermore, patients suffering from schizophrenia show a decreased density of OLs, down-regulation of myelin genes, and decreased white matter volume (Roberts et al., 2022). In addition, myelin defects also characterize several disorders of later life, e.g. age-related cognitive decline (Hinman and Abraham, 2007), major depression, and bipolar disorders (Sehmbi et al., 2018). Moreover, pathological signs of neurodevelopmental disorders (NDDs), like autism spectrum disorder (ASD) (Galvez-contreras et al., 2020), and cerebral palsy, include aberrant myelination (Kim et al., 2014). Brain magnetic resonance study in $Mecp2^{-/y}$ mice, a highly validated murine model of Rett syndrome, detected a significant reduction in the thickness of the corpus callosum (Confort-gouny et al., 2006). MOBP was found to be upregulated in Mecp2-null mice and to be directly regulated by MeCP2 through the binding of its promoter (Urdinguio et al., 2008). Moreover, both MBP and MAG show increased expression in the corpus callosum of Mecp2 deficient mouse (Vora et al., 2010). A conditional mutant mouse line lacking MeCP2 only in oligodendroglial lineage developed severe hind-limb clasping phenotype which was significantly ameliorated by restoration of MeCP2 along with the improved motor activity. Interestingly, this specific loss of MeCP2 in oligodendrocyte lineage does not affect the expression pattern of proteins MBP and PLP involved in the myelination (Jin et al., 2017). Finally, a diffusion tensor imaging study in Rett syndrome (RTT) patients shows a significant reduction in fractional anisotropy in the corpus callosum, indicating that white matter impairments are present in Rett syndrome patients (Bibat et al., 2010).

1.2 Neurodevelopmental disorder

NDDs are a group of conditions that occur during brain development before the child enters grade school. NDDs currently include Intellectual disabilities, communication disorders, autism spectrum disorder (ASD), attention deficit hyperactivity disorder (ADHD), specific learning disorders (SLD), and movement disorders as shown in Fig. 5 (Cainelli and Bisiacchi, 2022). They affect 1-2% of the population and are characterized by intellectual disability, behavioral abnormalities, cognitive impairments, speech and language deficits, and neurological dysfunction, which greatly impact personal, social, academic, and occupational function. The diagnostic criteria for NDDs are based on a constellation of behaviors and symptoms specified in the DSM-5 and WHO international classification of disease. The diagnosis mainly depends on the clinical presentation of the patient and deficits and delays in expected development (Ismail et al., 2019). NDDs likely result from a combination of genetic, biological, psychosocial, and environmental risk factors. Epidemiologic studies have reported various environmental factors associated with NDDs such as maternal health conditions, perinatal infection, malnutrition, trauma, and many others (Durbagula et al., 2022). Various epigenetic alterations or a polygenic contribution with multiple variants or polymorphisms also collectively result in NDD. Genetic mutations are also a prominent feature contributing to NDDs, as there are an enormous number of individually rare genetic conditions including chromosome copy number variants and single-gene disorders. Numerous NDDs are caused by single or multiple mutations of about 20% of genes located on X chromosome such as *CDKL5, SMC1A, USP9X, LAMP2, MECP2, DCX, DDX3X, OFD1, SHANK3, CNTNAP2, NRXN1, PTEN, FMR1, OPHN1,* and *TSC1*, etc. Most of these genes are highly expressed in the brain and play a crucial role in CNS functioning highlighted by numerous studies reporting that mutations of such genes are associated with severe forms of NDDs (Brand et al., 2021). For the rest of this dissertation, I am going to focus on one of these NDDs of monogenic origin: *CDKL5* deficiency disorder (CDD).

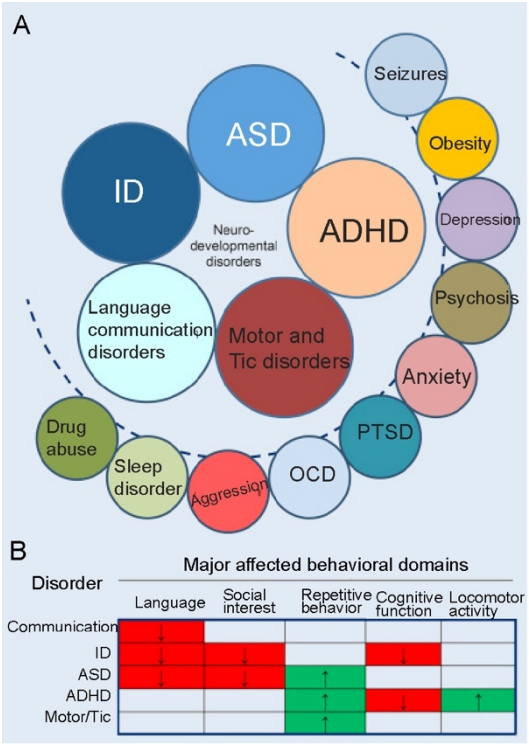

Figure 5: The spectrum nature of neurodevelopmental disorders (NDDs). ***(A) The spectrum*** *of NDDs and other related disorders.* ***(B)*** *Major affected behavioral domains and their heritability of common NDDs (red—reduced, green—increased). ASD—autism spectrum disorder, ID—intellectual disabilities, ADHD—attention deficit hyperactivity disorder, OCD—obsessive-compulsive disorder, PTSD—post-traumatic stress disorder.* Image modified from (Homberg et al., 2016)

1.3 *CDKL5* deficiency disorder

CDD is a rare NDD that is caused by mutations in the cyclin-dependent kinase-like 5 (*CDKL5*) gene, which is located on the short arm of the X chromosome. *CDKL5* encodes for a serine/threonine protein kinase and its mutations lead to almost complete loss of the functional protein leading to CDD pathology. The gene, *CDKL5*, was originally identified in 1998 during a transcriptional mapping project of the human X chromosome (Montini et al., 1998). Until a few years ago, the pathology produced by such mutations was identified as an "Early onset seizure variant of RTT" or "Hanefeld variant of RTT" because it shares several features with the classical form of Rett syndrome (RTT). RTT is another NDD linked to the X chromosome that is caused by mutations in the gene coding for the MeCP2 protein. RTT is a developmental encephalopathy affecting a patient's ability to communicate and perform simple motor tasks. It mainly affects females at a prevalence of 1:10,000. Indeed RTT and CDD patients have similar features

like stereotypic hand movement, growth retardation, regression of speech, laughing and screaming spells, breathing and peripheral vasomotor disturbances, and a range of dysmorphic features. Various RTT variants are described based on their characteristics such as preserved speech variant, categorized by the recovery of speech to some degree; the congenital variant (recognized from birth); and the ‘‘forme fruste’’, with a milder, incomplete clinical course (with regression occurring at between 1 and 3 years of age). Although RTT patients develop normally up to 6-18 months, showing a period of apparently normal development followed by a regression phase whereas, CDD is associated with high rates of infantile seizures (Weaving et al., 2004). Among these variants, the ‘‘early-onset seizure variant’’ was initially described by Hanefeld in 1985, who reported a girl showing infantile spasms with hypsarrhythmia in her early development (Hanefeld, 1985). Even if initially diagnosed as an early-onset seizure variant of RTT, it is now clear that such clinical condition was a case of CDD, which is currently recognized as an independent clinical entity associated with early-onset encephalopathy (Fehr et al., 2013; Katayama et al., 2020). Typically, epileptic seizures are the first sign of CDD, with the first episodes discovered in 90% of patients in the first three months of life and in 96.9% in the first six months (the mean first occurrence period is usually set at week 6 of postnatal development) (Olson et al., 2019).

CDD is characterized by severe intellectual disability, hypotonia, behavioral abnormalities, developmental delay, cognitive impairments, sensory, visual, and motor changes, autonomic and sleep disturbances, speech and language deficits, stereotypic hand movement, gastrointestinal disturbances, abnormal muscle tone, drug-resistant infantile epileptic seizures, and bruxism leading to impaired brain growth and neurological dysfunctioning (Fehr et al., 2013; Leonard et al., 2022). The estimated incidence of CDD is 1:40,000-60,000 live births, and it affects prevalently girls, i.e.: four females to every male. The higher incidence in females compared to males suggests that the disease is often more lethal in hemizygous males as they have only a mutated copy of the gene. However, the pathology affects critically and equivalently both the hemizygous males and heterozygous females although the lyonization mechanism (i.e: X-inactivation) can mitigate the severity of the disease in the latter group. (Demarest et al., 2019). Each female

cell can express either the mutant copy or the normal copy of the *CDKL5* gene as a result of the inactivation of one of the two X chromosomes, resulting in so-called somatic mosaicism. Although the extent to which somatic mosaicism influences the clinical phenomenology of CDD is still poorly understood, this phenomenon leads to a significant degree of symptom heterogeneity (Zhu and Xiong, 2019). The clinical profile of patients ranges from moderate forms, with independent walking and controlled epilepsy, to severe forms, with drug-resistant, untreatable, and refractory seizures in addition to microcephaly and the inability to fully develop motor skills (Olson et al., 2019). CDD patients exhibit an unusual seizure pattern, beginning with generalized tonic-clonic episodes and progressing to recurrent distal myoclonic jerks. Moreover, they frequently show cortical visual impairment (CVI), along with other characteristics such as autistic traits, language impairment, food intolerance, constipation, dysautonomia, sleep difficulties, and scoliosis (Bahi-Buisson et al., 2008; Fehr et al., 2013).

It is exceedingly difficult to establish a diagnosis, shortly after birth, as abnormalities on brain MRI scans are quite infrequent. Neuroimaging alterations became evident in about 50% of 6-year-old affected kids. Patients with *CDKL5* mutations have nonspecific abnormalities in their brains, as shown by MRI. The majority of them show temporal lobe white matter hyperintensities along with cortical atrophy (Bahi-Buisson et al., 2008). The EEG of temporal or tempo-occipital head regions frequently displays hypsarrhythmia or epileptiform discharges. Neuroimaging may reveal dentate nuclei and/or cerebral atrophy, hyperintensities in the posterior white matter, and delayed myelination of the temporal lobes (Morrison-Levy et al., 2021). Recent work by Y. Tang et al. shows quantitative MRI morphological defects in young children (3 years of age) with CDD. The subcortical regions of the brain showed the most notable volume reduction, while the occipital, parietal, and temporal lobes also showed volume loss and cortical thinning. Moreover, three distinct patterns of age-related morphological changes were also observed in CDD patients' brains (Tang et al., 2021), highlighting the interest in closely following the developmental trajectory of the consequences produced by *CDKL5* loss.

There is currently no cure available for CDD. Treatment plans for CDD patients rely on symptomatic medications to manage the most troubling symptoms that contribute to disability. The main concern affecting patients' and caregivers' quality of life is epilepsy,, however, 84% of CDD patients show antiepileptic medications resistance. According to an assessment of the anti-seizure medication response in 39 people with CDD, the responder rate (defined as a 50% reduction in seizures) was 69% at 3 months, 45% at 6 months, and then dropped to 24% at 12 months. The drugs that reduced seizures the most at three months were felbamate, vigabatrin, clobazam, valproic acid, steroids, lamotrigine, and zonisamide. Broad-range anti-seizure drugs such as clobazam, valproate, topiramate, levetiracetam, and vigabatrin were most frequently used in CDD, while 29.6% of patients received steroid or ACTH treatment.

1.4 *CDKL5* gene and protein

A positional cloning technique used in 1998 to identify and isolate the genes in Xp22, a region linked to a number of hereditary diseases, led to the discovery of CDKL5 (Montini et al., 1998). The CDKL5 protein belongs to the CMGC family of serine/threonine kinases, which also includes cyclin-dependent kinases (CDK), mitogen-activated protein kinases (MAP kinases), glycogen synthase kinases (GSK), CDK-like kinases. It is distinguished from other CDKL family members by an N-terminal catalytic domain (amino acids 13-297). In this family of kinases, CDKL5 is unique because it has an exceptionally long tail of over 600 amino acids, that is not clearly related to any other protein domains but is well conserved among the several CDKL5 orthologs, which differ only in the most extreme C-terminal regions (Fig 6; (Kilstrup-Nielsen et al., 2012). The Ser/Thr kinase elements that make up the 12-subdomain structure of the CDKL5 enzyme's catalytic domain are highly conserved throughout many species, from fish to mammals as represented in Fig 7 (Katayama et al., 2020). The majority of CDKL5 mutations are found between subdomains I–IV or between the C–terminal region of subdomain VIA and subdomain X, among the 12 subdomains. Across subdomain V and the initial part of subdomain VIA, very few changes have been found. This shows that CDKL5 activity is highly dependent on subdomains I to IV and the C-terminal regions of subdomains VIA and X. (Katayama et al., 2020). An activation cycle between subdomains VII and VIII of

the catalytic domain contains the TEY sequence as seen in MAPK family kinases. This activation cycle's autophosphorylation is believed to induce CDKL5's catalytic activities. Two nuclear localization signal sequences (NLS) and a nuclear export signal (NES) are found in the regulatory domain at the C-terminus of CDKL5. It has been shown that these signal sequences control the intracellular localization of CDKL5 in vitro (Rusconi et al., 2008).

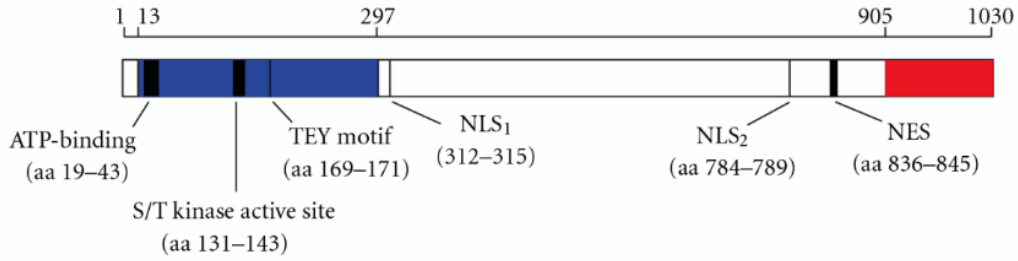

Figure 6: ***The CDKL5115 protein is shown schematically along with its functional domains.*** *Nuclear export signal (NES) and nuclear localization signal (NLS). Image taken from* (Kilstrup-Nielsen et al., 2012).

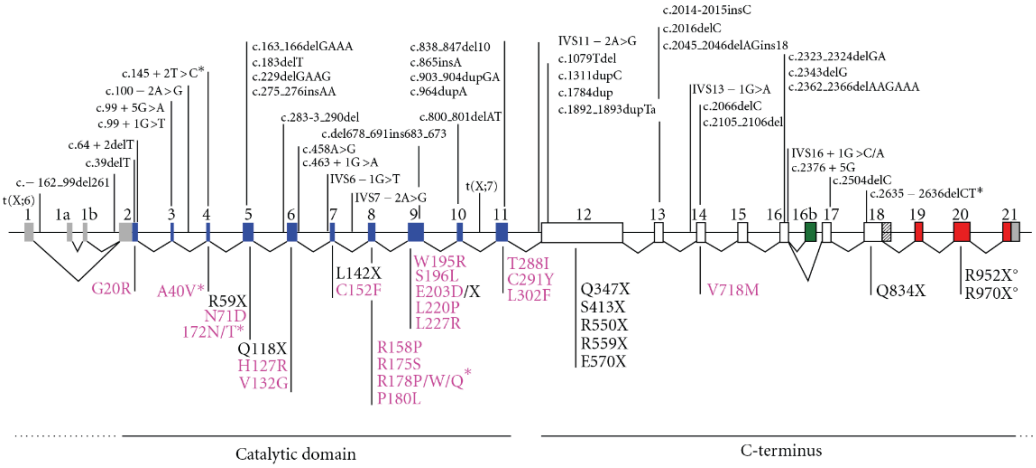

Figure 7: ***All the CDKL5 mutations that have been found are mentioned in the image.*** *Deletions, frameshift mutations, splice variations, and cDNA nomenclature are all demonstrated in the figure. Missense mutations are shown in bright pink, while nonsense mutations are shown in black. Image taken from* (Kilstrup-Nielsen et al., 2012)

The human CDKL5 gene encompasses a region of 228 kb on the short arm of the X chromosome (Xp22), and it has 27 exons that are organized into the 5'-UTR region, the coding region, and the 3'-UTR region (exons 19-22). By using alternative splicing, the exons are joined to create several CDKL5 transcripts, giving rise to five distinct transcription isoforms (hCDKL5 1–hCDKL5 5) (Fig 8). The hCDKL5 1 isoform is present in all tissues examined, indicating its ubiquitous nature. However, the central nervous system is where this isoform is

highest abundant. The CDKL5107 transcript previously reported encodes the same protein as this isoform (Williamson et al., 2012). The hCDKL5_1 isoform is present in all tissues, indicating its ubiquitous nature. However, the central nervous system is where this isoform is highest abundant. Exon 17 is present in the hCDKL52 isoform, which is homologous to hCDKL5 1 and has a larger coding sequence (123 bases, or 41 aa) than hCDKL5_1 (Fichou et al., 2011). The isoforms hCDKL5_3 and hCDKL5_4 are homologous to hCDKL5 1 and hCDKL5 2 respectively, although they lack 51 coding sequence bases at the 3' end of exon 11. These transcripts are anticipated to create a protein that is 17 amino acids (aa) shorter than hCDKL5_1 and hCDKL5_2. Although widely expressed, the three isoforms hCDKL5 2, hCDKL5 3, and hCDKL5 4 seem to be slightly less common than hCDKL5 1. The fifth isoform, hCDKL5 5 was only found in the testes, in contrast to the preceding four isoforms. Recent research showed that mice have five main transcription isoforms, each of which has a unique coding area. It has been determined that the first two isoforms, termed mCdkl5_1 and mCdkl5_2, are orthologous to human isoforms _1 and _2, respectively (Fig 9). Contrarily, the coding regions of the remaining three transcripts are known as mCdkl5_6, mCdkl5_7, and mCdkl5_8 since they do not exhibit complete orthology to human isoforms (Hector et al., 2016).

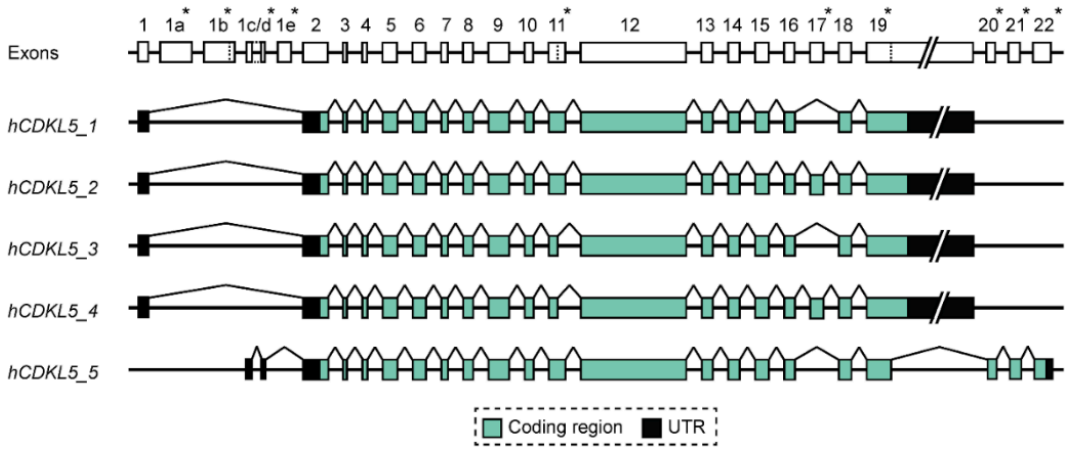

Figure 8: ***The human CDKL5 gene and its transcription isoforms.*** *Lines connecting the exons represent the splicing events, while dotted lines inside the exons represent the potential alternative splicing locations. Asterisks denote exons where variations between distinct isoforms were discovered. Image taken from* (Hector et al., 2016).

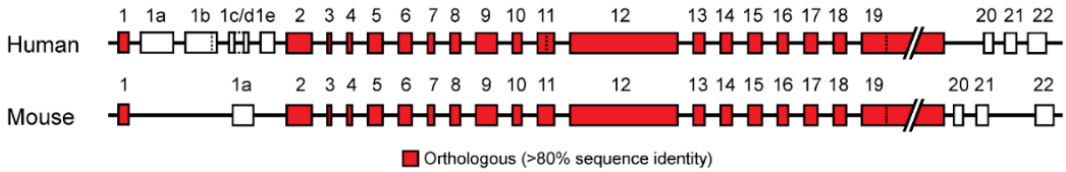

Figure 9: ***Structures of the Cdkl5 genes in humans and mice.*** *Image taken from Hector et al., 2016).*

1.4.1 *CDKL5* gene: mutations and genotype-phenotype correlation

De novo mutations are the cause of the majority of CDD cases. However, examples of *CDKL5* mutations with a family history have also been described; these cases are likely the consequence of germline mosaicism in one of the parents, from whom the child may inherit the mutant gene (Jakimiec et al., 2020). There are many types of pathogenic mutations that have been identified, such as missense and nonsense mutations, small and large deletions, frameshifts, and abnormal splicing (Kilstrup-Nielsen et al., 2012), as a consequence, the clinical variability of CDD may be impacted by this mutational heterogeneity. Moreover, it is important to note the phenotypic variations found among siblings with the same mutation, implying that both environmental and epigenetic factors, as well as the X chromosome's inactivation, have an impact on the final phenotypic profile of specific patients (Hagebeuk et al., 2015).

In 2021, Mackay and colleagues released the results of a ten-years study in which information provided by families of people suffering from CDD was reported and submitted to the International CDKL5 Disorder database (https://www.cdkl5.com/cdkl5-international-registry-database) (MacKay et al., 2021). As part of the data analysis, the CDKL5 variations were divided into four categories based on their projected functional effects: (1) no functional protein; (2) missense/inframe inside the catalytic domain; (3) truncations between amino acid (aa) 172 and aa 781; and (4) truncations after aa 781. Mackay and colleagues demonstrated that there are notable variations in the severity of some recurrent mutations in CDKL5 using a sizable multinational dataset. For instance, those who displayed the severe phenotypes, as represented by the poorest achievement of developmental stages, had missense variants, p. Arg178Trp and p. Arg178Gln, and nonsense variant, p. Arg559*. Those who carried the p.Arg134* and p.Arg550* mutations presented softer phenotypes and lower severity scores,

indicating a better developmental state. Although several clinical characteristics in individuals with the same mutation have been found to be quite homogeneous, research is still far from having a clear and conclusive understanding of the genotype-phenotype link This highlights the complexity and heterogeneity of this condition and prompts more future work in order to establish the cellular and circuits defects underlying the differential clinical outcomes.

1.4.2 Tissue expression and subcellular localization

CDKL5 mRNAs may be readily found in tissues like the testis, lung, spleen, prostate, uterus, and placenta, as well as in a lesser amount in the heart, kidneys, liver, and skeletal muscles (Kilstrup-Nielsen et al., 2012). However, studies on the expression of CDKL5/Cdkl5 mRNA in human and mouse tissues have revealed that is the brain where transcription levels are at their maximum (Kalscheuer et al., 2003). It has been demonstrated that the brain's CDKL5 expression levels peak throughout the differentiation and growth of this organ. CDKL5 is barely detectable throughout embryogenesis and is significantly induced in the early postnatal stages up to P14 (post-natal day 14) (Rusconi et al., 2008). A thorough examination of Cdkl5 expression in the mouse brain revealed that different brain areas had varying levels of Cdkl5 mRNA. In particular, the adult forebrain has exceptionally high quantities of it. It is intriguing to notice that higher levels of expression were discovered in the frontal cortical areas and in the more superficial cortical layers, which are involved in the connection of the two hemispheres through the corpus callosum. This suggests that CDKL5 has a function in the physiology of these brain regions. Moreover, the motor cortex and cingulate cortex, which are of special importance because they are the source of a wide range of mental diseases, have been found to have a significant quantity of CDKL5. Furthermore, all CA fields of the hippocampus exhibit extremely high levels of Cdkl5 mRNA, a region of the brain that largely shares the same evolutionary background as the cortex. Finally, Cdkl5 mRNA is expressed by Purkinje cells in all lobules of the cerebellum, but its levels there appear to be much lower than in other parts of the brain (Kilstrup-Nielsen et al., 2012). Interestingly, Cdkl5 is expressed at modest levels in non-neuronal brain cells (Chen et al., 2010). Among glial cells, it is expressed by both OPCs and OLs, little by astrocytes, and at extremely low levels by the microglia (Ye Zhang et al.,

2014; Zhang et al., 2016). It is clear that alternative splicing plays a role in the functional regulation of Cdkl5 because multiple Cdkl5 splice variants are present and exhibit varying relative abundances depending on their localization (Kilstrup-Nielsen et al., 2012). In the brain, Cdkl5 distribution differs not only according to region but also depending on the subcellular compartment. For instance, the cerebellum retains more than 80% of CDKL5 in the cytoplasm, while the cortex has a nearly equal distribution between the cytoplasm and nucleus (Rusconi et al., 2008). Additionally, it has been discovered that CDKL5 localization is prominent in excitatory postsynaptic compartments, where it governs dendritic spine development and expansion as well as excitatory synaptic function. The interaction of CDKL5 with the palmitoylated version of postsynaptic density protein 95 (PSD-95) mediates the protein's synaptic localization (Yonghong Zhang et al., 2014; Zhu et al., 2013).

1.4.3 Role of CDKL5 in the nucleus

CDKL5 is a kinase that moves back and forth between the cytoplasm and nucleus, suggesting that it may have functions in both cellular compartments. The nuclear speckles, sub-nuclear structures involved in the processing and storage of pre-mRNA splicing factors, are the location where CDKL5 mostly accumulates in the nucleus. The interaction and phosphorylation of MeCP2, which is to the best of knowledge only expressed in the nucleus, by CDKL5 raise the possibility that these two proteins are part of the same biochemical process (Mari et al., 2005). Trazzi and colleagues (2016) further confirmed the role of CDKL5 in epigenetic processes by demonstrating that CDKL5 directly regulates the subcellular location and function of the histone deacetylase 4. (HDAC4). Specifically, HDAC4 is kept in the cytoplasm by CDKL5 phosphorylation activity, which prevents HDAC4 from moving and acting as a transcriptional repressor (Katayama et al., 2020). All of these findings indicate that CDKL5 could regulate still unknown epigenetic modifications via MeCP2, HDAC4, and DNMT1, along with post-transcriptional processes by modulating pre-mRNA machinery and hence contributing to the mechanisms influencing gene expression (Fig 6). Moreover, it has been shown that CDKL5 nuclear localization in human neuroblastoma may also regulate cell cycle and neural development (Valli et al., 2012). In fact, CDKL5 actively inhibits cell cycle and promotes the development

of nerve cells. In support of this idea, it has been demonstrated that animals lacking CDKL5 show increased neural precursor proliferation and a concurrent decrease in fully differentiated neurons in the hippocampus (Fuchs et al., 2014b). However, to assess whether and how CDKL5 directly affects gene transcription, more in-depth investigation is required.

1.4.4 Role of CDKL5 in the cytoplasm

Through its interactions with F-actin in the growth cone and, upon BDNF activation, with Rac1 activity (a member of the Rho GTPases crucial for cytoskeletal remodeling) cytoplasmic CDKL5 has been proposed to play a significant role in neuronal morphogenesis and dendritic arborization (Chen et al., 2010). Moreover, the lab of Sila Ultanir used affinity-based separation of peptides derived from phosphorylated substrates that were discovered by mass spectrometry to identify phosphorylation substrates of CDKL5 (Fig. 10). This study assessed three microtubules (MT)-associated proteins — MAP1S, EB2, and ARHGEF2 — whose phosphorylation is compromised in CDKL5 mutant mice (Baltussen et al., 2018). Furthermore, CEP131, DLG5 and again MAP1S were recognized and validated as additional CDKL5 cellular substrates by Muñoz and colleagues (2018) using a phosphoproteomic approach (Fig. 7). Interestingly, these proteins are all involved in controlling both MT and centrosome function. Likely, irregular dendritic arborization of pyramidal neurons is a possible consequence of CDKL5 loss-of-function mutations that alters both cargo transport control and MT dynamics (Amendola et al., 2014a; Chen et al., 2010; Tang et al., 2017). Importantly, the discovery of these new substrates revealed the consensus pattern, RPXS*, which is recognized by CDKL5, a discovery that will provide with a favorable opportunity to look for other CDKL5 phosphorylation substrates. Recent research has demonstrated that CDKL5 directly interacts with the palmitoylated form of the post-synaptic density 95 protein (PSD-95) to target the PSD (Zhu et al., 2013).

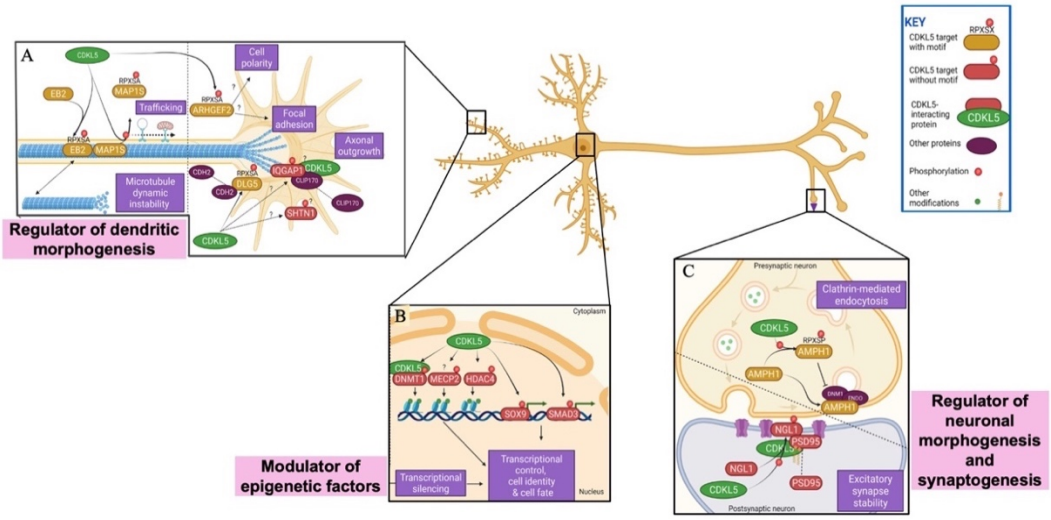

Figure 10: ***CDKL5 targets and affects neuronal processes.*** *CDKL5 targets possessing the consensus motif (yellow), CDKL5 phosphorylation targets without the consensus pattern or with an undetermined phosphorylation site (red), and related proteins (purple).* ***(A)*** *CDKL5 direct targets MAP1S and EB2 are implicated in neuronal microtubule dynamics, which may alter microtubule dynamic instability or cargo microtubule trafficking in neurons. ARHGEF2 and DLG5 are both CDKL5 direct targets. ARHGEF2 can attach to microtubules and is involved in the maintenance of neuronal processes such as dendritic spine integrity and focal adhesions. DLG2 regulates dendritic spine development and synaptic transmission in cortical neurons via regulating N-cadherin location (CDH2). SHTN1, CLIP170, and IQGAP1 are among the proteins that CDKL5 may interact with or potentially phosphorylate.* ***(B)*** *Other potential CDKL5 phosphorylation targets that do not include the consensus motif include the chromatin remodeling proteins MeCP2, DNMT1, and HDAC4, as well as the transcription factor SOX9 and the signal transduction protein SMAD3, which all have the ability to impact transcriptional regulation, govern cell identity, and influence cell death.* ***(C)*** *AMPH1 is a direct CDKL5 phosphorylation target, and phosphorylation inhibits clathrin-mediated endocytosis by preventing interaction with endophilin (ENDO) and dynamin (DNM1). Synaptic vesicle recycling, spine development, and axonal growth are all dependent on this. There is evidence that CDKL5 phosphorylates the cell adhesion component NGL1, which interacts with palmitoylated PSD95 to establish a scaffold for glutamatergic synaptic receptors. Image modified from* (Van Bergen et al., 2022).

Furthermore, Ricciardi and colleagues (2012) showed that CDKL5 binds and phosphorylation NGL-1 which stabilizes its interaction with PSD-95, and that this interaction is crucial for the preservation of both dendritic spines and excitatory neurotransmission. They also showed that dendritic spine structure is aberrant in neurons derived from induced pluripotent stem cells (iPSCs) of CDD patients, indicating that CDKL5 is involved in the structural organization of dendritic spines in human cells (Ricciardi et al., 2012). Importantly, an in vivo two-photon microscopy investigation revealed CDKL5 function in the dynamic of spines turnover in the cerebral cortex providing additional evidence for CDKL5 involvement in the dendritic spine assembly (Della Sala et al., 2016). This study demonstrated that the absence of CDKL5 causes a substantial rise in the rate of

spine elimination as opposed to spine growth/stabilization, which results in a decreased density of mature spines. This finding was supported by the downregulation of PSD-95 clustering at excitatory synapses. It is significant to note that these morphological abnormalities were associated with functional changes in the cortical circuits including weakened excitatory synaptic transmission and LTP maintenance (Della Sala et al., 2016). These findings, along with more recent investigations, clearly indicate that CDKL5 is essential for controlling both the stability of dendritic spines and the plasticity of synapses (Amendola et al., 2014a; Della Sala et al., 2016; Tang et al., 2019). While CDKL5 participates in dendritic arborization, axon extension, spine development, and stability in post-mitotic neurons, its function in proliferating cells is still largely unclear. In an analysis of the function of CDKL5 in these cells, Barbiero and colleagues discovered that it is localized in the centrosome and at the midbody of proliferating cells. They also discovered that the simultaneous absence of HIPK2 from the midbody and its cytokinesis target causes a multipolar spindle to develop when CDKL5 is acutely inactivated by RNA interference (histone H2B). In light of these findings, it is likely that CDKL5 plays a role in faithful cell division regulation by ensuring proper midbody HIPK2/H2B function (Barbiero et al., 2017). These findings further imply that abnormalities in cell cycle progression may contribute to the pathological characteristics associated with CDD as CDKL5 is crucially involved in proliferating cells.

1.4.5 Role of CDKL5 in glial cells

Glial cells do express CDKL5, although at a lower level than neurons, however there is extremely limited information on the role of this kinase in glial cell populations. Recently, a study by Galvani et al., 2021 showed that the brains of *Cdkl5*-KO mice had altered microglial cell shape and number, elevated levels of AIF-1 and proinflammatory cytokines, along with enhanced STAT3 signaling. Additionally, these authors have shown that such microglia overactivation is non-cell autonomous and may result from *Cdkl5* loss in neuronal cells. These results stemmed from studying a conditional *Cdkl5*-KO mouse in glutamatergic forebrain neurons (Emx1::Cre) showing similar microglial overactivation to *Cdkl5*-Ko mice (Galvani et al., 2021).

Growing evidence demonstrates that white matter abnormalities are frequently found in CDD patients. MRI scans of about 50% of children aged 6 with *CDKL5* mutations revealed extensive abnormalities in their brains. The majority of patients exhibit cortical atrophy and temporal lobe white matter hyperintensities, as shown in Fig 11 (Bahi-Buisson and Bienvenu, 2012). Moreover, the results of another neuroimaging study show cerebral atrophy, dentate nuclei hyperintensities in the posterior white matter, and delayed myelination of the temporal lobes (Morrison-Levy et al., 2021). Although this is intriguing information, no study on the impact of CDKL5 loss in myelin organization is so far available. Indeed, ASDs and fragile-X syndrome patients, who show overlaps with CDD pathological signs, have substantially impaired myelin sheath organization in the optic nerve, spinal cord, and corpus callosum (Zhao et al., 2018). Moreover, it is reported that CDKL5 is expressed in both OPCs and OLs in the human and mouse brain (Ye Zhang et al., 2014; Zhang et al., 2016), no study has assessed if/how CDKL5 loss impacts oligodendroglial cells.

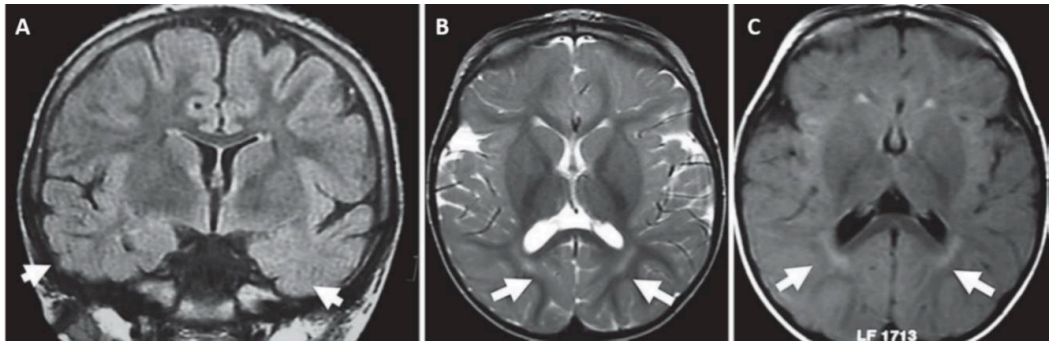

Figure 11: ***Brain MRI results in CDKL5 point mutation patients.*** ***(A)*** *A 12-year-old CDKL5 mutant patient with nonspecific hyperintensities in both temporal lobes (T2 FLAIR coronal section).* ***(B)*** *Nonspecific periventricular hyperintensities (T2 axial section) in a CDKL5 mutant patient aged 3 years.* ***(C)*** *Nonspecific periventricular hyperintensities (T2 FLAIR axial section) in a CDKL5 mutant patient 9 months old. The significant abnormalities in each figure are indicated by arrows* (Bahi-Buisson and Bienvenu, 2012).

1.5 Validation of pharmacological therapeutic approaches for CDD.

With the aim of reversing or at least mitigating the symptoms displayed by CDKL5 KO mice, numerous laboratories have set up preclinical evaluations of innovative therapeutics in recent years. These efforts have yielded some hopeful findings. For instance, Della Sala et al. (2016) discovered that an acute injection with IGF-1(which is an upstream activator of Akt/mTOR pathway) in mutant

mice restored synaptic abnormalities like aberrant dendritic spine turnover, PSD-95 expression, and rpS6 activation (Della Sala et al., 2016). On the other hand, Fuchs and colleagues tested two different selective GSK3β inhibitors SB216763 and Tideglusib on these mutants to counteract the upregulation of this signaling pathway that they found in the hippocampus of CDKL5 KO mice. (Fuchs et al., 2015). More recently, the same group used Tideglusib and showed a rescue in both hippocampus-dependent behavior and hippocampal connectivity, but the Tideglusib treatment in older animals was not effective (Fuchs et al., 2018). Additionally, they treated mutants with LMK235 which inhibits HDAC4 activity and restored synapse formation in the dentate gyrus of CDKL5 KO mice along with improving hippocampus-dependent learning and memory. They also demonstrate that sertraline, a selective serotonin reuptake inhibitor, can correct some of the behavioral and neurodevelopmental flaws seen in heterozygous CDKL5 female and CDKL5 KO male mice as these mice have reduced expression of serotoninergic receptors (5-HT7R) in both hippocampus and cortex (Fuchs et al., 2019). It's interesting to note that Vigli and colleagues (2019) also focused on the 5-HT7R using LP-211, a particular agonist already used to treat Fragile X syndrome and RTT mice models (Fuchs et al., 2020; Vigli et al., 2019). They showed that the activation of 5-HT7R partially corrects the behavioral and cerebral abnormalities, corrects abnormalities in prepulse inhibition, mitrochondrial dysfunctioning and, at the molecular level, reverses the aberrant phosphorylation of rpS6 observed in the CDKL5 KO cortex. (Vigli et al., 2019).

Finally, in order to make up for the mutated CDKL5 protein's inability to function, Prof. Ciani's team has developed a protein substitution therapy for CDD (Trazzi et al., 2018). Following in-vitro tests to confirm the effectiveness of the transduction, the TATĸ—GFP-CDKL51 was directly pumped into the lateral ventricle of CDKL5 KO mice. They discovered that this protein diffused into the brain, reaching the hippocampus and the deeper brain structures (Trazzi et al., 2018). They discovered that intracerebroventricular administration of TATĸ-GFP-CDKL51 significantly reversed cognitive deficits measured by the Morris water maze and passive avoidance paradigms, as well as dendritic abnormalities observed in CDKL5 KO animals (Trazzi et al., 2018).

1.6 CDD rodent models

In light of this condition's complexity and lack of knowledge, CDD models are crucial allies in raising the possibility of discovering efficient therapeutic strategies. Below described are available *Cdkl5*-KO mice models that display high construct and face validity. Wang and associates created the first *Cdkl5* knockout mice in 2012 by deleting the exon 6 of the *Cdkl5* gene (Wang et al., 2012). In 2014 a consecutive *Cdkl5*-KO allele was generated by germline deletion of exon 4 (Fig 12A) (Amendola et al., 2014). Lastly, In 2017, Tanaka's laboratory produced another *Cdkl5* mutant mouse by deleting exon 2 from the *Cdkl5* gene (Okuda et al., 2017). As a result of *Cdkl5* being located on the X chromosome, homozygous females (-/-), heterozygous females (-/x), and hemizygous males (-/y) are produced when the *Cdkl5* allele is deleted. In addition to mice models recently a novel rat model for CDD has also been developed by the deletion of exon 8 (de Oliveira et al., 2022).

1.6.1 Generation and validation of *Cdkl5*-KO mice

The Wang et al., model was validated with the help of an accelerating rotarod test, this mouse model demonstrated hyperlocomotion and poor motor control, which were both measured in a cage-like home setting. They also looked at sociability by probing these mutants in the three-chamber test because deficits in social interaction are a defining characteristic of ASDs and are common in CDD patients (Bahi-Buisson et al., 2008). They discovered that mice lacking *Cdkl5* exhibit profound impairment in social interaction. These mice also exhibit reduced anxiety, impaired learning and memory, and impaired social behavior in the home cage as measured by the nest-building test (hindlimb and forelimb clasping) (Olson et al., 2019). Jhang and colleagues examined autistic and ADHD-like behaviors in young *Cdkl5* mutant mice using the same animal paradigm. They discovered that *Cdkl5*-KO mice exhibit reduced social interaction in the three-chamber sociability maze, abnormal motor behavior, hyperactivity, and an increase in repetitive behaviors like digging as early as 4-5 weeks of age (Jhang et al., 2017). These findings collectively imply that *Cdkl5*-KO mice serve as a reliable model for researching features similar to autism.

Tanaka's *Cdkl5* mutant mice model was also verified by the authors using a battery of behavioral tests that revealed deficiencies in spatial and working memory as well as abnormal social interaction and anxiety-like behavior (Okuda et al., 2018). The majority of the behavioral impairments seen in CDD patients are recapitulated by both models, despite the fact that the two mouse lines were created using distinct methods. These mice do, in fact, suffer motor and cognitive deficiencies, but unlike patients, they do not demonstrate epileptiform activity in the EEG trace or behavioral seizures (Okuda et al., 2017; Wang et al., 2012). However, because these mice models don't have epileptic convulsions, which can have some confounding consequences, they are suitable for both the identification of the molecular and synaptic abnormalities brought on by the absence of *Cdkl5* and for the necessary behavioral assessments.

All research for my thesis was conducted using the *Cdkl5*-KO strain created in Dr. Cornelius Gross's lab at the EMBL in Rome, Italy, and primarily reported by Amendola et al (2014). Therefore, in the next part, I will outline the method utilized to create this mouse line along with the outcomes of the behavioral, molecular, and morphofunctional assessments. Since in my doctoral dissertation, I examined the cerebral cortex, below I'll concentrate primarily on its abnormalities. The deletion of *Cdkl5* in this model was demonstrated by molecular biology and biochemical methods such as semi-quantitative PCR analysis (Fig 12B), and western blotting (Fig 12C) along with morphological analyses (i.e. immunofluorescence; Fig 12D)

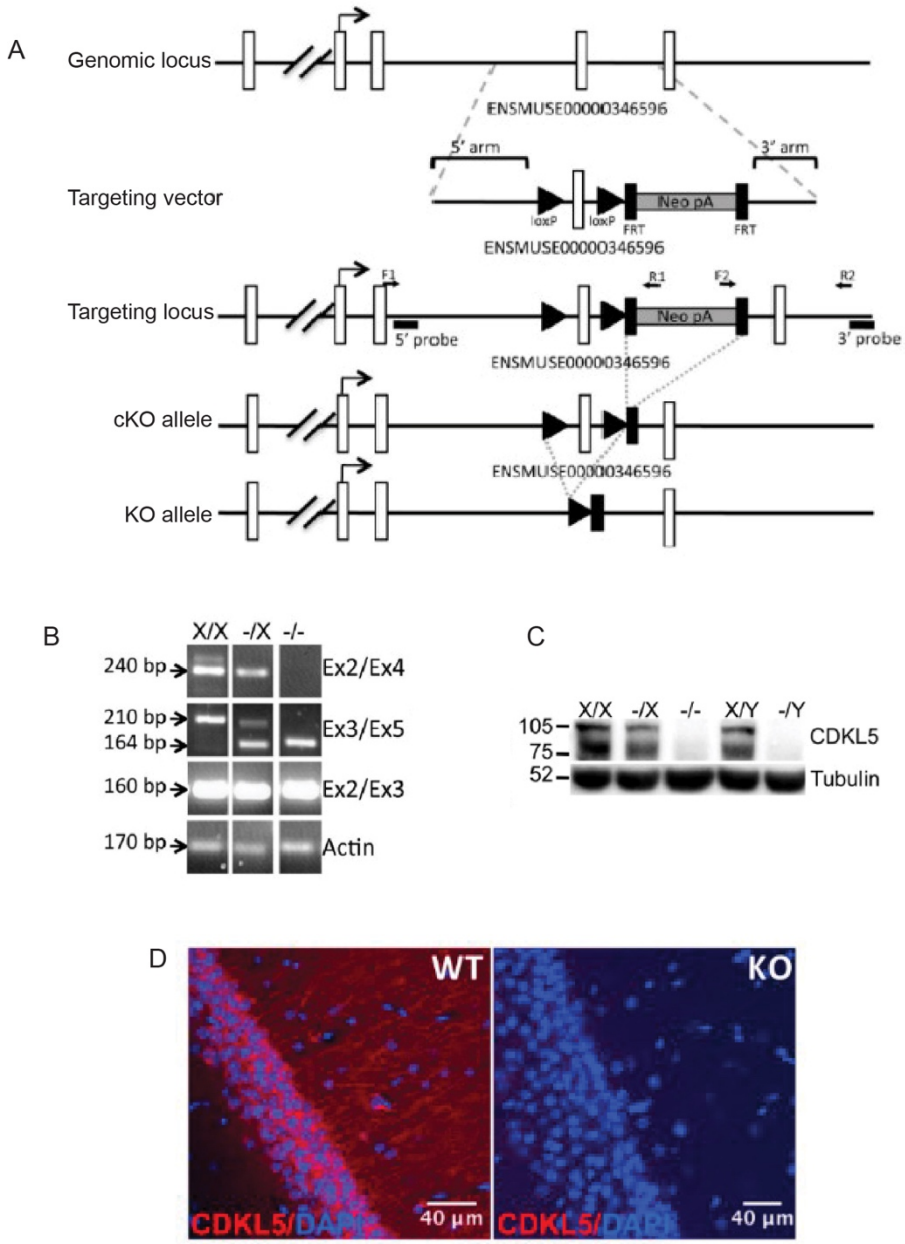

Figure 12: ***(A)*** *Genomic arrangement of the Cdkl5 locus demonstrating the importance of exon 4 (ENSMUSE00000346596), the targeting vector that specifically targeted the Cdkl5 gene, the FRT-deleted conditional Cdkl5-KO allele, and the Cre- deleted constitutive Cdkl5-KO allele used in the current investigation.* ***(B)*** *Exon 4 was not present in any of the mice, although exon 2, 3, and 5 levels were all within normal ranges confirmed by semi-quantitative PCR analysis on total brain RNA.* ***(C)*** *The absence of* CDKL5 *in mutant animals was verified by Western blot analysis of whole brain protein extracts from WT (X/X), heterozygous (X/-), and homozygous (-/-) female Cdkl5-KO mice as well as WT (X/Y) and hemizygous (-/Y) male Cdkl5-KO mice.* ***(D)*** *Examples of CA1 hippocampal brain slices from WT and Cdkl5-KO mice that have undergone Cdkl5 immunostaining were displayed in micrographs (red signal). Hoechst dye was used as a counterstain for cell nuclei (DAPI- blue signal). Scale bar: 40 µm (images modified from Amendola et al., 2014).*

1.6.2 Analysis of *Cdkl5*-KO mice's behavior

Male hemizygous as well as heterozygous and homozygous female *Cdkl5*-KO animals have all been validated (Amendola et al., 2014a; Fuchs et al., 2018). However, the majority of the work was performed on CDKL5 KO male mice to examine the CDKL5 loss of functional consequences and to uncover endophenotypes and biomarkers related to the human condition. CDkl5 KO male phenotype was the closest one that replicates male CDD patients' pathology and serves as the most efficient tool to explore CDKL5 functions in-vivo. Amendola's mouse model exhibits a wide range of behavioral flaws, including hind limb clasping as shown in Fig 13, hypolocomotion, and significant locomotor deficits only in the home cage but not in an open arena (Fig. (Amendola et al., 2014a). In addition, when compared to their WT littermates, male and female mutant animals show gait deficits, aberrant motor learning, and coordination on the accelerating rotarod test (Sivilia et al., 2016)

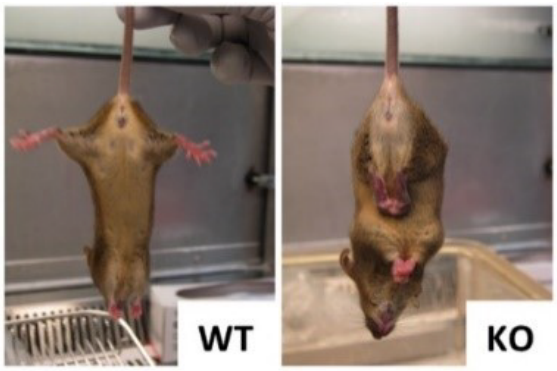

Figure 13: ***Cdkl5 deficient mice display hind limbs clasping.*** *(Image taken from Amendola et al., 2014)*

Cdkl5-KO mice were put through the Y-Maze, Morris water maze, and passive avoidance tests to assess their cognitive ability. In an interesting turn of events, these analyses showed that null mice consistently display abnormalities in hippocampus-dependent learning and memory, indicating that *Cdkl5* plays a role in the proper circuit development underlying these processes (Fuchs et al., 2018, 2014a; Trazzi et al., 2016). Additionally, *Cdkl5* heterozygous and KO females were shown to have all of these defects. (Amendola et al., 2014; Fuchs et al., 2018, 2014) Since CDD patients exhibited behaviors similar to autism, *Cdkl5* mutant mice were also examined for these flaws. In fact, autistic-like characteristics in *Cdkl5* heterozygous and KO female mice are analyzed with

home-cage social behavior observations (such as the capacity to build nests) and environmental interest (such as marble burying). Interestingly, this mouse line like the other two *Cdkl5* mutants exhibit comparable autistic-like behaviors in both young and old animals further supporting the validity of these mutants in the preclinical CDD research (Fuchs et al., 2018). (Jhang et al., 2017; Okuda et al., 2018; Wang et al., 2012). Locomotor dysfunctions are also present in the Amendola mouse model, and more critically, these mutant animals replicate the profound vision abnormalities observed in CDD patients. It has been discovered that *Cdkl5*-KO mice exhibit abnormalities in cortical visual responses in both *Cdkl5* null male mice and heterozygous females using both visual evoked responses (VEPs) and intrinsic optical imaging (IOS) (Lupori et al., 2019a; Mazziotti et al., 2017). These experiments demonstrated that visual cortical responses significantly reduce amplitude as early as P27–P28 (Mazziotti et al., 2017). In addition, adult *Cdkl5* mutant mice had reduced visual acuity as determined by VEPs (Amendola et al., 2014a). These findings support the notion that visual impairments and cortical visual responses are reliable preclinical CDD indicators. In order to identify the circuits responsible for the mice's visual deficiencies, the same team also performed the morphological examination of the visual pathway from the retina to the primary visual cortex (V1) (Lupori et al., 2019a). They discovered that while the structure of the retina is intact, a lack of *Cdkl5* causes incorrect dendritic spine shape, a decrease in PSD-95 expression, and an increase in $VGAT^{+}$ inhibitory synapses in the dorsal and lateral geniculate nuclei as well as the V1 cortex (Lupori et al., 2019a). Moreover, they also used a conditional cre mouse line i.e., $EMX1^{cre}$ in which *Cdkl5* was specifically deleted in excitatory neurons and these mice demonstrated that selective cortical deletion of *Cdkl5* is sufficient to recreate the impairments in visual cortical responses.(Lupori et al., 2019a).

Electroencephalographic (EEG) recordings have not yet shown spontaneous seizures in any of the produced *Cdkl5* mutant mice lines, despite the fact that early-onset seizures are the most recognizable symptom of CDD. However, a distinct reaction was revealed by the pharmacological production of seizures with kainic acid in KO mice (Amendola et al., 2014a). These studies revealed that although *Cdkl5*-KO and WT littermates had similar latency to kainic acid-induced

epileptiform activity bursts, *Cdkl5*-KO mice had longer mean high-amplitude burst durations and lower frequency. This suggests that *Cdkl5* null mice may be more susceptible to seizure induction (Amendola et al., 2014a). Since epilepsy is the major feature of CDD patient pathology here I also want to highlight the findings from Tanaka and colleagues. Tanaka's team intriguingly discovered that *Cdkl5* affects seizure susceptibility in the exon-2 animal model and controls the post-synaptic location of GluN2B-containing NMDARs in the hippocampus (Okuda et al., 2017). They focused on synaptic dysfunction and epileptic susceptibility in the hippocampus and demonstrated that mutant animals exhibit considerable hyperexcitability in response to NMDA treatment but not kainic acid. Moreover, They discovered a postsynaptic overaccumulation of NMDARs with the GluN2B subunit in the hippocampus, which these scientists claimed to be the main cause of epileptogenesis linked to the absence of *Cdkl5* (Okuda et al., 2017). In line with this hypothesis, they found that acute injection of the GluN2B-selective antagonist Ifenprodil eliminates NMDA-induced hyperexcitability in *Cdkl5* mutant mice. These findings thus imply that *Cdkl5* is crucial for regulating the postsynaptic location of NMDARs that contain GluN2B in the hippocampus, which in turn controls the seizure susceptibility (Okuda et al., 2017).

1.6.3 Anatomical and cellular signaling abnormalities shown by *Cdkl5*-KO mice.

Neuroanatomical changes in the cortex and hippocampus are linked to all the behavioral and functional abnormalities seen in *Cdkl5*-KO animals. Although *Cdkl5* mutant mice did not display any abnormalities in brain weight compared to WT controls, they show a significant loss in thickness in each of these brain locations (Fig 14A) (Amendola et al., 2014a). It was demonstrated that both cortical and hippocampal pyramidal neurons of *Cdkl5* mutant mice have shorter apical dendritic arbors and less dendritic branching, which is consistent with the decreased thickness of these areas (Fig 14A). Further, Fuchs et al., (2014) discovered that the proliferation rate of dentate gyrus neural precursors is higher in *Cdkl5*-KO animals than in WT animals. An increase in apoptotic cell death, which mostly affects immature granule neurons and results in a decrease in the overall number of mature granule cells, occurs along with this impairment.

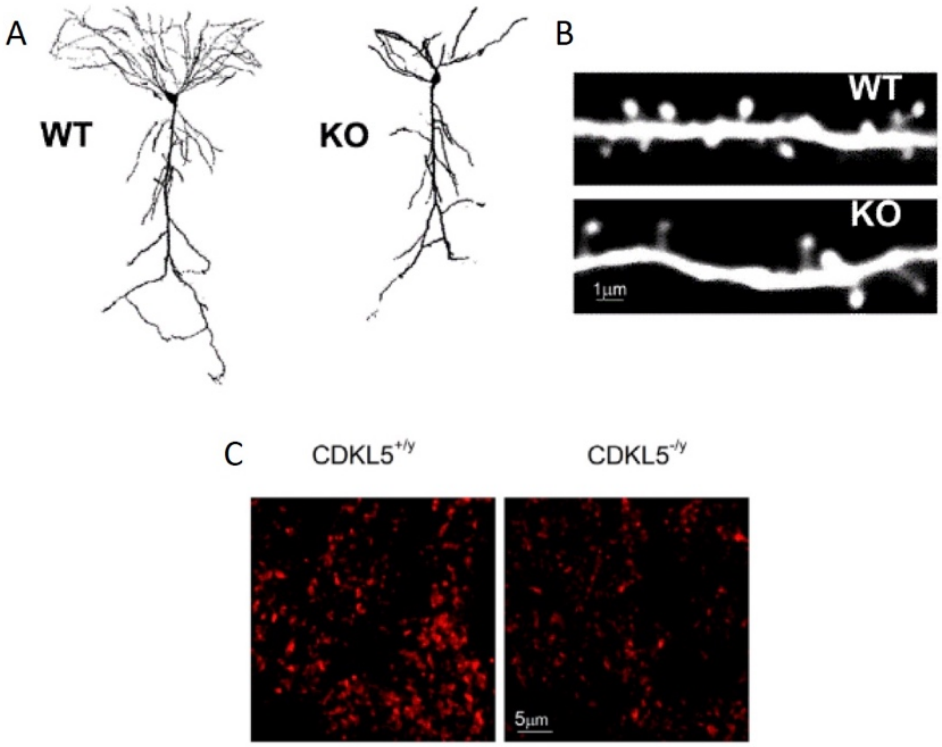

Figure 14: ***(A)*** *Representative images of adult WT and Cdkl5-KO mice rebuilt neurons demonstrating lower dendritic arborization in mutant mice(image taken from* (Amendola et al., 2014a). ***(B)*** *Image of an adult WT and KO mouse dendritic branch demonstrating lower spine density in Cdkl5 mutants.* ***(C)*** *Confocal images of PSD-95^{+} puncta from Cdkl5$^{+/y}$ and Cdkl5$^{-/y}$ mice in the neuropil of S1 layers II–III. Scale bar:5* μm; (modified from Sala et al., 2016)

In addition, Della Sala et al., (2016) discovered that *Cdkl5* deletion causes a decrease in dendritic spine density in the somatosensory cortex (S1). Two-photon microscopy techniques made it possible to comprehend that the lack of *Cdkl5* causes increased amounts of spine turnover, which in turn causes this synaptic abnormality. Instead of faults in spine production, this greater turnover causes an increase in the rate of spine removal. The results demonstrating that the synaptic location of PSD-95 is substantially compromised in *Cdkl5* mutants support the hypothesis that dendritic spines cannot grow correctly in the absence of *Cdkl5* as shown in Fig 14B, C. Therefore, when *Cdkl5* is absent, dendritic spines are unstable and get inappropriately eliminated at greater rates as a result of disrupted PSD organization. It's interesting to note that these morphological flaws were connected to reduced spontaneous excitatory postsynaptic current frequency (EPSC) and impaired long-term potentiation (LTP) maintenance in the brain of *Cdkl5*-KO animals (Della Sala et al., 2016).

It has been discovered that the cortex of *Cdkl5*-KO mice exhibits decreased levels of the phosphorylated forms of phosphorylated ribosomal protein S6 (rpS6), indicating that *Cdkl5* loss impacts the Akt/mTOR pathway, a molecular cascade essential for protein synthesis (Amendola et al., 2014a). This finding sheds light on the molecular mechanism by which loss of *Cdkl5* may alter brain development. Hippocampal *Cdkl5*-KO neurons exhibit this impairment as a result of altered AKT/mTOR/GSK-3 signaling pathways (Fuchs et al., 2015; Okuda et al., 2017). Fuchs and colleagues discovered, in particular, that a change in GSK-3 causes an abnormally high rate of granule cell precursor proliferation in the dentate gyrus of the hippocampal nucleus of mutant mice (Fuchs et al., 2015). Additionally, these cells have a diminished arborization with fewer branches, indicating that GSK-3 deficiencies may negatively affect these morphological features (Fuchs et al., 2015). Moreover, I here want to highlight that AKT/mTOR/GSK-3 signaling pathway defects have also been discovered in other reported *Cdkl5*-KO mice models. In fact, Okuda and colleagues indicated that these defects may contribute to impairments in neurogenesis and neuronal maturation as well as to the enhancement of NMDAR-mediated EPSCs and LTP in the CA1 area (Okuda et al., 2017). The absence of CDKL5 may affect the mTOR pathway differently during development, however, as evidenced by the increased phosphorylation of rpS6 in mutant mice at an advanced disease stage (i.e., 9–12 months) (Vigli et al., 2019).

2. AIMS

In a recent MRI study on CDD patients, severe cortical atrophy and white matter abnormalities were demonstrated. In addition, growing evidence indicates that the white matter and myelin sheath organization are substantially compromised in NDDs such as ASD and fragile-X syndrome, which are strongly related to CDD pathophysiology. Despite these suggestive indications, there are no studies currently available on the role of CDKL5 in oligodendroglial cells and in myelin organization.

To start filling this lack of knowledge, in the present thesis I studied sensory cortices of both Cdkl5 mouse mutants and WT littermates to compare among these groups:

- The localization and numerosity of OPCs and myelinating OLs during the postnatal development of the cerebral cortex.
- The developmental trajectory of cortical myelination by analyzing the expression of important molecules modified by myelin deposition or axonal injury.
- The ultrastructural organization of myelin sheath and g-ratio values.
- The axo-myelinic arrangements at nodal and paranodal structures.
- The effect of stimulating mGluR5 receptors on myelination.

Furthermore, during the Ph.D. program, I had the opportunity to collaborate on a study that for the first time assessed the consequences of *Cdkl5* loss on the expression of mGluR5 receptors and in the pathological signs produced in a mouse model of CDD. In this preclinical study that I co-authored "**mGluR5 PAMs repair cortical and behavioral deficits in a mouse model of CDKL5 deficient condition**. Gurgone et al., 2022)", I employed positive allosteric modulators (PAM) of these receptors that resulted very efficient in reversing several endophenotypes and behavioral symptoms showed by *Cdkl5*-KO mice. This study inspired the experiments where I utilized the same class of drugs to look for myelination effects. Therefore, for the sake of clarity, I included the results of crucial experiments from Gurgone et al., 2022 work at the beginning of this dissertation. All the information related to the materials and methods used to

generate these results and relative discussion is presented in the original article (see annexure) that is included at the end of my thesis.

3. MATERIALS AND METHODS

Animals and pharmacological treatment

Animal care and handling throughout the experimental procedures were conducted in accordance with European Community Council Directive 2010/63/UE for the care and use of experimental animals with protocols approved by the Italian Minister for Scientific Research (Authorization number 175/2015-PR) and the Bioethics Committee of the University of Torino, Italy. Animal suffering was minimized, as was the number of animals used. Mice for testing were produced by crossing *Cdkl5*$^{-/x}$ females with *Cdkl5*$^{-/y}$ males or with *Cdkl5*$^{+/y}$ males. To assess how the cell-specific deletion of *Cdkl5* might affect myelination, two different mouse CRE lines were employed. Cdkl5^{flox} females were crossed with either Emx1^{Cre} male (to specifically delete *Cdkl5* in forebrain pyramidal neurons) (Iwasato et al., 2004) or with Sox10^{Cre} male (to delete *Cdkl5* in the oligodendroglial population) (Matsuoka et al., 2005) B6; CBA-Tg (Sox10^{Cre})1Wdr/J, The Jackson Laboratory). Littermate controls were used for all the experiments. After weaning, mice were housed 4 per cage on a 12 h light/dark cycle (lights on at 7:00 h) in a temperature-controlled environment (21 ± 2◦C) with food and water provided ad libitum. For this study, 2 and 6 weeks old (post-natal days 15 and 56) males were used as the CDD phenotype in male mice is more closer to CDD patients' pathology. These ages were chosen because CDKl5 expression peaks around P14 and the most rapid phase of myelination occurs between P14 and P50. In pharmacological rescue experiments, animals were treated with the selective positive allosteric modulator (PAM) of mGluR5 RO6807794 (RO68) (Kelly et al., 2018). The drug was freshly prepared by dissolving it in 0.3% of Tween 80 and the volume was made up of normal saline. Mice received an intraperitoneal injection of 0.3 mg/kg of RO68 or vehicle every day from P3 to P15 at 9.00 am and then placed back in their home cage. 24 hours after the last injection mice were sacrificed for brain analyses.

Post-mortem brain tissue from CDKL5 patients and controls

The Harvard Brain Tissue Resource Center, Belmont (USA), and the University of Maryland, via the NIH NeuroBioBank, Baltimore, provided the flash-frozen and formalin-fixed human brain tissue blocks of two female CDD patients and neurotypical controls, respectively. The primary visual cortex was utilized in the

current investigations since it is a cortical region that has been widely studied (Brodmann Area 17) and is also seen affected in my mice studies. The samples were specifically matched for gender, age, and hemisphere. A 5.7-year-old female (P1) with a frameshift mutation (c.2153 2154dupTG) in exon 15 of the CDKL5 gene, which causes a premature stop codon, and a 29-year-old female (P2) with a loss of exons 1-3 in CDKL5 were the used samples from CDD patients. The CDD patient samples came from a 5.7-year-old female (P1) with a frameshift mutation (c.2153 2154dupTG) in exon 15 of the CDKL5 gene, which causes a premature stop codon, and from a 29-year-old female (P2) with a loss of exons 1-3 in CDKL5. Contrarily, controls were made up of two females who had no genetic changes and were 4 years old (C1) and 29 years old (C2). These experiments were performed in collaboration with Dr. Riccardo Pizzo and Debora Comai in our laboratory.

Cortical lysates preparation

Young and adult mice (P15: WT=8; KO=5; P56: WT=7; KO=9) were euthanized by decapitation, the entire cortex was rapidly moved and tissue was processed as in (Pavlowsky et al., 2010) and (Huttner et al., 1983). The cerebral cortex was dissected and homogenized in ice-cold lysis buffer (0.32 M sucrose, and HEPES 1X at pH 7.4 and 1 mM EGTA, 1mM Na-Orthovanadate, 1 mM DTT, phenylmethylsulphonyl fluoride, and 1 mM sodium fluoride and protease inhibitors (SIGMAFASTTM Protease Inhibitor Cocktail Tablets, EDTA-Free), using a glass Teflon tissue grinder. The homogenates were centrifuged at 10,000 rpm for 45 min at 4°C. The supernatant was collected and stored at −80 C. The protein content was determined by bicinchoninic acid assay (Pierce, Rockford, IL, USA).

Magnetic-activated cell sorting (MACS) isolation of OPCs

Young mice (P10, n = 3 each genotype) were euthanized by decapitation, the whole brain was rapidly removed and tissue was placed in papain solution. The tissue was dissociated and centrifuged at 1000 rpm for 10 min at 4°C. The pellet was then resuspended and placed in the MACs buffer (Miltenyi Biotech GmbH, Bergisch Gladbach, DE). Mouse OPCs were enriched by positive selection using an anti-PDGFRα antibody conjugated to magnetic beads, according to the

instructions of the manufacturer. Magnetic labeled OPCs were separated by placing cell suspension in the column and washed with MACs buffer. MAC-sorted OPCs were then centrifuged at 1000 rpm for 10min, the supernatant was discarded, and the pellet was stocked at -80°C. The stored sample is ready for the identification of proteins of interest. The isolation of OPCs was performed in collaboration with Prof. Annalisa Buffo and Dr. Martina Lorenzati at Neuroscience Institute Cavalieri Ottolenghi (NICO), University of Turin.

Western blotting

The cortical lysates or MACs isolated OPCs were boiled in an SDS sample buffer, separated by SDS–PAGE, and the proteins were then blotted to the PVDF membrane following a standard protocol (Grasso et al., 2017). Next, PVDF membranes were blocked in milk 5% for 1h and incubated with the primary antibody (MBP 1:500, NF 1:500, pNF 1:5000, or CDKL5 1:500) O/N at 4°C. After washes with TBS 0.1% Tween 20, the membranes were incubated with the secondary antibody (anti-rat, anti- mouse, anti-rabbit 1:5000; Sigma, Italy) for 1h at RT. The chemiluminescent signal was visualized using ClarityTM Western ECL Blotting Substrates (Bio-Rad; Italy) and acquired with Bio-Rad ChemiDocTM Imagers (Bio-Rad; Italy) and analyzed with Image J software (NIH, USA).

Transmission electron microscopy

Adult mice (P56: WT=3; KO=3) were anesthetized using a mix of tiletamine/zolazepam (40mg/kg) and xylazine (4-5 mg/kg) and then transcardially perfused with ice-cold 2% PFA and 2.5% glutaraldehyde in 0.1 M phosphate buffer (PB; pH 7.4). After perfusion, brains were postfixed in the same solution overnight at 4°C and then washed several times in 0.1 M PB. Vibratome sections (500 mm) were coronally cut through the hemispheres, postfixed with 0.5% osmium tetroxide (in 0.1 M cacodylate buffer) for 20 min on ice, dehydrated in a crescent series of ethanol (30%–100%), and embedded flat with epon-araldite resin in rubber molds. Ultrathin serial sections (70 nm) were cut with an ultramicrotome (Leica Ultracut) and collected on single-slot grids coated with a Pioloform solution. Grids were counterstained with uranyl acetate and lead citrate and were observed in a JEM-1400 Flash transmission electron microscope (JEOL,

Tokyo, Japan), and images were acquired from the alveus of the hippocampus of P56 *Cdkl5*$^{+/y}$ and *CDkl5*$^{-/y}$ mice with a high-sensitivity sCMOS camera. Embedding of samples for electron microscopy and ultrathin sectioning was performed in collaboration with Prof. Chiara Salio and Dr. Patrizia Aimar (Dept. of Veterinary Sciences). The extent of myelination was analyzed on micrographs taken at 5,000x magnification by calculating the g-ratio, which equals the diameter of the axon divided by the diameter of the myelinated fiber, on at least 100 fibers from each animal.

Immunofluorescence staining

Animals were anesthetized using a mix of tiletamine/zolazepam (40mg/kg) and xilazine (4-5 mg/kg) and then transcardially perfused with about 10 ml of 0.01M PBS followed by 80 ml of ice-cold 4% paraformaldehyde in 0.1M PB. After the brains were dissected, they were kept in the same fixative solution O/N at 4°C, cryoprotected by immersion in raising sucrose-PB 0.1M solutions, cut into 30 µm sections with a cryostat, and stored at −20°C in a cryoprotective solution containing 30% ethylene glycol and 25% glycerol until use. Cryosections were subsequently washed in PBS solution three times every 10 minutes free-floating. Further, they were blocked by immersion in 0.1M PBS solution containing 3% normal donkey serum (NDS) and 0.5% Triton X for 1h followed by an overnight incubation at 4°C with the following primary antibodies: anti-MBP; (1:500-Abcam, cat ab7349); anti-phospho-neurofilament marker (NF) (1:5000-Biolegend cat SMI-31P); anti-NF marker (1:500-Biolegend cat SMI-312); anti-Caspr (1:500-NeuroMab cat 75-001); anti-Opalin (1:500- cat: sc-374490); anti-NG2 (1:300-Merck Millipore cat: AB5320). For Opalin staining, the sections were processed for antigen retrieval procedure before blocking using sodium citrate buffer (10 mM Sodium citrate, 0.05% Tween 20, pH 6.0) for 5 minutes at 95°C temperature. The following day sections were rinsed with 0.01M PBS and incubated with the appropriate fluorescent secondary antibodies (anti-rat, anti-rabbit, or anti-mouse, 1:1000 -Jackson ImmunoResearch, West Grove, PA, USA) for 1h at RT. The sections were then washed three times with 0.01M PBS, mounted on gelatine-coated glass slides, and coverslipped with Dako fluorescence mounting medium (Dako Italia, Italy).

Processing of post-mortem brain tissue, and histochemical methods

Formalin-preserved tissue blocks were immersed in 15% and 30% sucrose solution and washed for three nights at 4°C in 0.1M phosphate buffer (PB), pH 7.4. They were then placed in a freezer at -80°C and quickly frozen in 2-methylbutane. Using a cryostat (Leica), serial sections (30 m) were cut and kept at -20 °C in a solution of 30% ethylene glycol and 25% glycerol until use.

Sudan Black B staining

It is a method used in histology and pathology to identify lipids and neutral glycosphingolipids in tissue sections. As mentioned above brains were dissected and cut into 30 µm sections with a cryostat, and stored at −20°C in a cryoprotective solution containing 30% ethylene glycol and 25% glycerol until use. The sections were processed with the Sudan Black B (SBB) dye (Merck KGaA, Darmstadt, Germania) which allows the visualization of myelin with a high-resolution (Bordeleau et al., 2021). After three 10 minutes of rinses in 0.01M PBS (pH 7.4), sections were mounted on glass slides and immersed into a 0.1% SBB/70% ethanol solution previously filtered, for 10 minutes. After several rinses in 0.01M PBS, sections were coverslipped with a Eukitt® mounting medium (O. Kindler GmbH, Freiburg, Germany).

Images acquisition and analysis

All analyses were carried out by an investigator who was blinded to the animal's genotype or treatment and to the type of plasmids transfection in cells. The immunofluorescence on tissue sections was acquired with a confocal microscope (LSM 900; Zeiss, DE; and Axio Imager.Z2; Zeiss, DE, Germany) equipped with a 20x (0.50 numerical aperture), or 40× oil objective (1.4 numerical aperture) and the pinhole set at 1 Airy unit. For brain section analyses, the layers of the primary somatosensory and visual (S1 and V1) cortices were identified as previously reported (Srubek et al., 2014; Morello et al., 2018). Images for MBP, NF, pNF immunofluorescence staining were acquired using a 20x objective on 7 serial optical sections (0.5 µm Z-step size) from P15 and P56 mice brains. Images were acquired in two corresponding coronal and sagittal sections from at least seven animals per group. For OPCs and OLs staining was acquired using a 40x

objective on 7 serial optical sections (0.5 µm Z-step size) from all cortical layers, and cells were counted manually with Image J. Digital boxes spanning from the pial surface to the corpus callosum were superimposed at matched locations on each section and divided into 10 equally sized sampling areas (bins; layer I: bin 1; layer II/III: bins 2–3; layer IV: bins 4–5; layer V: bins 6–7; layer VI: bins 8–10). Based on this separation of layers from I-VI, supragranular i.e., layer I-III, granular i.e., layer IV, and infragranular i.e., layer V-VI was recognized. The analysis of both integrated density (sum of all the pixels within a selected region) and percentage of area fraction (area covered by fibers in the selection have been highlighted using threshold tool divided by the total area) was performed using dedicated Image J tools. For paranodal and nodal length, the MBP and Caspr immunofluorescence staining was acquired using a 40x objective on 5 serial optical sections (0.5 µm Z-step size) from layer V. The plot intensity profiles of Caspr fluorescence obtained with image J were used to measure the length of paranodes and nodes of Ranvier. Sections processed for Sudan Black B staining were imaged with the Axio Imager.Z2 (Zeiss, DE, Germany) in the brightfield modality equipped with a CDD camera (Axiocam HRc, Carl Zeiss) using a 20x objective (0.50 numerical aperture).

Statistical analysis

All statistical analyses were performed using Prism software (Graphpad, La Jolla, CA, USA). For the analyses, Student's t-test or two-way ANOVA followed by Fisher's LSD post hoc test were performed, as indicated in the text. Significance was set as follows: *$P < 0.05$, **$P < 0.01$, ***$P < 0.001$. The results are expressed as mean ± s.e.m.

4. RESULTS: mGluR5 PAMs rescue cortical and behavioral defects in a mouse model of CDKL5 deficiency disorder (Gurgone et al., 2022)

4.1 Altered mGluR5/Homer1bc organization in the cerebral cortex of *Cdkl5*$^{-/y}$ mice.

We focused on mGluR5 because of their role in mechanisms involved in CDD such as synaptogenesis, dendritic spines formation/maturation, and synaptic plasticity (Ballester-rosado et al., 2016; Chen et al., 2010). Moreover, mGluR5 must interact with Homer1bc, which is downregulated in the cortex of *Cdkl5*$^{-/y}$ mice to exert signaling functions within the PSD (Lupori et al., 2019b; Mazziotti et al., 2017). First, we evaluated the strength of mGluR5-Homer1bc binding in mutant mice. Intriguingly, coimmunoprecipitation (co-IP) assays of cortical synaptosomal fraction (Fig. 15A) revealed that the amount of mGluR5 immunoprecipitated with Homer1bc was significantly reduced in *Cdkl5*$^{-/y}$ mice compared to *Cdkl5*$^{+/y}$ animals (O.D mGluR5/Homer1bc *p < 0.05; Fig. 15B), while the total amount of both Homer1bc and mGluR5 did not change between genotypes (O.D mGluR5/Act and O.D Homer1b/Act p > 0.05; Fig. 15C). We next assessed mGluR5 expression in the neuropil by performing immunofluorescence experiments on S1 cortices from *Cdkl5*$^{-/y}$ and *Cdkl5*$^{+/y}$ mice (Fig. 15D). By using a fixation/staining protocol improved for postsynaptic protein localization (Morello et al., 2018; Pizzo et al., 2016), mGluR5 immunofluorescence (Fig. 15D) resulted in discrete puncta that were found closely localized, but only rarely overlapping, with PSD95^{+} puncta in agreement with previously reported perisynaptic localization of mGluR5 (Lujan and Somogyi, 1996). Interestingly, the density of mGluR5-puncta was strongly reduced in layers II-III and V of S1cortex in *Cdkl5*$^{-/y}$ mice compared to controls (layers II-III and V *p < 0.05; Fig. 15D, E). These data indicate that *Cdkl5* loss interferes with Homer1bc-dependent insertion/stabilization of mGluR5 in the postsynaptic membrane.

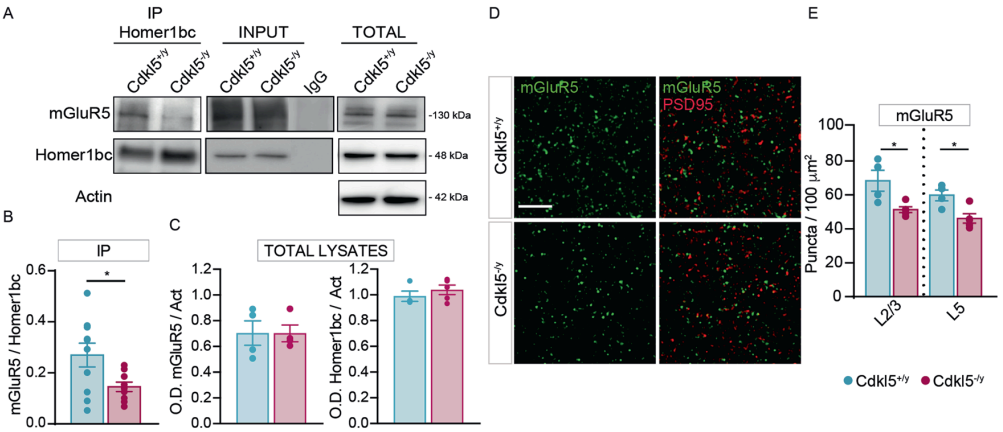

Figure 15: ***CDKL5 loss is responsible for both the disruption of mGluR5-Homer1bc interaction and the reduction of mGluR5 localization in the cortical neuropil.*** ***(A)*** *Co-IP of cortical synaptosomal fraction (P2) from P56 mice by using anti-Homer1bc. IgG: control lane in the absence of antibodies. Immunoprecipitates, inputs (P2), and total cortical lysates were analyzed by immunoblotting for mGluR5 and Homer1bc. Bar graphs showing* ***(B)*** *Co-IP and* ***(C)*** *total cortical lysates quantitation expressed as optical density (O.D.).* ***(D)*** *Confocal microscopy images showing mGluR5^{+} (green) and PSD-95^{+} (red) immunopuncta in layers II/III of S1 cortex (scale bar: 5 µm).* ***(E)*** *Bar graphs displaying the density of mGluR5^{+} puncta. Student T test *p < 0.05 (Co-IP: n = 8; WB: n = 4 IFL: n = 4). Image taken from* (Gurgone et al., 2022)

4.2 Excitatory neurotransmission and mGluR5-mediated signaling are severely disrupted in *Cdkl5*$^{-/y}$ cortical neurons.

Our data suggest that the mGluR5 function might be compromised in the absence of *Cdkl5* (Aloisi et al., n.d.; Kammermeier and Worley, 2007). To test this idea, we recorded spontaneous miniature excitatory postsynaptic currents (mEPSCs) in neuronal cultures of the S1 cortex from both *Cdkl5*$^{+/y}$ and *Cdkl5*$^{-/y}$ mice (Fig. 16A–D, upper part), before and after mGluR5 activation. As we reported previously in acute cortical slices (Della Sala et al., 2016), mEPSCs recorded from *Cdkl5*-null neurons showed an increased inter-event interval (IEI) (*Cdkl5*$^{+/y}$ vs *Cdkl5*$^{-/y}$ *p < 0.05; Fig. 16D) while the mean peak amplitude was similar between genotypes (*Cdkl5*$^{+/y}$ vs *Cdkl5*$^{-/y}$ p > 0.05; Fig. 16C). Intriguingly, 2-minutes stimulation with the selective mGluR5 agonist DHPG (100 µM) produced a significant increase in the IEI of mEPSCs in *Cdkl5*$^{+/y}$ cultures (Moult et al., 2006; Verpelli et al., 2011) but not in *Cdkl5*$^{-/y}$ neurons (Fig. 16E). Next, we tested NMDA-mediated responses because these receptors activity can be modulated by mGluR5 [36]. When NMDA currents were elicited by the application of NMDA (50 µM) (Marcantoni et al., 2020), *Cdkl5*$^{-/y}$ cultures showed a significant reduction of I_{NMDA} compared to *Cdkl5*$^{+/y}$ neurons (*Cdkl5*$^{+/y}$ vs *Cdkl5*$^{-/y}$ **p < 0.01; Fig. 16F). Intriguingly, the application of NMDA together

with DHPG (100 μm) increased I_{NMDA} in *Cdkl5*$^{+/y}$ cells, (Fig. 16G) while it produced a small decrease in *Cdkl5*$^{-/y}$ neurons, as illustrated by the sharp difference in the percentage of I_{NMDA} variation between genotypes (DHPG-*Cdkl5*$^{+/y}$ vs DHPG-*Cdkl5*$^{-/y}$ *p < 0.05; Fig. 16G). Strikingly, while 73% of *Cdkl5*$^{+/y}$ cortical neurons (11/15 cells) showed potentiated I_{NMDA} after the application of DHPG, most of *Cdkl5*$^{-/y}$ neurons did not respond to DHPG (10/14; 71%) as shown by plotted data (Fig. 16H). These results disclose that loss of *Cdkl5* disrupts excitatory neurotransmission at multiple sites and severely affects mGluR5 normal function.

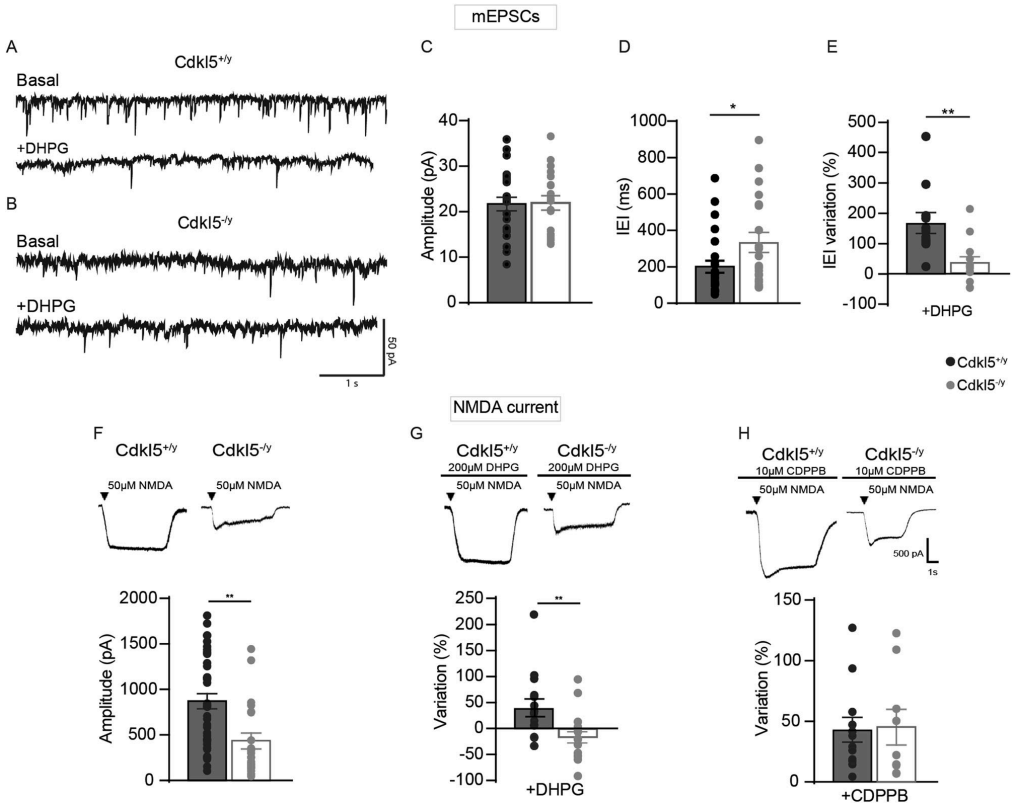

Figure 16: ***Cdkl5 loss tampers with both mEPSCs and NMDA current.*** ***(A)*** *Sample traces of miniature excitatory postsynaptic current (mEPSC) recorded from Cdkl5*$^{+/y}$ *neurons (**A**, upper part) and Cdkl5*$^{-/y}$ *neurons (**B**, upper part) and after the application of DHPG (**A, B** lower part). Bar graphs showing the mean average amplitude **(C)** and the inter-event interval (IEI) of mEPSCs **(D)**. **(E)** Bar graphs displaying the % of IEI variation IEI after the application of DHPG (100 μM). **(F)** Representative traces of currents obtained with patch-clamp recordings on S1 neurons cultures from Cdkl5*$^{+/y}$ *and Cdkl5*$^{-/y}$ *embryos after NMDA (50 μM) application (upper part), bar graphs showing differences of* I_{NMDA} *current between genotypes (lower part). **(G)** Representative traces of NMDA currents on S1 neurons after 2-min application of DHPG (100 μM-upper part); bar graphs showing the % change of* I_{NMDA} *after the application of DHPG (lower part). **(H)** Representative traces of NMDA after 2-min CDPPB + NMDA application (upper part), bar graphs showing the % change of* I_{NMDA} *current after the application of CDPPB (lower part). Student's t-test, chi-square, two-way ANOVA followed by Fisher's multiple comparison test, *p < 0.05, **p < 0.01, ***p < 0.001 (mEPSC Cdkl5*$^{+/y}$ *n = 22 cells, Cdkl5*$^{-/y}$ *n = 28; minis+DHPG*

Cdkl5$^{+/y}$: n = 12 cells; minis+DHPG Cdkl5$^{-/y}$: n = 13 cells. NMDA: Cdkl5$^{+/y}$ n = 36 cells, Cdkl5$^{-/y}$ n = 23 cells; NMDA + DHPG Cdkl5$^{+/y}$ n = 15 cells and NMDA + DHPG Cdkl5$^{-/y}$ n = 14 cells; NMDA + CDPPB Cdkl5$^{+/y}$ n = 12 cells; NMDA + CDPPB Cdkl5$^{-/y}$ n = 9 cells). Image taken from (Gurgone et al., 2022)

4.3 CDPPB potentiates NMDAR current in cortical neurons lacking *Cdkl5*.

We and others have previously shown that in conditions where I_{NMDA} is not sensitive to DHPG, the application of selective mGluR5 PAMs can instead elicit the strengthening of this current (Auerbach et al., 2011; Vicidomini et al., 2017). Among these, 3-Cyano-N-(1,3-diphenyl-1H-pyrazol-5-yl) benzamide (CDPPB) offers several advantages compared to agonist drugs such as higher subtype selectivity, reduced desensitization, and more subtle modulatory effects on receptor function. Thus, we examined the effect produced by CDPPB on cortical neurons by measuring NMDA current. Intriguingly, 2 min bath application of CDPPB (10 μM) preceding NMDA (50 μM) administration produced a comparable increase of I_{NMDA} (Fig. 15F, lower part) in both genotypes (CDPPB-*Cdkl5$^{+/y}$* vs CDPPB-*Cdkl5$^{-/y}$* $p > 0.05$; Fig. 15H) when compared to the average amplitude of I_{NMDA} measured after administration of NMDA alone. Consistently, in the case of CDPPB application, the majority of both *Cdkl5$^{-/y}$* and *Cdkl5$^{+/y}$* neurons showed potentiated I_{NMDA} (*Cdkl5$^{+/y}$*: 13/18, 78%; *Cdkl5$^{-/y}$* 10/12, 83%) resulting in a significant increase compared to DHPG-treated *Cdkl5$^{-/y}$* neurons (chi-square DHPG-*Cdkl5$^{-/y}$*: 29% vs CDPPB-*Cdkl5$^{-/y}$*: 83% ****$p < 0.0001$). These results show that positive allosteric modulation can rescue mGluR5-dependent strengthening of NMDA-mediated activation in *Cdkl5$^{-/y}$* neurons.

4.4 CDPPB treatment ameliorates visual, sensorimotor and memory functions in *Cdkl5$^{-/y}$* mice.

Encouraged by the positive effects we obtained on synaptic currents, we evaluated the therapeutic potential of CDPPB by treating mice with one intraperitoneal injection (i.p.) of CDPPB (3 mg/Kg), as in (Vicidomini et al., 2017), that were subsequently exposed to a battery of tests. We investigated cortical visual responses by transcranial intrinsic optical signal (IOS) imaging before and after CDPPB administration in the same animals. As expected from our previous data (Lupori et al., 2019b; Mazziotti et al., 2017), the baseline response amplitude of *Cdkl5$^{-/y}$* mice was strongly decreased compared to *Cdkl5$^{+/y}$*

littermates (*Cdkl5*$^{+/y}$ vs vehicle-*Cdkl5*$^{-/y}$ / CDPPB-*Cdkl5*$^{-/y}$ **p < 0.01, Fig. 17A, B). After CDPPB treatment, visual responses approached *Cdkl5*$^{+/y}$ levels (*Cdkl5*$^{+/y}$ vs CDPPB-*Cdkl5*$^{-/y}$ post-injection p = 0.6; *Cdkl5*$^{+/y}$ vs vehicle-*Cdkl5*$^{-/y}$ post-injection *p < 0.05) significantly increasing from their baseline values (vehicle-*Cdkl5*$^{-/y}$ post-injection vs CDPPB-*Cdkl5*$^{-/y}$ post-injection *p < 0.05; CDPPB-*Cdkl5*$^{-/y}$ baseline vs CDPPB-*Cdkl5*$^{-/y}$ post-injection *p < 0.05; vehicle-*Cdkl5*$^{-/y}$ baseline vs vehicle-*Cdkl5*$^{-/y}$ post-injection p = 0.90). By contrast, visual response remained impaired in vehicle-treated mutants. These experiments indicate that cortical response to visual stimulation is ameliorated by CDPPB treatment in *Cdkl5*$^{-/y}$ mice. When assessed for sensorimotor responses in the adhesive tape-removal test, *Cdkl5*$^{-/y}$ mice displayed a significant increase in time-to-contact the tape compared to *Cdkl5*$^{+/y}$ mice (vehicle-*Cdkl5*$^{+/y}$ vs vehicle-*Cdkl5*$^{-/y}$ **p < 0.01; Fig. 17C). Importantly, a single CDPPB injection produced a reduction of the latency exclusively in mutant mice whose performance became similar to controls (vehicle-*Cdkl5*$^{+/y}$ vs CDPPB-*Cdkl5*$^{-/y}$ p> 0.4; Fig. 17C). Moreover, the number of correct spontaneous alternations in the Y-maze paradigm for working memory was decreased in *Cdkl5*$^{-/y}$ mice compared to *Cdkl5*$^{+/y}$ animals (vehicle-*Cdkl5*$^{+/y}$ vs vehicle-*Cdkl5*$^{-/y}$ **p < 0.01; Fig. 17D), confirming previous observations (Fuchs et al., 2014b). Intriguingly, working memory was rescued in *Cdkl5*$^{-/y}$ mice by CDPPB (vehicle-*Cdkl5*$^{+/y}$ vs CDPPB-*Cdkl5*$^{-/y}$ p > 0.4; Fig. 17D), while it did not affect memory in *Cdkl5*$^{+/y}$ mice. Also, total number of arms entries did not change between genotypes under either treated or untreated conditions (Fig. 17E). To assess locomotor activity, we used the open field test. As previously reported (Terzic et al., 2021), *Cdkl5*$^{-/y}$ mice showed an increase in both total distance traveled (vehicle-*Cdkl5*$^{+/y}$ vs vehicle-*Cdkl5*$^{-/y}$ *p < 0.05; Fig. 17F) and speed (vehicle-*Cdkl5*$^{+/y}$ vs vehicle-*Cdkl5*$^{-/y}$ *p < 0.05; Fig. 17G) that was not changed by CDPPB treatment (vehicle-*Cdkl5*$^{-/y}$ vs CDPPB-*Cdkl5*$^{-/y}$ p > 0.4; Fig. 17F, G). These data indicate that the action of CDPPB can reverse atypical visual cortical response, sensorimotor and short-term memory impairments in *Cdkl5*$^{-/y}$ mice, but not locomotor activity.

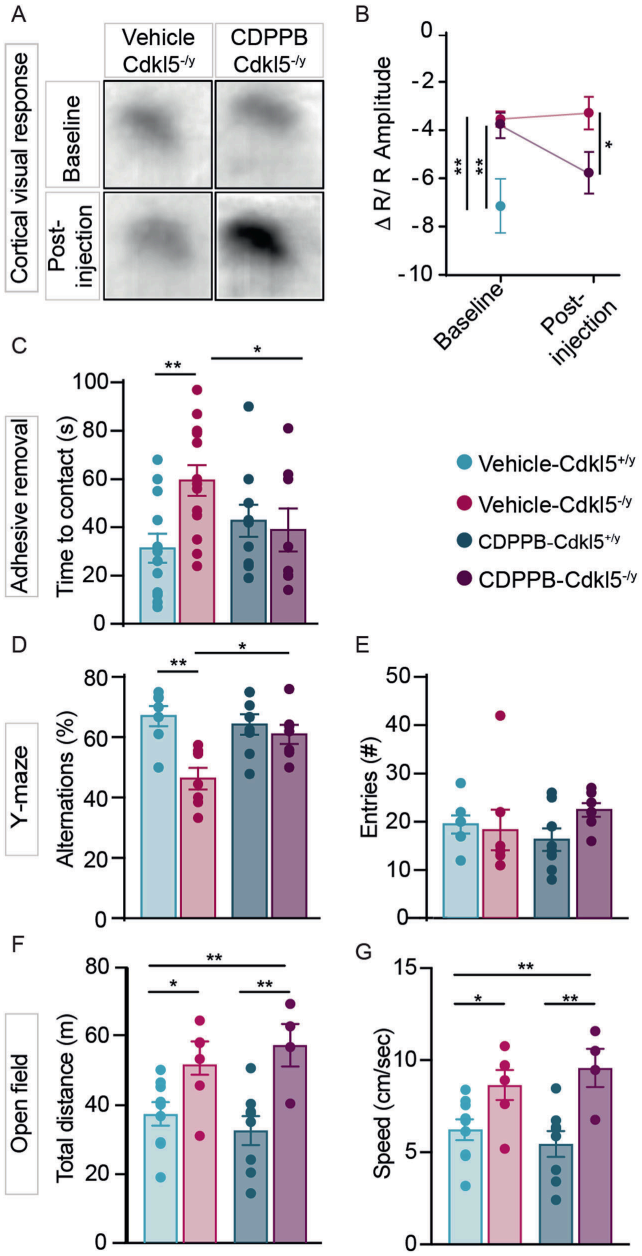

Figure 17: ***Acute CDPPB treatment rescues visual response, sensorimotor and memory deficits in Cdkl5$^{-/y}$ mice. (A)*** *Samples images showing differences of IOS evoked responses in vehicle- and CDPPB-treated Cdkl5$^{-/y}$ mice.* ***(B)*** *Trajectory of the IOS amplitude in vehicle-Cdkl5$^{+/y}$, vehicle-Cdkl5$^{-/y}$ and CDPPB-Cdkl5$^{-/y}$ treated mice.* ***(C)*** *Bar graphs showing contact latency with the tape placed under mice's forepaws. Bar graphs showing the percentage of the correct alternations* ***(D)*** *and the number of entries* ***(E)*** *made by Cdkl5$^{+/y}$ and Cdkl5$^{-/y}$ mice, treated with either vehicle or CDPPB, in the Y-maze. Bar graphs showing the total distance traveled* ***(F)*** *and the mean speed* ***(G)*** *in the open field arena of mice treated with either vehicle or CDPPB. One-way ANOVA followed by Tukey's multiple comparison; two-way ANOVA followed by Sidak or Bonferroni's multiple comparison test, *p< 0.05, **p< 0.01 (IOS: vehicle-Cdkl5$^{+/y}$ n = 3, vehicle-Cdkl5$^{-/y}$ n = 8, CDPPB-Cdkl5$^{-/y}$ n = 6; behavioural tests: vehicle-Cdkl5$^{+/y}$ n = 12, vehicle-Cdkl5$^{-/y}$ n = 13, CDPPB-Cdkl5$^{+/y}$ n = 8, CDPPB-Cdkl5$^{-/y}$ n = 7). Image taken from* (Gurgone et al., 2022)

4.5 mGluR5 PAMs rescue both synaptic and activity defects in *Cdkl5*$^{-/y}$ cerebral cortex.

In parallel with the observed behavioral and functional rescues, acute CDPPB treatment normalized both the number and organization of postsynaptic sites as well as neuronal activity in primary cortices of *Cdkl5*$^{-/y}$ mice. CDPPB increased the density of Homer1bc^{+} puncta in both S1 and V1 cortices of *Cdkl5*$^{-/y}$ mice (S1: layers II-III and V vehicle-*Cdkl5*$^{-/y}$ vs CDPPB-*Cdkl5*$^{-/y}$ **p < 0.01. V1: layers II-III and V vehicle-*Cdkl5*$^{-/y}$ vs CDPPB-*Cdkl5*$^{-/y}$ *p < 0.05; Fig. 18A, B), reproducing *Cdkl5*$^{+/y}$ mice conditions (S1 and V1: layers II-III and V: vehicle-*Cdkl5*$^{+/y}$ vs CDPPB-*Cdkl5*$^{-/y}$ p > 0.3; Fig. 18A, B). Intriguingly, CDPPB treatment also normalized mGluR5^{+} puncta density in both S1 and V1 cortices of *Cdkl5*$^{-/y}$ mice (S1: layers II-III and V: vehicle-*Cdkl5*$^{-/y}$ vs CDPPB-*Cdkl5*$^{-/y}$ ***p < 0.001; vehicle-*Cdkl5*$^{+/y}$ vs CDPPB-*Cdkl5*$^{-/y}$ p > 0.3. V1: layers II-III and V: vehicle-*Cdkl5*$^{-/y}$ vs CDPPB-Cdkl5$^{-/y}$ *p < 0.05. S1 and V1: vehicle-Cdkl5$^{+/y}$ vs CDPPB-Cdkl5$^{-/y}$ p > 0.3; Fig. 18C, D). Finally, the density of cells expressing ARC, an immediate-early gene (IEG) induced by mGluR5 activation (Me, 2012; Wang and Zhuo, 2012), was restored in the V1 cortex of *Cdkl5*-mutants after a single CDPPB administration (layers I-VI: vehicle-*Cdkl5*$^{+/y}$ vs vehicle-*Cdkl5*$^{-/y}$ **p < 0.01; vehicle-*Cdkl5*$^{-/y}$ vs CDPPB-*Cdkl5*$^{-/y}$ ***p < 0.001; Fig. 18E, F).

To increase the reproducibility of our study, we treated another group of *Cdkl5*$^{-/y}$ and *Cdkl5*$^{+/y}$ animals with a different mGluR5 PAM, the RO6807794 (RO68) compound (Kelly et al., 2018). Two hours after an i.p. injection with RO68 (0.3 mg/kg as in (Me, 2012)), the density of Homer1bc^{+} puncta in the S1 cortex of *Cdkl5*$^{-/y}$ mice was increased (S1: layers II-III and V vehicle-*Cdkl5*$^{-/y}$ vs CDPPB-*Cdkl5*$^{-/y}$ *p < 0.05. V1: layers II-III and V vehicle-*Cdkl5*$^{-/y}$ vs CDPPB-*Cdkl5*$^{-/y}$ *p < 0.05; Fig. 19A, B) reproducing *Cdkl5*$^{+/y}$ mice conditions (S1 layers II-III and V: vehicle-*Cdkl5*$^{+/y}$ vs CDPPB-*Cdkl5*$^{-/y}$ p > 0.3; Fig. 19A, B). Intriguingly, RO68 was also able to restore neuronal activity in S1 cortex in *Cdkl5*$^{-/y}$ mice (Fig. 19C) throughout cortical layers (vehicle-*Cdkl5*$^{+/y}$ vs vehicle-*Cdkl5*$^{-/y}$ ***p < 0.001; vehicle-*Cdkl5*$^{-/y}$ vs RO68-*Cdkl5*$^{-/y}$ ***p < 0.001), as indicated by c-Fos^{+} cell density (Fig. 19D; see also (Pizzo et al., 2016)), that reached the magnitude of *Cdkl5*$^{+/y}$ mice (vehicle-*Cdkl5*$^{+/y}$ vs CDPPB-*Cdkl5*$^{-/y}$ p > 0.05). These results strongly support the idea that the atypical circuit organization,

both structural and molecular, shown by the cerebral cortex of *Cdkl5*$^{-/y}$ mice can be rescued by activating mGluR5-mediated signaling.

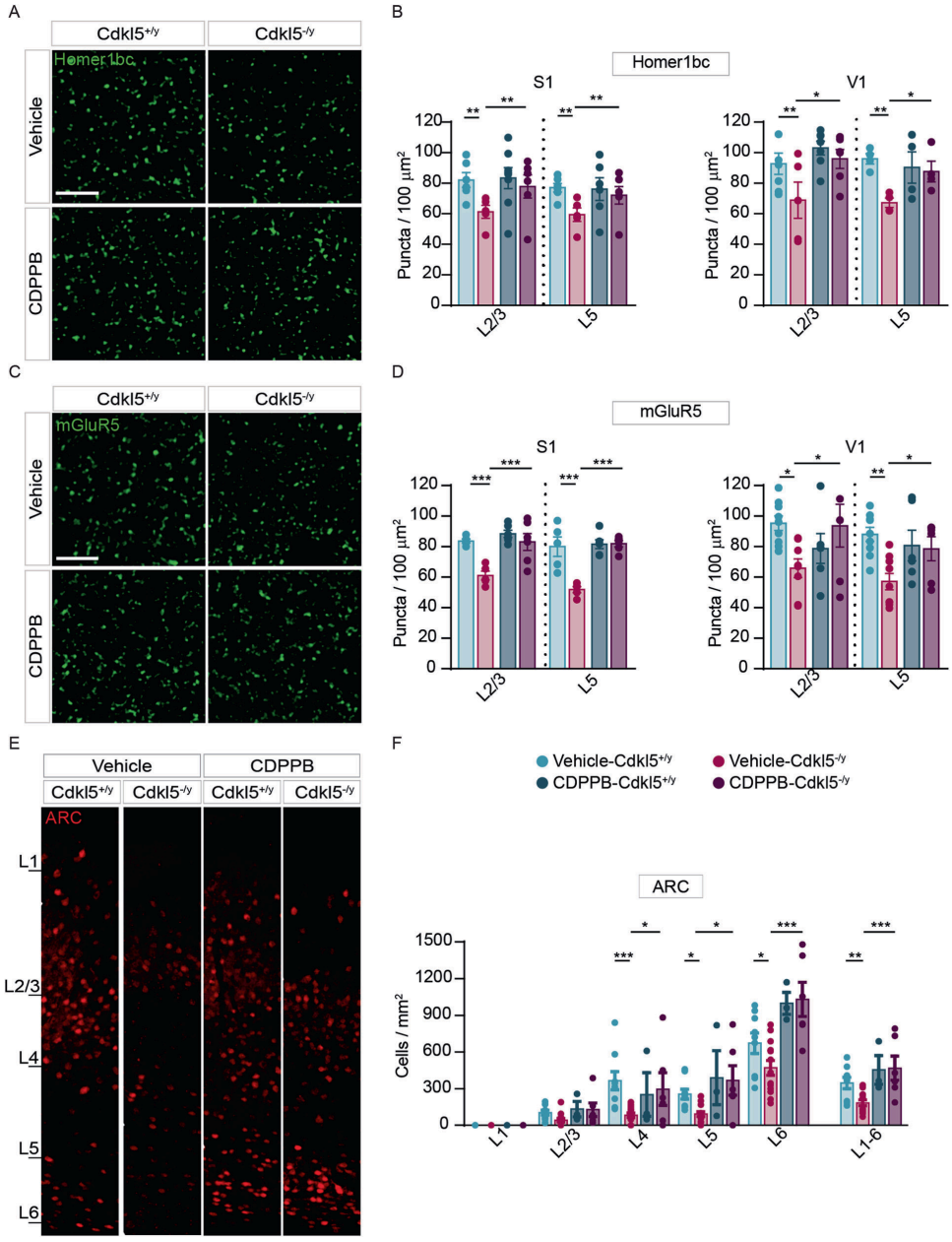

Figure 18: ***Structural defects exhibited by Cdkl5$^{-/y}$ mice cortices are rescued by an acute CDPPB injection.*** *Representative confocal images showing Homer1bc^{+}* ***(A)*** *and mGluR5^{+}* ***(C)*** *puncta in layer II-III of S1 cortex from either vehicle- or CDPPB-treated mice (scale bar: 5 µm). Bar graphs showing both Homer1bc^{+}* ***(B)*** *and mGluR5^{+}* ***(D)*** *immunopuncta density in layers II-III and V of both S1 and V1 cortices in either vehicle or CDPPB-treated mice.* ***(E)*** *Confocal images of ARC immunostaining on coronal sections of the V1 cortex from mice treated with vehicle or CDPPB (scale bar: 25 µm), and* ***(F)*** *relative ARC^{+} cells density quantitation throughout the cortical layers. Two-way ANOVA followed by Fisher's multiple comparison test, *p < 0.05, **p < 0.01, ***p < 0.001; (n = 6 animals per genotype). Image taken from* (Gurgone et al., 2022)

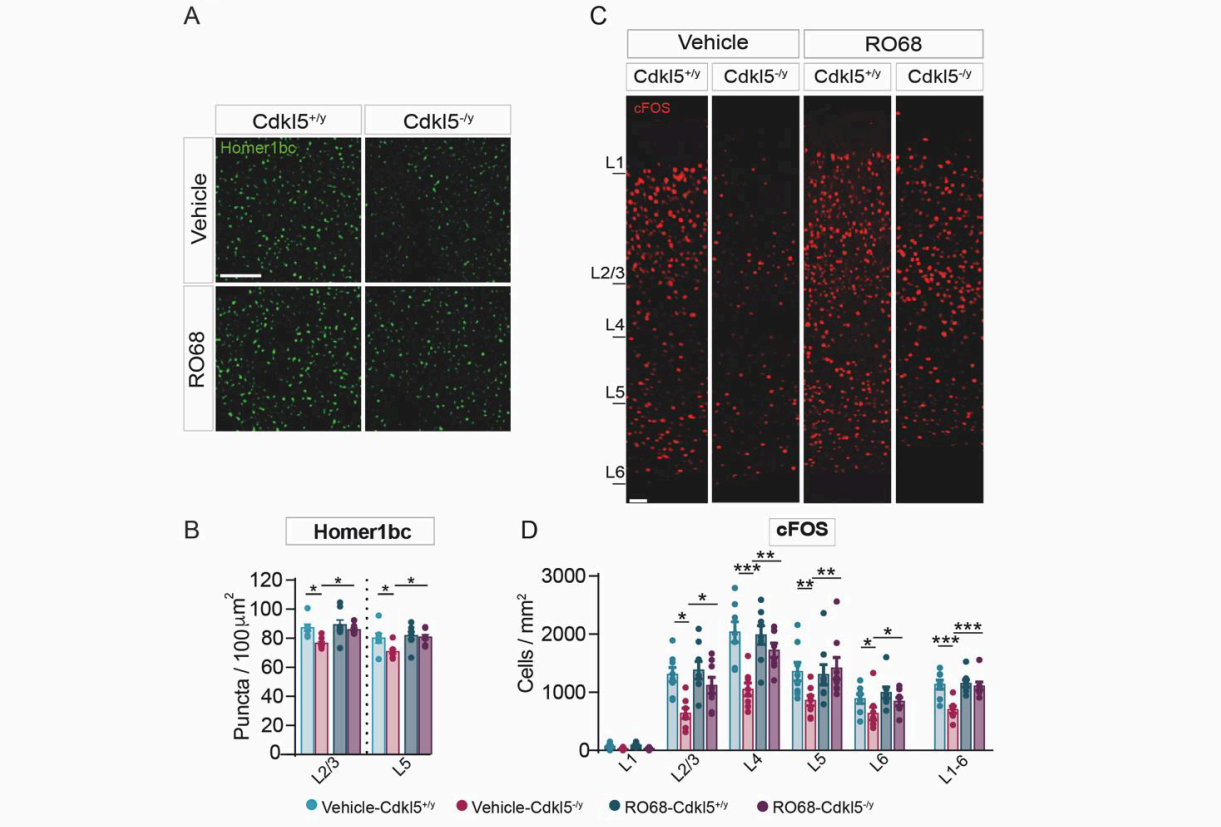

Figure 19: ***Acute administration of RO6807794 (RO68) rescues the morpho-functional defects shown by Cdkl5$^{-/y}$ mice. (A)*** *Representative confocal images showing Homer1bc^{+} puncta in layer II-III of S1 cortex from either vehicle- or RO68-treated Cdkl5$^{+/y}$ and Cdkl5$^{-/y}$ mice (scale bar: 5 µm).* ***(B)*** *Bar graphs showing differences between genotypes in Homer1bc^{+} immunopuncta density counted from layers II-III and V of S1 cortices in either vehicle- or RO68-treated mice.* ***(C)*** *Confocal images of c-FOS^{+} immunostaining in sections of the S1 cortex from Cdkl5$^{+/y}$ and Cdkl5$^{-/y}$ mice, treated with vehicle or RO68 (scale bar: 50 µm), and* ***(D)*** *relative cFOS^{+} cells density quantitation throughout layers of V1 cortex. Two-way ANOVA followed by Fisher's multiple comparison test, *p < 0.05, ** p < 0.01, *** p < 0.001; (n = 8 animals per genotype). Image taken from* (Gurgone et al., 2022)

4.6 A protracted treatment with CDPPB effectively restores *Cdkl5*$^{-/y}$ mice deficits.

To assess the therapeutic potential of mGluR5 activation, we treated animals for five consecutive days with CDPPB that 24h as shown in Fig. 20A after the last injection were behaviourally tested and then sacrificed for brain analyses. The density of Homer1bc^{+} puncta was restored in both upper and deeper layers of the S1 cortex in treated mutant mice (layers II-III and V: vehicle-*Cdkl5*$^{-/y}$ vs CDPPB-*Cdkl5*$^{-/y}$ **p < 0.01; Fig. 20B, C), while protracted CDPPB had no effect on Homer1bc expression in *Cdkl5*$^{+/y}$ animals (layers II-III and V: vehicle-*Cdkl5*$^{+/y}$ vs CDPPB-*Cdkl5*$^{+/y}$ p =0.9; Fig. 20B, C). Next, we analyzed hind-limb clasping, a sign displayed by *Cdkl5*$^{-/y}$ mice (Wang and Zhuo, 2012). In line with previous

studies, vehicle-treated mutants showed increased hindlimb clasping compared to controls (vehicle-*Cdkl5*$^{+/y}$ vs vehicle- *Cdkl5*$^{-/y}$ ***p < 0.001; Fig. 20D and [12]) whereas after CDPPB treatment *Cdkl5*$^{-/y}$ mice spent significantly less time clasping their hind paws (vehicle-*Cdkl5*$^{-/y}$ vs CDPPB-*Cdkl5*$^{-/y}$ **p < 0.01; Fig. 20D). Moreover, the differences shown by the two genotypes in the adhesive tape-removal test were abolished by 5-days CDPPB treatment (vehicle-*Cdkl5*$^{+/y}$ vs. CDPPB-*Cdkl5*$^{-/y}$ p > 0.7; Fig. 20E). Intriguingly, the visual response was also significantly improved after the prolonged CDPPB treatment. While the baseline response amplitude was strongly reduced in *Cdkl5*$^{-/y}$ mice compared to *Cdkl5*$^{+/y}$ littermates (*Cdkl5*$^{+/y}$ vs vehicle-*Cdkl5*$^{-/y}$ **p < 0.01; *Cdkl5*$^{+/y}$ vs CDPPB-*Cdkl5*$^{-/y}$ *p < 0.05, fig 20F, G), no differences were shown by the two *Cdkl5*$^{-/y}$ groups (vehicle-*Cdkl5*$^{-/y}$ vs pre-CDPPB-*Cdkl5*$^{-/y}$ p > 0.3; Fig. 20F). After CDPPB treatment, mutants showed robust changes in response amplitude (pre-CDPPB-*Cdkl5*$^{-/y}$ vs post- CDPPB-*Cdkl5*$^{-/y}$ **p < 0.01) highlighting a substantial effect of treatment during time. Importantly, after CDPPB-treatment, *Cdkl5*$^{-/y}$ mice reached amplitude values significantly different from vehicle-treated mutants (CDPPB-*Cdkl5*$^{-/y}$ vs vehicle-*Cdkl5*$^{-/y}$ postinjection **p < 0.01). Finally, we evaluated the effects of sub-chronic CDPPB treatment on cortical activation assessing both c-Fos and ARC expression. Intriguingly, the reduction of IEGs expression shown by mutant mice (c-FOS: vehicle-*Cdkl5*$^{+/y}$ vs vehicle-*Cdkl5*$^{-/y}$ **p < 0.01 Fig. 20H, I; ARC: vehicle-*Cdkl5*$^{+/y}$ vs vehicle-*Cdkl5*$^{-/y}$ **p < 0.01; Fig. 20J, K) was abolished by the treatment (c-FOS and ARC vehicle-*Cdkl5*$^{+/y}$ vs CDPPB-*Cdkl5*$^{-/y}$ p > 0.05; Fig. 20I, K).

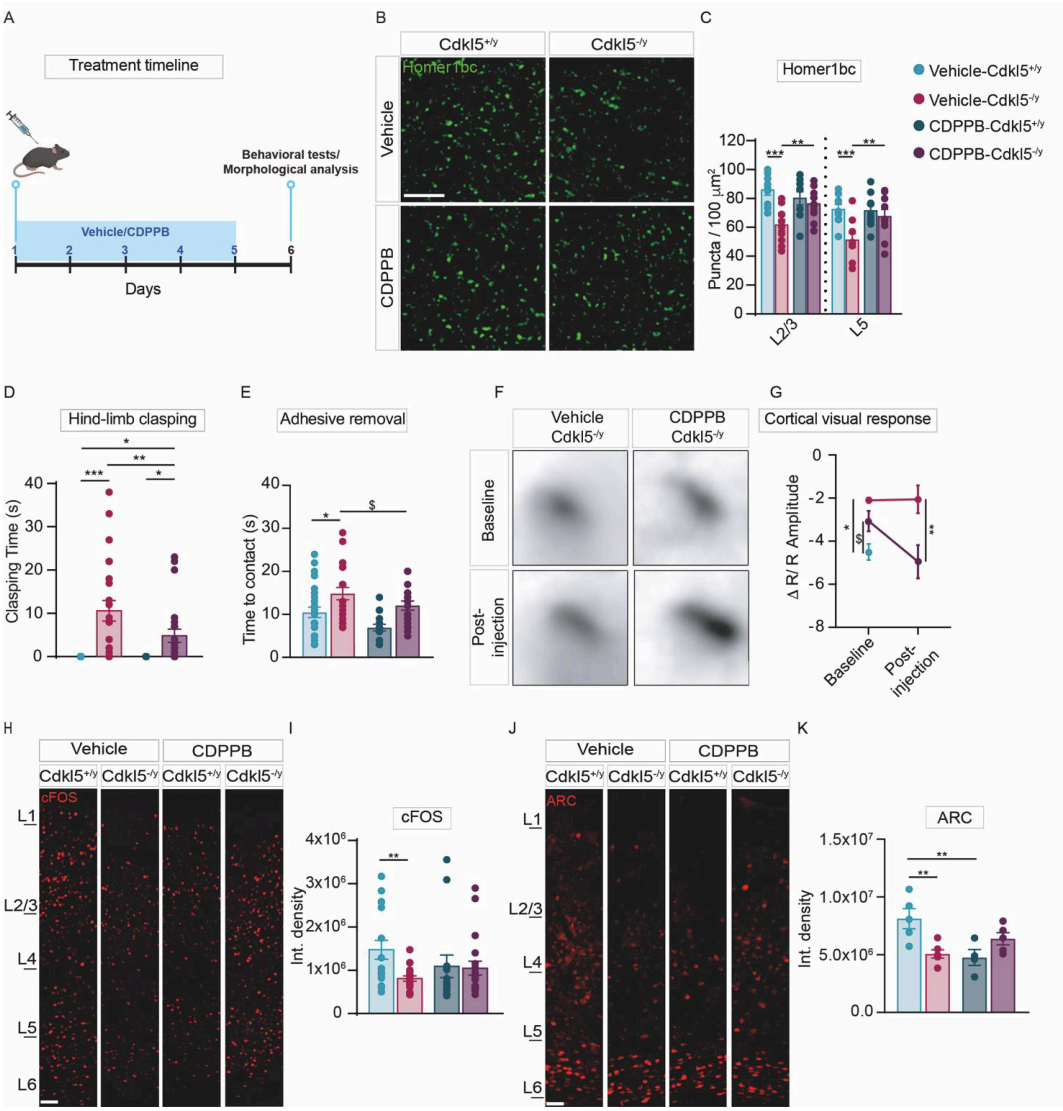

Figure 20: ***Subchronic treatment with CDPPB restores morphofunctional defects in Cdkl5$^{-/y}$ mice.*** ***(A)*** *Schematic illustration of the experimental timeline for the 5-day CDPPB treatment.* ***(B)*** *Representative confocal images of Homer1bc^{+} (green) immunofluorescence in layers II-III of the S1 cortex.* ***(C)*** *Bar graphs showing Homer1bc^{+} puncta density in layers II-III and V of the S1 cortex of either vehicle- or CDPPB-treated mice.* ***(D)*** *Bar graphs showing time spent clasping in vehicle-treated and CDPPB-treated mice.* ***(E)*** *Bar graphs showing latencies to touch the tape of the different animal groups.* ***(F)*** *Samples images showing differences of IOS evoked responses in vehicle-treated and CDPPB-treated Cdkl5$^{-/y}$ mice.* ***(G)*** *Trajectory of the IOS amplitude in vehicle-Cdkl5$^{+/y}$, vehicle-Cdkl5$^{-/y}$ and CDPPB-Cdkl5$^{-/y}$ treated mice. Representative images of c-Fos and* ***(H)*** *ARC* ***(J)*** *immunoreactive cells in S1 of vehicle- and CDPPB-treated mice (scale bar 50 µm). Bar graphs showing the integrated density analysis of c-Fos* ***(I)*** *and ARC* ***(K)*** *immunofluorescence in the S1 of vehicle- or CDPPB-treated mice. One-way ANOVA followed by Tukey multiple comparison; two-way ANOVA followed by Sidak or Fisher's LSD: * $p < 0.05$, ** $p < 0.01$, *** $p < 0.001$; $ $p = 0.05$ (Homer1bc^{+} puncta: $n = 9$ for each group; clasping and c-Fos vehicle-Cdkl5$^{+/y}$ $n = 34$, vehicle-Cdkl5$^{-/y}$ $n = 23$, CDPPBCdkl5$^{+/y}$ $n = 17$, CDPPB-Cdkl5$^{-/y}$ $n = 23$; adhesive tape-test vehicle-Cdkl5$^{+/y}$ $n = 27$, vehicle-Cdkl5$^{-/y}$ $n = 21$, CDPPB-Cdkl5$^{+/y}$ $n = 17$, CDPPB-Cdkl5$^{-/y}$ $n = 19$; IOS: vehicle-Cdkl5$^{+/y}$ $n = 5$, vehicle-Cdkl5$^{-/y}$ $n = 3$, CDPPB-Cdkl5$^{-/y}$ $n = 5$; ARC vehicle-Cdkl5$^{+/y}$ $n = 6$, vehicle-Cdkl5$^{-/y}$ $n = 6$, CDPPB-Cdkl5$^{+/y}$ $n = 4$ CDPPB-Cdkl5$^{-/y}$ $n = 5$). Image taken from* (Gurgone et al., 2022)

4.7 The BA17 cortex of CDD patients recapitulates the synaptic defects shown by *Cdkl5*$^{-/y}$ mice.

To assess the translational potential of our findings, we examined excitatory synaptic structures in the 2 postmortem CDD patient brains available worldwide that were obtained from the Harvard Brain Tissue Resource Center (Belmont; USA). These experiments were performed on sections from the primary visual cortex (BA17) of CDD cases and age/sex-matched neurotypical controls. Intriguingly, the results showed a clear reduction of both postsynaptic proteins PSD-95^{+} and Homer1bc^{+} as well as of the presynaptic marker VGluT1^{+}, irrespective of case age (5 and 30 years old), compared to NTs (Fig. 21A). Moreover, although a statistical comparison was not performed with only 2 cases, the analysis of immunopuncta revealed a reduction in the cortices of CDD patients with respect to controls (Fig. 21A–D), indicative of an overall reduction of glutamatergic synapses. We next evaluated Homer1bc, PSD-95, and mGluR5 expression by western blotting on BA17 cortical lysates. Intriguingly, as shown in Fig. 21E–H, the BA17 area from CDD samples showed a robust reduction of their expression compared to controls. Although derived from a limited dataset, these results suggest that both structural and molecular signatures of *Cdkl5* loss in the cerebral cortex largely overlap between mice and humans and support the translational potential of a mGluR5-directed therapeutic strategy.

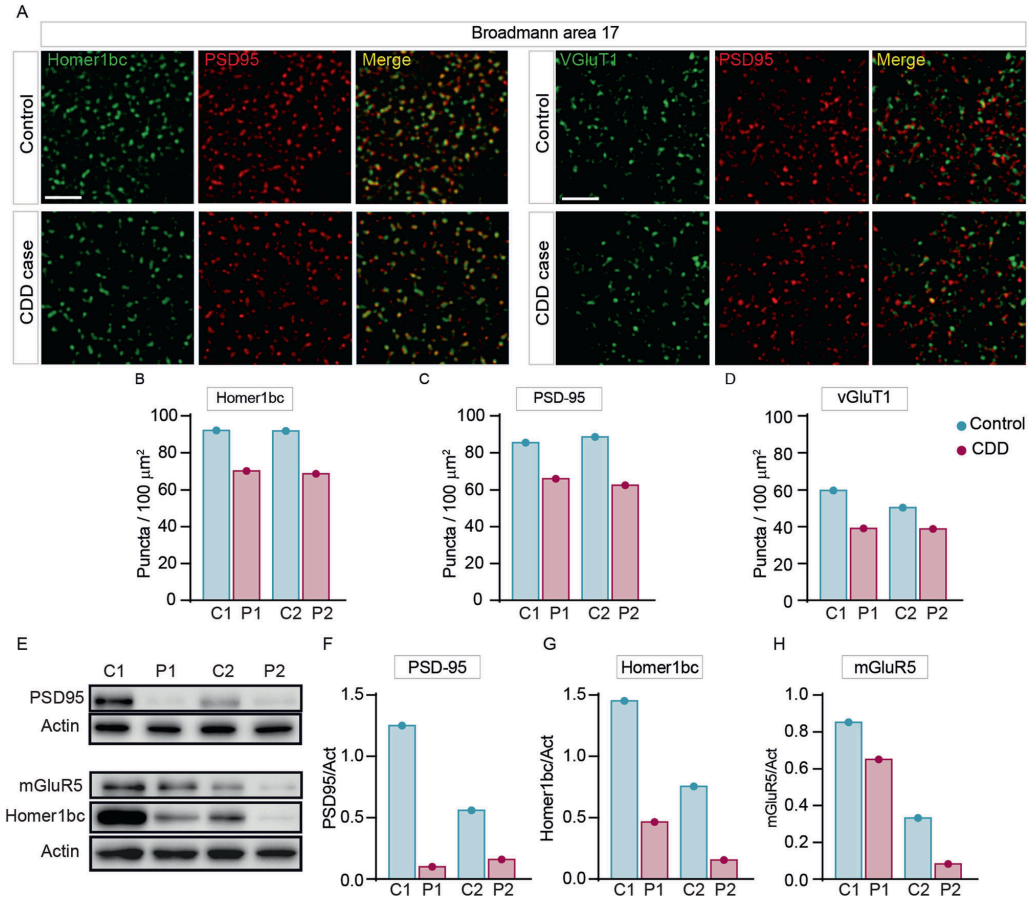

Figure 21: ***Aberrant expression of excitatory synaptic proteins in the BA17 cortex of CDD patients***. ***(A)*** *Illustrative confocal images taken from layers II-III of the BA17 cortex. PSD-95^{+}(red), Homer1bc^{+}(green), VGluT1^{+}(green) immunofluorescence puncta. Note the virtually complete overlapping of PSD-95 and Homer1bc immunofluorescence (scale bar: 5 µm).* ***(B–D)*** *Bar graphs showing the analysis of puncta density in layers II-III of BA17 cortices.* ***(E)*** *Western blotting showing the expression of PSD-95, Homer1bc and mGluR5 in lysates from BA17 cortices. Bar graphs displaying the optical density (O.D.) analysis of PSD-95* ***(F)****, Homer1bc* ***(G)*** *and mGluR5* ***(H)*** *expression. Student's t-test, *p < 0.05, **p < 0.01 (C1 = F, 4 years old; P1 = F, 5.7 years old; C2 = F, 29 years old; P2 = F, 30 years old). Image taken from* (Gurgone et al., 2022)

5 RESULTS: Investigating the impact of CDKL5 on grey matter myelination through mouse models analysis

5.1 Expression of CDKL5 in MACs isolated OPCs.

It is reported that *Cdkl5* is expressed not only in neurons but also in both OPCs and OLs (Ye Zhang et al., 2014; Zhang et al., 2016). However, the expression of CDKL5 protein in this glial cell lineage has not been previously assessed. Thus, to investigate this, I first isolated these cells by using the magnetic-activated cell sorting technique from the whole brain of P10 mice, and then I used these cell lysates to explore the expression of CDKL5 by western blotting. As shown in Fig. 22, CDKL5 is expressed in OPCs extract from *Cdkl5*$^{+/y}$ mice, although at a lower level than in the whole cortex. This experiment shows for the first time, to the best of my knowledge, that CDKL5 is expressed in OPCs. These findings encouraged us to explore the function of this protein in the development and maturation of OPCs, and in white matter organization.

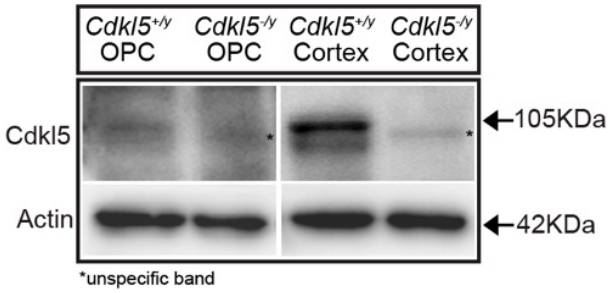

Figure 22: ***Expression of* CDKL5 *protein in the cortex and whole brain OPCs.*** *Western blotting of CDKL5 and actin expression in MACs isolated OPCs (lane 1- Cdkl5*$^{+/y}$*, lane 2- Cdkl5*$^{-/y}$*) and total cortical lysates (lane 3- Cdkl5*$^{+/y}$*, lane 4- Cdkl5*$^{-/y}$*) of P10 mice. * Represents an unspecific band present in the Cdkl5-KO sample.*

5.2 Lack of *Cdkl5* results in the decreased intensity of Sudan black B staining in most brain regions.

As *Cdkl5* expression peaks around P14, as well as it's the most rapid phase of myelination, I started assessing if the loss of *Cdkl5* can impact the anatomical organization of white matter in the brain by performing Sudan black B (SBB) staining, an established method to visualize the overall myelination in brain sections from P15 and P56 animals. As shown in Fig. 23A, the results of this qualitative analysis revealed a widespread reduction of the staining intensity in coronal brain sections from P15 *Cdkl5* mutant mice compared to WT controls in

almost all brain areas. Moreover, SBB staining appeared less intense also in P56 mutants than in control animals although this reduction seems milder compared to the juvenile animal's group (Fig. 23B), especially in the corpus callosum tract.

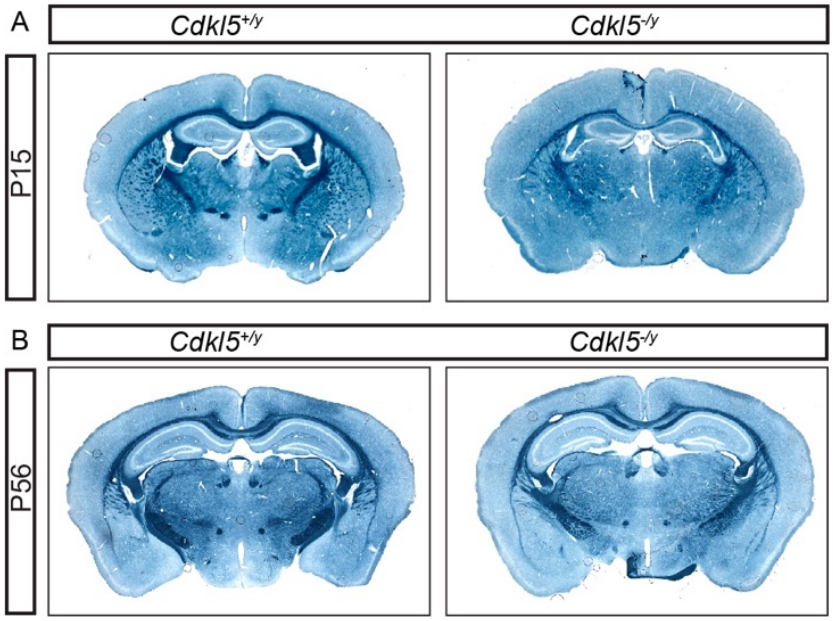

Figure 23: ***Sudan Black B staining in a coronal section of the mouse brain.*** *Bright-field images of SBB staining showing different brain regions of Cdkl5$^{+/y}$ and Cdkl5$^{-/y}$ mice at the age of P15* ***(A)*** *and P56* ***(B)****.*

5.3 Lack of *Cdkl5* leads to a reduction of mature OLs density, but not OPCs, in the mouse primary somatosensory cortex.

Based on the SBB results I decided to do a thorough anatomical and biochemical examination of the myelination process in the *Cdkl5*-lacking mice. Moreover, as I have shown that *Cdkl5* is expressed by OPCs but no studies so far have addressed whether this gene may play a role in the proliferation and/or survival of these glial cells. To shed light on this issue, I assessed the density of NG2-labeled OPCs by quantitatively analyzing cerebral cortical sections using IFL and confocal microscopy (Fig. 24A). This analysis showed no differences in NG2^{+} cells density between *Cdkl5*$^{+/y}$ and *Cdkl5*$^{-/y}$ mice in the primary somatosensory cortex (S1) of both young (P15) and adult (P56) animals (NG2^{+} cell/mm^2 $p > 0.05$; Fig. 24B). Several studies suggest that during the myelination process, a high density of mature myelinating OLs is required in white matter tracts for myelin generation (Meschkat et al., 2022). Based on this evidence, I next analyzed the density of myelinating OLs by using an antibody against opalin to label mature OLs (Fig.

24C). Intriguingly, this experiment showed that the density of OLs in the S1 cortex of adult *Cdkl5*$^{-/y}$ mice was significantly decreased compared to *Cdkl5*$^{+/y}$ littermates (opalin^{+} cells/mm^{2} $p < 0.01$; Fig. 24D). These results indicate that absence of *Cdkl5* has no impact on the density of OPCs generation but it can affect their maturation into myelinating OLs.

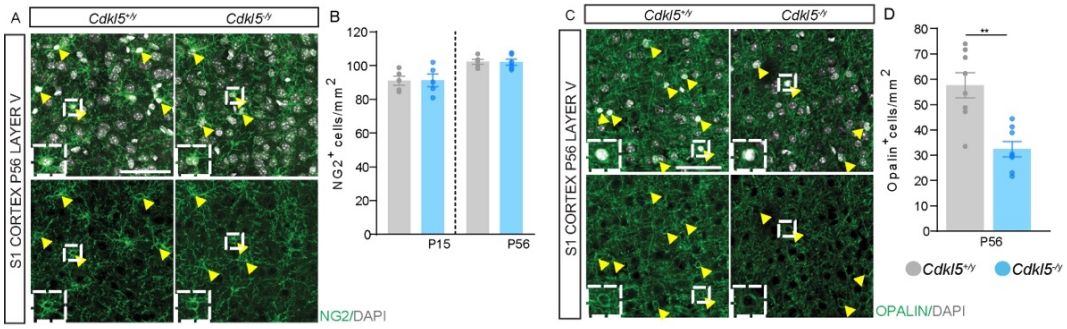

Figure 24: ***Cdkl5*$^{-/y}$ *mice show a decreased density of myelinating OLs.*** *Confocal images of NG2^{+} OPCs (green; **A**) and opalin^{+} OLs (green; **C**) co-labeled with DAPI (grey) in the S1 of Cdkl5$^{+/y}$ and Cdkl5$^{-/y}$ mice. Scale bar: 50 µm. Arrowheads point at examples of immunolabelled cells. Insets (bottom-left corner) show higher magnifications of the boxed areas. Bar graphs showing the density of NG2^{+} OPCs (**B**; n = 6 per genotype) and opalin^{+} OLs (**D**; n = 8 per genotype) throughout all layers of the S1 cortex in Cdkl5$^{+/y}$ and Cdkl5$^{-/y}$ mice. Statistical analysis: Student's t-test, ** p < 0.001.*

5.4 Myelin basic protein expression is reduced in the primary cortices of both young and adult *Cdkl5*$^{-/y}$ mice.

The observation that OLs density is sharply reduced in *Cdkl5* mutant mice led me to investigate whether myelination is affected in these animals. Myelin basic protein (MBP) is the major component of the myelin sheath and is produced by OLs. I, therefore, evaluated whether the lack of *Cdkl5* could impact the expression of MBP during post-natal development. As shown in Fig. 25A, S1; 25E, V1 the MBP immunofluorescence signal was strongly reduced in the S1 as well as V1 cortices of young mutant mice (P15) compared to WT littermates. The quantitative analysis of MBP immunofluorescence was obtained using the Image J software to measure both the proportion of stained pixels (% of area fraction) and the fluorescence intensity (integrated density, ID) throughout the cortical layers in each section. These quantitative analyses revealed that *Cdkl5*$^{-/y}$ mice show a profound decrease of MBP expression across layers I-VI of both S1 and V1 cortex compared to WT animals (% area fraction: S1 $p < 0.01$, V1 $p < 0.05$; Fig. 25B, F and ID: S1 $p < 0.001$, V1 $p < 0.05$; Fig. 25B', F'). In particular, these

alterations were found in the infragranular layer ($p < 0.001$) of the cortex and not in granular or infragranular layers. Cortical laminae contain unique information on the signal flow within the brain. In primary sensory cortices, thalamocortical connections providing sensory information arrive primarily in central (granular) layers. In contrast, supragranular layers are the primary origin and termination of corticocortical connections, whereas infragranular layers connect the cortex with subcortical and corticospinal regions (Kandel et al., 2021). Therefore, I measured whether the absence of *Cdkl5* could differentially produce MBP expression changes within the cortical laminae.

To establish whether the reduction of MPB is retained, or even reinforced, into adulthood, I next analyzed P56 mice and, as illustrated in Fig. 25C, S1; 25G, V1. I found that MBP immunostaining was strongly reduced in mutant mice compared to WT littermates across layers I-VI of both S1 and V1 cortex (% area fraction: S1 $p < 0.01$, V1 $p < 0.05$; Fig. 25D, H, and ID: S1 $p < 0.01$, V1 $p < 0.01$; Fig. 25D', H'). Interestingly, in contrast to young mice, in adult animals, MBP expression was significantly different in both granular ($p < 0.05$) and infragranular cortical layers ($p < 0.001$). Consistently, western blot (Fig. 26A) analysis of total cortical lysates confirmed lower expression levels of two isoforms of MBP, both in young and adult *Cdkl5*$^{-/y}$ mutants (O.D.: MBP/actin $p < 0.05$; Fig. 26B) compared to *Cdkl5*$^{+/y}$ mice. Thus, these data show that the effect of *Cdkl5* loss on MBP expression is generalized to the entire cortex.

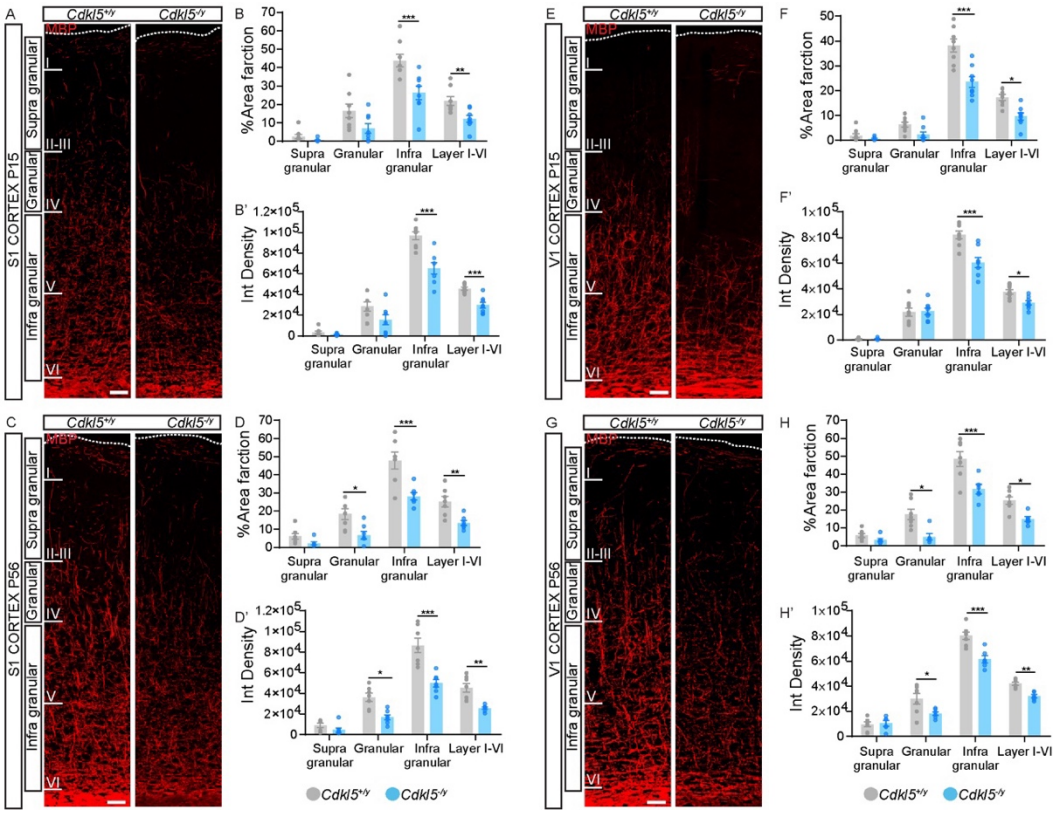

Figure 25: ***Reduced expression of MBP in the cortex of both P15 and P56 Cdkl5 KO mice.*** *Confocal images of MBP (red) immunofluorescence in primary cortices of both P15: S1, **A**; V1, **E** and P56: S1, **C**; V1, **G** Cdkl5$^{+/y}$ and Cdkl5$^{-/y}$ mice. Scale bar: 50 µm. Bar graphs show analysis of % of area fraction (P15: S1, **B**; V1, **F**; P56: S1, **D**; V1, **H**) and the integrated density (P15: S1, **B'**; V1, **F'**; P56: S1, **D'**; V1, **H'**) in both P15 (n= 8 each genotype) and P56 (n= 7,6 each genotype) mice. Statistical analysis: Student's t-test, *p < 0.05, ** p < 0.01, and Two-way ANOVA followed by Tukey's multiple comparisons *p < 0.05, **p < 0.01, *** p < 0.001.*

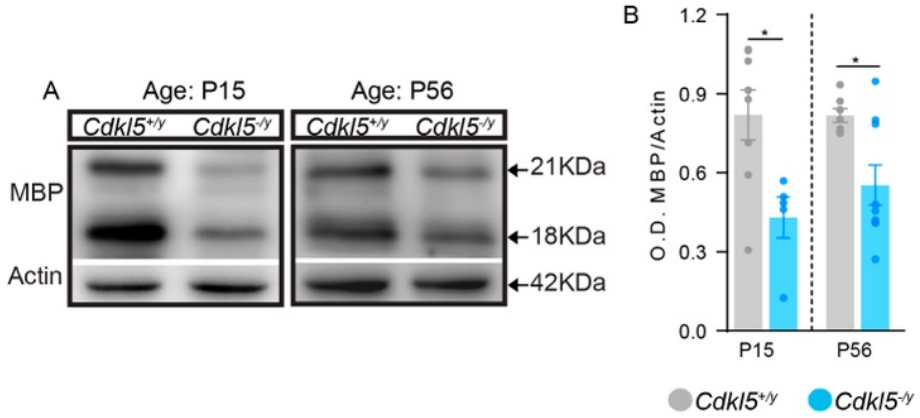

Figure 26: ***Lower expression levels of* MBP *protein in the cortex of young and adult mutant mice. (A)*** *Western blotting of MBP (18KDa and 21KDa isoform) and actin expression in total cortical lysates. **(B)** Optical density (O.D.) analysis of two isoforms of MBP protein in P15 (n= 7, 5 each genotype) P56 (n= 6, 8 each genotype) mice. Statistical analysis: Student's t-test, *p < 0.05.*

5.5 Neurofilaments phosphorylation is greatly compromised in the cerebral cortex of *Cdkl5*$^{-/y}$ mice.

Next, we investigated the phosphorylation of neurofilaments (NF), an accurate proxy of both myelin abnormalities, and axonal injury. it is known that NF phosphorylation is decreased in dysmyelinating conditions and axonal dysfunctioning. I, therefore, assessed whether loss of *Cdkl5* could affect the expression of either the total or the phosphorylated form of NFs. To this aim, I first performed immunofluorescence experiments using antibodies that specifically label either total NF or phosphorylated NF (pNF). As shown in Fig. 27 the expression of NFs did not show major differences between genotypes in both the S1 (Fig. 27A, P15; 27C, P56) and V1 (Fig. 27E, P15; 27G, P56) cortical areas at the ages analyzed. This qualitative observation was confirmed by the quantitative analysis that revealed no differences in NFs immunofluorescence with respect to genotype, cortical areas, laminae, and age (% area fraction: P15 Fig. 27B, S1; 27F, V1; P56 Fig. 27D, S1; 26H, V1; $p > 0.05$, and ID: P15 Fig. 27B', S1; 27F', V1; P56 Fig. 27D', S1; 27H', V1; $p > 0.05$).

Importantly as shown in Fig. 28, I found a sharp reduction of pNF immunosignal in the S1 (Fig. 28A, P15; 28C, P56) and V1 (Fig. 28E, P15; 28G, P56) cortices of *Cdkl5*$^{-/y}$ mice compared to *Cdkl5*$^{+/y}$ at both P15 and P56 mice. Furthermore, the quantitative analysis in both ages also suggests that the pNF IFL in mutants was found significantly declined in deeper laminae including both granular and infragranular layers except the supragranular layer (% area fraction: P15 Fig. 28B, S1; 28F, V1; $p < 0.01$, P56 Fig. 28D, S1; $p < 0.01$, 28H, V1; $p < 0.05$, and ID: P15 Fig. 28B', S1; $p < 0.01$, 28F', V1; $p < 0.001$, P56 Fig. 28D', S1; $p < 0.05$, 28H', V1; $p < 0.001$). Finally, I performed western blot analysis (Fig. 29A) on total cortical lysates of both young and adult mice in order to separate the analysis between the NFH and NFM subunits. As already predictable by looking at the bands' intensities, the quantitative analysis of these western blot experiments shows a significant decrease in the phosphorylation of both NF subunits in *Cdkl5*$^{-/y}$ mice compared to *Cdkl5*$^{+/y}$ littermates (O.D.: pNF/NF/actin P15 $p < 0.05$; *Fig. 29B, and P56* $p < 0.05$; *Fig. 29C*). Interestingly, no changes were observed in the total form of NF. These results indicate that the loss of *Cdkl5* directly or indirectly

tampers with the phosphorylation of NF, an alteration that could underlie both myelination and glial alterations in *Cdkl5* mutants.

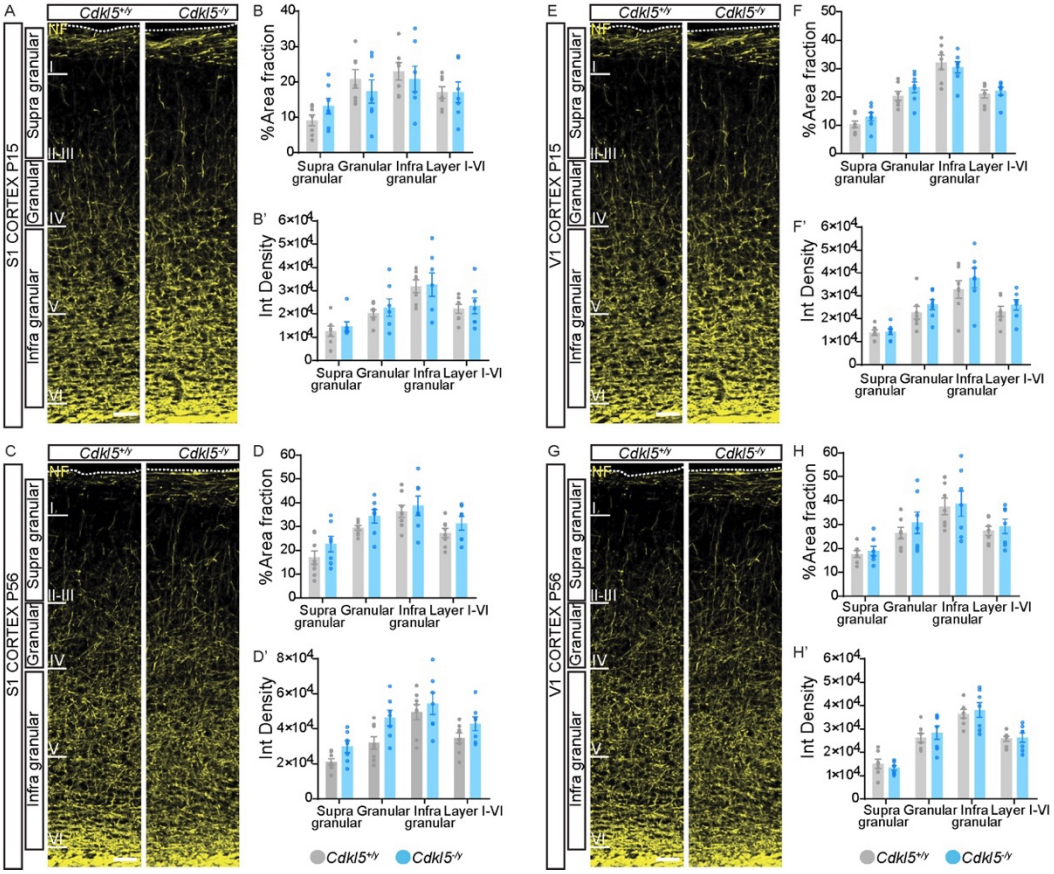

Figure 27: ***No changes in NF expression were found in S1 and V1 cortices of Cdkl5 mutant mice.*** *Confocal images of NF (yellow) immunofluorescence in S1 and V1 cortex of both P15: S1,* ***A****; V1,* ***E*** *and P56: S1,* ***C****; V1,* ***G*** *Cdkl5$^{+/y}$ and Cdkl5$^{-/y}$ mice. Scale bar: 50 µm. Bar graphs show analysis of % of area (P15: S1,* ***B****; V1,* ***F****; P56: S1,* ***D****; V1,* ***H****) and the integrated density (P15: S1,* ***B'****; V1,* ***F'****; P56: S1,* ***D'****; V1,* ***H'****) of both P15 (n= 8 each genotype) and P56 (n= 7,6 each genotype) mice. Statistical analysis: Student's t-test, p > 0.05, ** p < 0.01, and Two-way ANOVA followed by Tukey's multiple comparisons p > 0.05.*

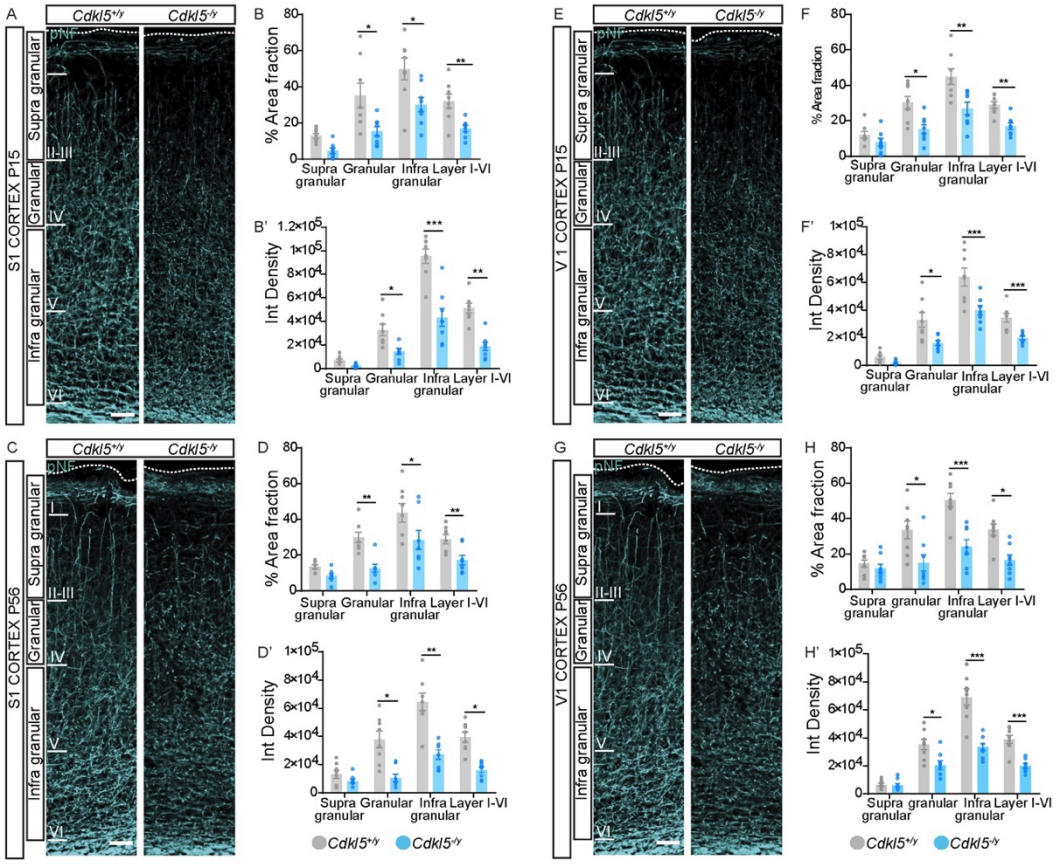

Figure 28: ***Expression of pNF in the cortex of both P15 and P56 Cdkl5-KO mice.*** *Confocal images of pNF (cyan) immunofluorescence in S1 (P15, **A**; P56, **C**) and V1 (P15, **E**; P56, **G**) cortex of P15 (left panel) and P56 (right panel) Cdkl5$^{+/y}$ and Cdkl5$^{-/y}$ mice. Scale bar: 50 µm. Analysis of immunofluorescence for pNF showing % of area fraction (P15: S1, **B**; V1, **F**; P56: S1, **D**; V1, **H**) and the integrated density (P15: S1, **B'**; V1, **F'**; P56: S1, **D'**; V1, **H'**) in both young (upper panel, n= 8 each genotype) and adult (lower panel, n= 7, 6 each genotype) animals. Statistical analysis: Student's t-test, *p < 0.05, **p < 0.01, *** p < 0.001, and Two-way ANOVA followed by Tukey's multiple comparisons *p < 0.05, **p < 0.01, *** p < 0.001.*

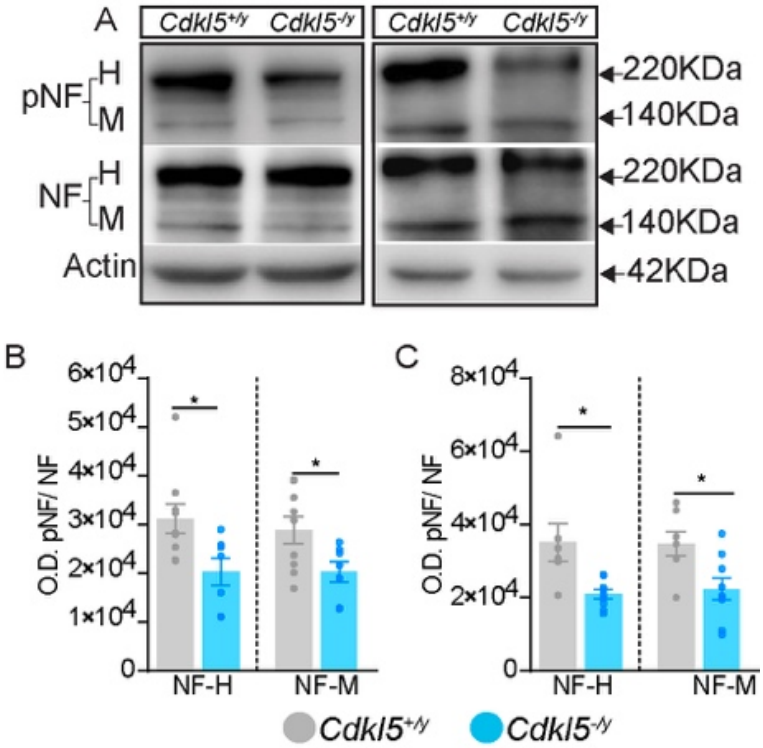

Figure 29: ***Decreased expression levels of* pNF *protein in the cortex of young and adult mutant mice.*** ***(A)*** *Western blotting on total cortical lysates immunoblotted with anti-NF, anti-pNF, and anti-actin antibodies. Bar graphs show O.D. values for NFH and NFM phosphorylation in both P15 (n =9, 7;* ***B****) and P56 (n = 7, 9;* ***C****) mice. Statistical analysis: Student's t-test, *p < 0.05.*

5.6 The lack of *Cdkl5* affects myelin sheath thickness.

The amount of MBP, along with various other proteins, is essential for the correct distribution and compaction of myelin sheath on neuron's axonal processes. In view of the decrease of both MBP and pNF expression in *Cdkl5* null mice, we decided to use transmission electron microscopy to assess myelination at the ultrastructural level. We directed our observations to the alveus of the hippocampus on coronal ultrathin sections from both *Cdkl5*$^{+/y}$ and *Cdkl5*$^{-/y}$ adult mice to assess the thickness of the myelin sheath (Fig. 30A). By measuring both the axonal area and the myelinated fiber area with the help of an ImageJ tool we plotted the g-ratio values (Fig. 30B). This analysis revealed that the mean g-ratio of myelinated fibers in mutant mice was significantly higher compared to WT littermates (g-ratio: $p < 0.01$; *n = 3 per genotype, 100 axons/animal*), indicating that the myelin sheath is significantly thinner in *Cdkl5* deficient mice. Moreover, we found that both genotypes show similar axonal areas, and the reduced myelin sheath thickness is independent of axonal size (Fig. 30C).

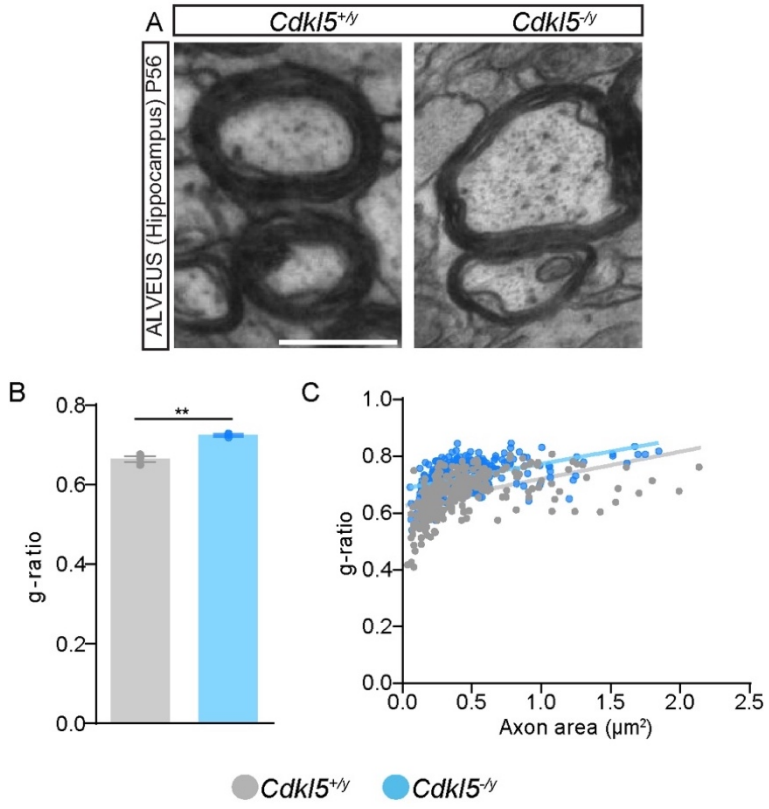

Figure 30: ***Decreased myelin sheath thickness in P56 Cdkl5$^{-/y}$ mice represented by increased g-ratio.*** ***(A)*** *Transmission electron micrographs of coronal ultrathin sections through the alveus of the hippocampus from Cdkl5$^{+/y}$ and Cdkl5$^{-/y}$ mice. Scale bar 500 nm.* ***(B)*** *The bar graph shows a significantly increased g-ratio of myelinated fibers in Cdkl5$^{-/y}$ mice.* ***(C)*** *Scatter plot of g-ratio vs. axonal area (n = 3 per genotype; 100 axons/animal). Statistical analysis: Student's t-test, **p < 0.01.*

5.7 *Cdkl5* loss is associated with alterations in the axo-myelinic morphology at nodal/paranodal structures.

In addition to the thickness of the myelin sheath, its distribution along the axons to generate internodes and nodes of Ranvier is also an important phase of the myelination process. The internodes and nodes of Ranvier, flanked on both sides by a domain called paranode, which is a site of contact between myelinating glial cell and axon, play a crucial role in the optimization and fast conduction of action potentials (Hedrick, 2008). These complex and prominent axonal structures allow energy-efficient saltatory propagation and their length contributes to tuning the conduction velocity (Benamer et al., 2020). To examine whether the decreased myelination in *Cdkl5*-null mice is associated with alterations in the axo-myelinic organization, I next evaluated the morphology of the nodal/paranodal region. To this aim, I performed double immunofluorescence in layer V of S1 cortical sections using antibodies against MBP (to label two consecutive myelinated

internodes) and CASPR (a protein expressed only at the paranodal region) that I imaged using high-resolution confocal microscopy from both young and adult mice as illustrated in Fig. 31A (P15), and 31B (P56). By using the plot intensity profiles of CASPR immunofluorescence I first measured the length of the nodes of Ranvier (i.e., the distance between two paranodes). Remarkably, I found a sharp increase in node length in the S1 cortex of *Cdkl5*$^{-/y}$ compared to *Cdkl5*$^{+/y}$ mice at both developmental ages (mean node length (µm): $p < 0.01$; Fig. 31C). Moreover, this increase was confirmed by the assessment of no267de length distribution, showing a significant shift towards longer node values in mutant mice compared to controls at both ages (distribution (%): $p < 0.001$; Fig. 31D, P15; 31E, P56). In addition, when I analyzed the density of nodes it showed a decreased density of nodes in the S1 cortex of *Cdkl5*-KO mice compared to WT littermates (nodes/mm^2 $p < 0.01$; Fig. 31F). Intriguingly, the length of CASPR-labeled paranodes, as shown in Fig. 31G, was significantly shorter in both young and adult mutants compared to *Cdkl5*$^{+/y}$ mice (paranode length (µm): $p < 0.01$; Fig. 31G). Thus, these data indicate that *Cdkl5* is required for the mechanisms underlying the complex cell-to-cell interactions that are established between OLs and neurons at nodal/paranodal sites along the axon.

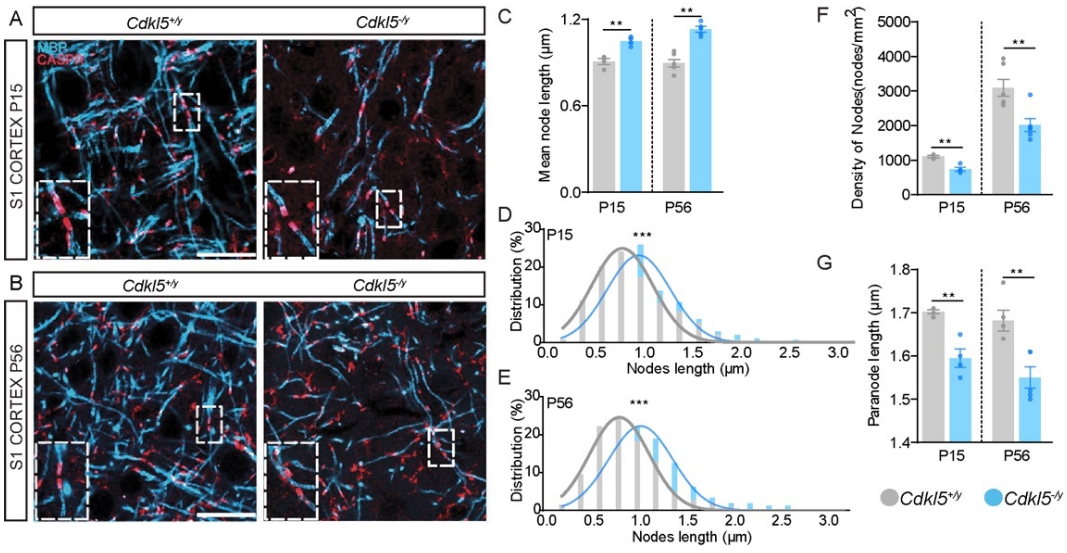

Figure 31: ***Cdkl5*$^{-/y}$ *mice show severe alterations of the nodal and paranodal structures in the S1 cortex.*** *Confocal images of Caspr-expressing paranodes (red) co-labeled with MBP (cyan) in layer V of S1 cortex from P15* ***(A)*** *and P56* ***(B)*** *mice. Scale bar 20 µm. Insets (bottom left corner) represent higher magnifications of boxed areas.* ***(C)*** *Bar-graphs showing a significant increase in mean node length of Cdkl5*$^{-/y}$ *mice compared to WT controls. (n = 6, 5 each genotype; 80 nodes/animal). Length distribution of nodes in P15* ***(D)*** *and P56* ***(E)*** *mice; fitted lines show differences in Gaussian distributions between genotypes. Bar graph showing the nodes density* ***(F)***

and the paranodes length ***(G)*** *(n = 6/5 each group; 160 nodes/animal) in S1 cortex of both young and adult Cdkl5$^{+/y}$ and Cdkl5$^{-/y}$ mice. Statistical analysis: Student's t-test, ** p< 0.01; Gaussian fit, ***p-value< 0.001.*

5.8 Neuronal, but not Oligodendroglial, expression of *Cdkl5* is required for typical MBP expression.

Next, I assessed whether myelin abnormalities, i.e., MBP expression, are a primary consequence arising from *Cdkl5* loss in the oligodendroglial population or a secondary dysfunction caused by neuronal defects. To this aim, I crossed two different CRE mouse lines, i.e., Sox10^{Cre} (expressed mainly in oligodendroglial cells (Matsuoka et al., 2005) and Emx1^{Cre} (expressed specifically in forebrain pyramidal neurons (Iwasato et al., 2004), with a Cdkl5^{flox} mouse line (Amendola et al., 2014b), so to obtain cell-specific deletion of *Cdkl5*. Surprisingly, the expression of MBP in the S1 cortex of both young (P15: Fig. 32A) and adult (P56, Fig. 32C) Cdkl5^{flox}/Sox10^{Cre} mice was not different from Cdkl5^{flox} controls. Importantly, the quantitative analysis of the IFL signal confirmed these observations (of % area fraction: $p > 0.05$; Fig. 32B-P15, 32D-P56, and ID: $p > 0.05$; Fig. 32B'-P15, 32D'-P56) revealing no changes in MBP expression between genotypes at both ages. In contrast, Cdkl5^{flox}/Emx^{Cre} mice showed a severe reduction of MBP positive fibers in the cortical layers of the S1 cortex compared to controls (Fig.: P15-32E, P56-32G), a difference that was highlighted by the image analysis (% area fraction: $p < 0.05$; Fig. 32F-P15, 32H-P56, and ID: $p < 0.05$; Fig. 32F'-P15, 32H'-P56). Interestingly, young conditional Emx1/Cdkl5 mutants show changes in the deeper layers of the cortex whereas in adult animals these changes are significant both in granular and infragranular layers of the S1 cortex.

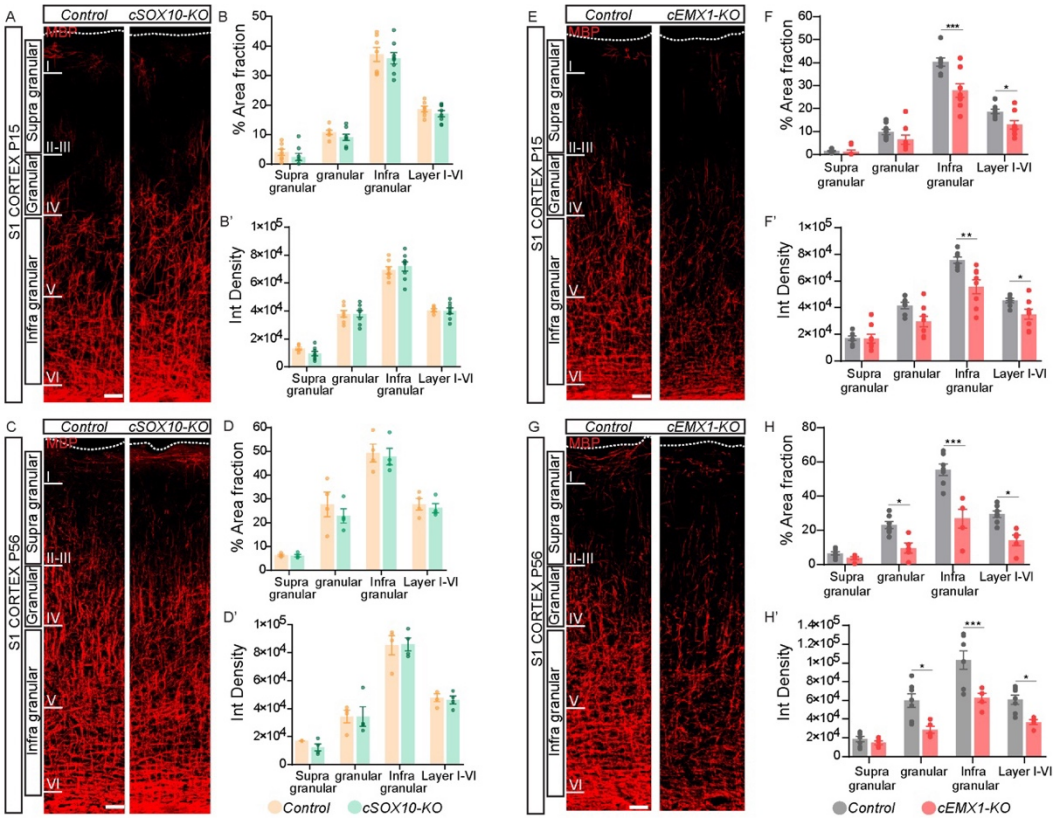

Figure 32: ***MBP expression in both Cdkl5^{flox}/SOX10^{Cre} and Cdkl5^{flox}/EMX1^{Cre} mice.*** *Representative confocal images of MBP immunofluorescence staining in all cortical layers of Cdkl5^{flox}/SOX10^{Cre} (P15: n=7, 8 each genotype; **A**, and P56: n=4 each genotype; **C**) and Cdkl5^{flox}/EMX1^{Cre} (P15: n=8, 9 each genotype; **E**, and P56: n=7, 5 each genotype; **G**) mice with specific conditional controls, Scale bar 20um. Histograms showing analysis of MBP immunosignal in all cortical layers of the S1 cortex of Cdkl5^{flox}/SOX10^{Cre} (% of area fraction: P15, **B**; P56, **D**; and the integrated density: P15, **B'**; P56, **D'**) and Cdkl5^{flox}/EMX1^{Cre} mice (% of area fraction: P15, **F**; P56, **H** and the integrated density: P15, **F'**; P56, **H'**). Statistical analysis: Student's t-test, p > 0.05, *p < 0.05, **p < 0.01, *** p < 0.001, and Two-way ANOVA followed by Tukey's multiple comparisons p > 0.05, *p < 0.05, **p < 0.01, *** p < 0.001.*

5.9 The primary visual cortex of CDD patients exhibits disorganized myeloarchitecture.

To investigate whether atypical myelin organization also occurred in CDD patients, I examined postmortem human brains. I first evaluated myelin architecture on sections of formalin-fixed tissue blocks of the BA17 cortex of both CDD and NT subjects using Sudan Black B staining. As shown in Fig. 33A, the levels of SBB staining in sections from CDD specimens were much lower than in NT sections, as confirmed by optical density (Fig. 33B) and percentage of cortical area covered by SBB (Fig. 33C) analyses. Furthermore, I tested the expression of MBP by western blot on snap-frozen BA17 tissues (Fig. 33D), and the results showed reduced levels of MBP in CDD compared to NT samples (Fig.

33E), a result consistent with the histological analyses. Thus, both histological and biochemical analyses confirm that CDD is associated with defective myelin synthesis and deposition in the cerebral cortex, a defect that is more pronounced with aging.

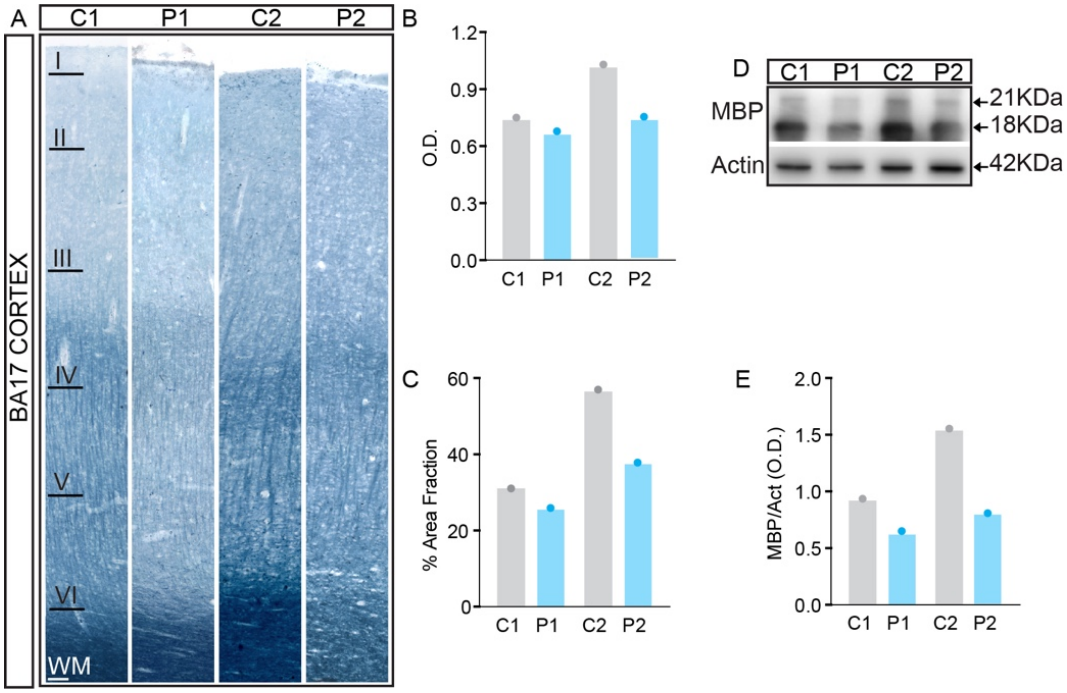

Figure 33: ***Atypical myeloarchitecture in BA17 of CDD patients.*** ***(A)*** *Images of Sudan Black B staining of formalin-fixed sections from both BA17 of NTs (C1, C2) and CDD patients (P1, P2), scale bar: 100 µm. Histograms of the optical density* ***(B)*** *and % of area fraction covered by SBB staining* ***(C)****. Western blot showing MBP expression levels in total protein extracts from BA17 of NTs and CDD patients* ***(D)*** *and relative quantitative analysis* ***(E)****. Actin was used as a loading control.*

5.10 Positive allosteric modulation of mGluR5 activity rescues MBP expression in *Cdkl5*$^{-/y}$ mice

A bidirectional communication between oligodendroglia and neurons plays a crucial role in regulating OPCs differentiation and mature OLs integration into neuronal circuits in the myelination process (Thornton and Hughes, 2020). According to the literature, mGluR5 is crucially involved in such communication. Indeed, recent evidence indicates that targeting metabotropic glutamate receptors might represent a novel therapeutic approach for multiple sclerosis and other demyelinating conditions (Luyt et al., 2006; Spampinato et al., 2018). Encouraged by the positive effects produced by the treatment with the mGluR5-PAM RO68 illustrated in Fig. 19 of this thesis (Gurgone et al., 2022), we treated WT and

Cdkl5-KO animals from P3 to P15 with this compound, and after 24 hr MBP immunofluorescence was analyzed (Fig. 34A). Intriguingly, this treatment produced a complete rescue of MBP expression in the S1 cortex of treated mutant mice (% area fraction: $p < 0.05$; Fig. 34B, and ID: $p < 0.01$; Fig. 34C) without affecting MBP expression in WT animals. These results support the idea that the activation of mGluR5-mediated signaling using positive allosteric modulators can rescue MBP expression, and likely hypomyelination, in *Cdkl5* null mice.

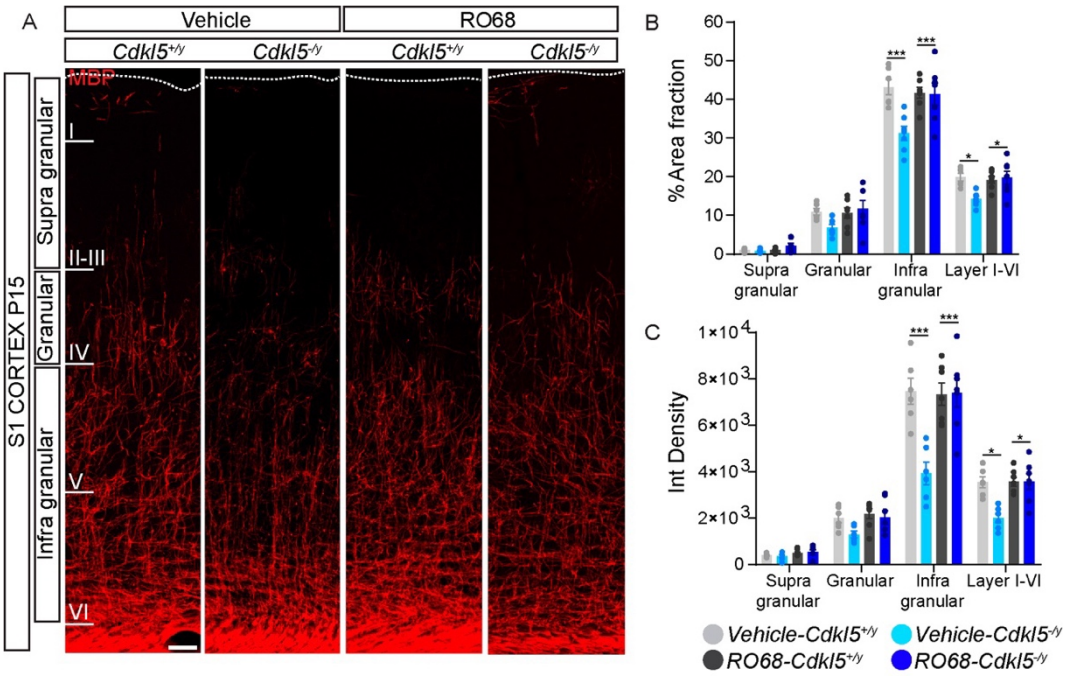

Figure 34: ***MBP immunofluorescence is restored by the chronic treatment with R068. (A)*** *Confocal images of MBP immunofluorescence throughout the cortical layers of vehicle and R068 treated young Cdkl5$^{+/y}$ and Cdkl5$^{-/y}$ mice. Scale bar: 20 µm. Bar graphs showing MBP immunosignal quantitative analysis as % of area fraction* ***(B)*** *and integrated density* ***(C)*** *values in S1 cortex laminae. Statistical analysis: Student's t-test, *p < 0.05, **p < 0.01, and Two-way ANOVA followed by Tukey's multiple comparisons, *** p < 0.001. (Vehicle-Cdkl5$^{+/y}$ n = 7, vehicle-Cdkl5$^{-/y}$ n = 7, RO68-Cdkl5$^{+/y}$ n = 6, RO68-Cdkl5$^{-/y}$ n = 8.)*

6. DISCUSSION

Infancy is the most common stage for neurodevelopmental disorders to arise, and they typically progress slowly over the course of a lifetime. They are a diverse range of illnesses that interfere with brain development. My thesis is focused on a monogenic NDD, i.e., CDKL5 deficiency disorder, a condition with monogenetic origin having a devastating impact on patients and their families. Unfortunately, these conditions have no known cure, rather, treatment consists of symptomatic and palliative medications that, in certain mild cases, might minimize some of the most severe symptoms, such as seizures and behavioral difficulties. However, because there is no cure and patients need ongoing care, this lack of therapeutic options has a significant negative impact on both patients and caregivers' quality of life and also stresses the healthcare system. Assessing both the pathophysiology of the disease and prospective therapeutic options is possible thanks to the availability of animal models with high face validity, that is reproducing various crucial aspects of the human condition (Van Bergen et al., 2022). However, to quantitatively monitor brain activity, there is a critical need for unbiased biomarkers with high translational value. In recent years, researchers have begun to investigate the use of myelination as a biomarker for neurodevelopmental disorders such as ASD and schizophrenia, an endophenotype that can be monitored by non-invasive brain imaging. These studies have shown that individuals with ASD have reduced myelination in certain areas of the brain, specifically in the prefrontal cortex, which is responsible for social behavior, communication, and decision-making (e.g., Deoni et al., 2015). Additionally, it has also been found that individuals with schizophrenia have a reduction in myelination in the anterior cingulate cortex, which is associated with cognitive control and emotion regulation (Haigh et al., 2019).

The assessment of myelination can be obtained through imaging techniques such as magnetic resonance imaging which can detect the amount and organization of myelinated tracts in the brain. This allows for a non-invasive and precise way of identifying abnormal myelination patterns in individuals with NDDs. Furthermore, the use of myelination as a biomarker can also aid in the early detection and intervention of the disease state which could greatly improve the pathological outcome for individuals with NDDs. MRI studies from CDD patients

have shown white matter abnormalities including reduced fractional anisotropy and increased mean diffusivity in the corpus callosum, the internal capsule, the cerebellum, and the brainstem (Bahi-Buisson and Bienvenu, 2012). These findings suggested that the white matter in CDD patients is atypically organized and more diffused than in neurotypical individuals. These white matter abnormalities may be caused by a number of factors, including abnormal development and function of nerve cells, aberrant communication between nerve cells and oligodendroglial cells, or unusual migration and/or function of this glial lineage during development. Thus, understanding the underlying causes of such white matter abnormalities and myelin organization is an important, but still, unexplored, area of research in CDD, as it will provide novel insights into the underlying mechanisms of the disorder and may help the development of new treatments.

The *Cdkl5* mRNA is known to be expressed in brain cells, including neurons, OPCs, and OLs (Ye Zhang et al., 2014; Zhang et al., 2016). However, if the protein CDKL5 is expressed by OPCs has never been directly addressed. The results shown in this thesis confirm that CDKL5 is present in OPCs and suggest that it may play a role in the development and maturation of OPCs, as well as in the organization of white matter in the nervous system. To shed light on these issues, I visualized the overall pattern of myelination in the brain by using the Sudan Black B staining technique, which is a non-toxic dye that can bind to lipids of the myelin sheath resulting in a blue-black stain in the processed brain sections. The examination of this staining, both at a very early developmental age i.e., P15, and an adult stage i.e., P56, shows that SBB intensity is decreased in *Cdkl5*$^{-/y}$ mice compared to *Cdkl5*$^{+/y}$ littermates, irrespective of age but with stronger differences in the young group of animals. This strong reduction in lipid content suggested that it could be the result of the lack/reduction of myelinating OLs or the reduced expression of proteins directly involved in myelin deposition. Indeed, Proteins such as MBP and PLP have been shown to interact with lipids for the deposition and compaction of the myelin sheath (Ruskamo et al., 2022). Based on these ideas, I then investigated the density of both OPCs and myelinating OLs, as well as the abundance of myelin-related proteins during postnatal development of primary sensory cortical areas in light of the significant sensory (i.e., tactile,

visual and auditory) abnormalities shown by the CDD mouse models and also reported in patients.

The results of these experiments show that the density of OPCs in the S1 cortex is not affected by *Cdkl5* loss in both P15 and P56 animals. However, adult *Cdkl5*$^{-/y}$ mice show considerably fewer myelinating OLs in this area compared to *Cdkl5*$^{+/y}$ littermates. These data imply that while *Cdkl5* deficiency does not affect OPCs production during embryogenesis, it directly or indirectly impacts their maturation into myelinating OLs during postnatal stages. Because it is known that a high density of mature myelinating OLs is required for myelin generation and the maintenance of white matter tracts (Meschkat et al., 2022), I next assessed the molecular organization of myelin in the Cdkl5 mutants. To this end, I examined the expression of MBP in both S1 and V1 cortical areas from young and adult mice. According to the analysis of immunofluorescence, both S1 and V1 cortices from *Cdkl5*$^{-/y}$ mice exhibit a substantial reduction in MBP expression in layers I to VI compared to WT animals. Interestingly, I found that, unlike young mice which display MBP impairments only in the infragranular layers, adult animals exhibit significant abnormalities in both granular and infragranular laminae. By using Western blot analyses of whole cortical lysates, I could also show that the expression levels were different for two MBP isoforms, bearing distinct molecular weights (i.e.,18KDa and 21KDa), suggesting that the loss of *Cdkl5* has a generalized effect on cortical myelination rather than only in S1 and V1.

These data support the idea that a reduction in the number of myelinating OLs produces a severe decline in MBP expression in *Cdkl5* mutant mice. To further validate these findings, I tested the phosphorylation of NF in these animals as a further readout of axonal health that has been shown to depend on several factors including myelin alterations (Gafson et al., 2020). According to my findings, in both S1 and V1 cortical regions of young and adult *Cdkl5*-deficient mice total NF expression was unaffected while phospho-NF was significantly diminished in both granular and infragranular layers at both ages. Moreover, various studies suggest that the phosphorylation of NFH and NFM subunits is critically increased by the myelination process (Yuan et al., 2017). For this reason, using Western blot analyses of whole cortical lysates, I could also show that the phosphorylation

of both NFH (220KDa) and NFM (180KDa) isoforms, was reduced in mutant mice of both ages. These results in association with MBP strengthen the fact that loss of *Cdkl5* causes myelin abnormalities. Importantly, by using electron microscopy, I was able to demonstrate that changes in the molecular organization of myelin and axonal cytoskeleton are accompanied by a reduced thickness of the myelin sheath around axonal fibers. Indeed, the results show a significant change in the g-ratio in the fibers sampled from the alveus of the hippocampus from adult *Cdkl5*$^{-/y}$ that is irrespective of the axonal size.

Axon morphology is also shaped by interruption of myelination at periodical sub-axonal loci by the development of the nodes of Ranvier and related paranodal membrane areas. Because in *Cdkl5* null animals infragranular neurons of the S1 cortex exhibit the most substantial myelin changes, I investigated the nodal/paranodal compartments in layer V of both young and adult mice. Interestingly, these experiments show the node's length is increased in mutant mice a sign that is accompanied by a reduction of Ranvier's node density. Additionally, by using a specific marker to visualize paranodes (i.e.: anti-CASPR labeling), I found that in layer V these structures are shorter in the absence of *Cdkl5*, highlighting the possibility that *Cdkl5* plays a role in axo-glial communication. This idea is supported by several previous studies showing that CASPR along with contacin1 and glial components such as NF155 participate in a molecular complex at paranodes, where OLs communicate with axons during the myelination process (Duncan et al., 2021). Because the paranodal length is recurrently found altered in hypo-/dys-myelinating conditions (Ruff et al., 2013), my results further validate the severity of myelin alterations shown by the cerebral cortex of *Cdkl5*$^{-/y}$ mice.

Numerous investigations conducted over the past few decades have demonstrated that neurons and cells of the oligodendrocyte lineage collaborate in bidirectional communication throughout life to support normal brain function. In other words, to adequately myelinate axons, OLs must be in close contact with neurons and must receive signals from them. OLs expresses a wide range of intracellular signaling pathways, growth factors, signaling molecules, neurotransmitters, and neuromodulator receptors, the modulation of which is controlled by the neuronal activity (Thornton and Hughes, 2020). It is well established that variations in

neuronal activity can control myelination, differentiation, and proliferation to aid in the development and function of neural circuits. It is then plausible that the myelination defect shown by Cdkl5 mutant mice could result from either cell-autonomous or non-cell-autonomous mechanisms, i.e.: OLs or neuronal, or from a mix of the two possibilities. Surprisingly, at least for MBP distribution, my results show that the neuronal expression of CDKL5 is necessary for its correct establishment. Indeed, I found that Sox10^{Cre}: *Cdkl5*^{flox} mice did not show changes of MBP neither in young nor in adult animals whereas in the Emx1^{Cre}: *Cdkl5*^{flox} mouse line a significant reduction of MBP starts from P15 and is retained into adulthood. Thus, these data indicate that, at least for MBP expression, myelin deficiencies seen in *Cdkl5*$^{-/y}$ mice are produced by secondary dysfunctions brought on by neuronal defects rather than a primary impairment resulting from the absence of Cdkl5 in oligodendroglial cells. Further experiments are currently ongoing using these conditional mutants to better understand the role of CDKL5 in myelination mechanisms (e.g., testing the density of myelinating OLs, components, and organization of nodal/paranodal structures, etc.). The defects that I observed might be caused due to loss of activity of molecules involved in axo-glial communication as I found a decrease in one of the important membrane proteins i.e., CASPR. Of note, further studies will be needed to examine the oligodendroglial components and other proteins involved in such communication for eg. NF155. Moreover, as it is evident that mGluR5 receptors are expressed in the oligodendroglial population and are involved in two-way communication between OL and neurons (Luyt et al., 2006; Thornton and Hughes, 2020), they may also be a contributing factor to these deficits. In fact, as shown in the results from Gurgone et al., *Cdkl5-KO* animals as well as CDD patients show lower expression of these receptors, which may involve in disrupting axo-glial communication.

The findings reported here on myelin defects shown by two postmortem CDD brains closely resemble those observed in the *Cdkl5*$^{-/y}$ mouse model and underscore the need for further research to comprehend the underlying mechanisms and develop effective treatments for this condition. Intriguingly, because at least two signs are mirrored by human and mouse brains (i.e. faulty overall myelination and MBP expression), the use of this animal model to look

for therapeutic remedies is strongly encouraged also for this pathological aspect of CDD. I am aware that the extremely small size of the human CDD samples, without the support of statistical analysis (which is not feasible to be run with an n = 2), makes drawing final conclusions very difficult. However, it is my goal to investigate in the future other regions of the human brain and perform additional research on other important aspects of myelination to validate these findings. These results will also guide future animal studies with the goal to increase our understanding of the mechanisms underlying CDD and to develop effective treatments.

In line with this therapeutic goal, the final section of my thesis tackles with the identification of molecular targets that might be manipulated to ameliorate the myelin abnormalities observed in Cdkl5 null mice. In the work by Gurgone et al. (2022), we demonstrated the preclinical therapeutic value of positively modulating the mGluR5 activity, a group I metabotropic glutamate receptor that is highly expressed in both mouse and human cerebral cortex. According to this work, the reduced expression and function of mGluR5 and both synaptic and behavioral abnormalities displayed by CDKL5 mutants can be rescued by treating animals with different mGluR5 PAMs. Interestingly, mGluR5 signaling plays a critical role in the bidirectional communication between oligodendroglia and neurons that controls OPCs differentiation and mature OLs integration into neuronal circuits throughout myelination (Thornton and Hughes, 2020). In addition, current research suggests that metabotropic glutamate receptor modulation may constitute a cutting-edge treatment strategy for treating multiple sclerosis and other demyelinating diseases. As a matter of fact, mGluR5 expression and activity abnormalities have been found in various animal models of both neurodevelopmental and demyelinating disorders that were rescued by treatments using either positive or negative allosteric modulators of these receptors (Spampinato et al., 2018; Vicidomini et al., 2017). As reported in the results of Gurgone et al. (2022), the RO68 compound is apparently more potent than the PAM CDPPB as it is efficacious at lower concentrations, and it has the advantage to be dissolved in a non-toxic vehicle solution compared to CDPPB. Intriguingly, our findings strongly support the idea that MBP expression, and hopefully hypomyelination (that remains to be tested directly), can be rescued in

Cdkl5 deficient mice by mGluR5-mediated signaling activation employing positive allosteric modulators. Importantly, these findings raise the possibility that targeting mGluR5 activity might represent a promising new therapeutic approach for treating demyelinating diseases.

In summary, in this Thesis, I report that myelination and associated processes are severely reduced or altered in primary cortical areas of CDD mice and human patients. Importantly, *Cdkl5* significantly impacts myelination by directly or indirectly influencing the development of OPCs to OLs. Additionally, *Cdkl5* plays a role in axo-glial communication, which most likely depends on the abnormal neuronal activity as demonstrated by the myelination defect shown by Emx1^{Cre}: *Cdkl5*^{flox} mice. These findings disclose a novel role of CDKL5 activity, likely of pivotal importance for CDD patients' pathology. Moreover, this study strongly encourages the use of MRI to minimally-invasively identify abnormal myelination patterns in individuals with CDD as a biomarker, an urgent clinical need for this condition. Finally, our preclinical evidence that activation of mGluR5 signaling sharply improves critical signs in *Cdkl5* mutant mice opens novel therapeutic avenues for the treatment of this, and hopefully others, devastating condition.

7. BIBLIOGRAPHY

Aloisi E, Corf K Le, Dupuis J, Zhang P, Ginger M, Labrousse V, Spatuzza M, Haberl MG, Costa L, Shigemoto R, Tappe-theodor A, Drago F, Piazza PV, Mulle C, Groc L, Ciranna L, Catania MV, Frick A. n.d. in Fmr1 knockout mice. *Nat Commun*. doi:10.1038/s41467-017-01191-2

Amendola E, Zhan Y, Mattucci C, Castroflorio E, Calcagno E, Fuchs C, Lonetti G, Silingardi D, Vyssotski AL, Farley D, Ciani E, Pizzorusso T, Giustetto M, Gross CT. 2014a. Mapping pathological phenotypes in a mouse model of CDKL5 disorder. *PLoS One* **9**:5–16. doi:10.1371/journal.pone.0091613

Amendola E, Zhan Y, Mattucci C, Castroflorio E, Calcagno E, Fuchs C, Lonetti G, Silingardi D, Vyssotski AL, Farley D, Ciani E, Pizzorusso T, Giustetto M, Gross CT. 2014b. Mapping pathological phenotypes in a mouse model of CDKL5 disorder. *PLoS One* **9**:e91613. doi:10.1371/journal.pone.0091613

Auerbach BD, Osterweil EK, Bear MF. 2011. Mutations causing syndromic autism define an axis of synaptic pathophysiology. *Nature* **480**:63–68. doi:10.1038/nature10658

Bahi-Buisson N, Bienvenu T. 2012. CDKL5-Related Disorders: From Clinical Description to Molecular Genetics. *Mol Syndromol* **2**:137–152. doi:10.1159/000331333

Bahi-Buisson N, Nectoux J, Rosas-Vargas H, Milh M, Boddaert N, Girard B, Cances C, Ville D, Afenjar A, Rio M, Héron D, N'Guyen Morel MA, Arzimanoglou A, Philippe C, Jonveaux P, Chelly J, Bienvenu T. 2008. Key clinical features to identify girls with CDKL5 mutations. *Brain* **131**:2647–2661. doi:10.1093/brain/awn197

Bakhti M, Snaidero N, Schneider D, Aggarwal S, Möbius W, Janshoff A. 2013. Loss of electrostatic cell-surface repulsion mediates myelin membrane adhesion and compaction in the central nervous system. doi:10.1073/pnas.1220104110

Ballester-rosado XCJ, Sun H, Huang J, Lu H. 2016. mGluR5 Exerts Cell-Autonomous Influences on the Functional and Anatomical Development of Layer IV Cortical Neurons in the Mouse Primary Somatosensory Cortex **36**:8802–8814. doi:10.1523/JNEUROSCI.1224-16.2016

Baltussen LL, Negraes PD, Silvestre M, Claxton S, Moeskops M, Christodoulou E, Flynn HR, Snijders AP, Muotri AR, Ultanir SK. 2018. Chemical genetic identification of CDKL 5 substrates reveals its role in neuronal microtubule

dynamics . *EMBO J* **37**:1–18. doi:10.15252/embj.201899763

Bansal R, Goebbels S, Nave K, Kochanek PM. 2014. NIH Public Access **61**:1595–1606. doi:10.1002/glia.22523.Role

Barbiero I, Valente D, Chandola C, Magi F, Bergo A, Monteonofrio L, Tramarin M, Fazzari M, Soddu S, Landsberger N, Rinaldo C, Kilstrup-Nielsen C. 2017. CDKL5 localizes at the centrosome and midbody and is required for faithful cell division. *Sci Rep* **7**:6228. doi:10.1038/s41598-017-05875-z

Barbin G, Charles P. 2005. Axonal signals in central nervous system myelination , demyelination and remyelination **233**:67–71. doi:10.1016/j.jns.2005.03.029

Bibat G, Zhan A, Farage L, Horska A, Mori S. 2010. White Matter Impairment in Rett Syndrome : 295–299. doi:10.3174/ajnr.A1792

Bongarzone ER, Jacobs E, Schonmann V, Kampf K, Campagnoni CW, Campagnoni AT. 2001. Differential Sensitivity in the Survival of Oligodendrocyte Cell Lines to Overexpression of Myelin Proteolipid Protein Gene Products **492**:485–492.

Bordeleau M, Fernández de Cossío L, Lacabanne C, Savage JC, Vernoux N, Chakravarty M, Tremblay M-È. 2021. Maternal high-fat diet modifies myelin organization, microglial interactions, and results in social memory and sensorimotor gating deficits in adolescent mouse offspring. *Brain, Behav Immun - Heal* **15**:100281. doi:https://doi.org/10.1016/j.bbih.2021.100281

Brand BA, Blesson AE, Smith-hicks CL. 2021. brain sciences The Impact of X-Chromosome Inactivation on Phenotypic Expression of X-Linked Neurodevelopmental Disorders.

Cainelli E, Bisiacchi P. 2022. Neurodevelopmental Disorders: Past, Present, and Future. *Child (Basel, Switzerland)* **10**. doi:10.3390/children10010031

Castelo-branco G, Liu J. 2020. Epigenetic regulation of oligodendrocyte differentiation : From development to demyelinating disorders 1619–1630. doi:10.1002/glia.23820

Chen C, Lu H, Brumberg JC. 2010. mGluR5 Knockout Mice Display Increased Dendritic Spine Densities 1–6.

Chernoff GF. 1981. Shiverer: an autosomal recessive mutant mouse with myelin deficiency. *J Hered* **72**:128. doi:10.1093/oxfordjournals.jhered.a109442

Confort-gouny S, Le Y, Villard L, Cozzone PJ. 2006. Brain magnetic resonance study of Mecp2 deletion effects on anatomy and metabolism **340**:776–783. doi:10.1016/j.bbrc.2005.12.080

de Oliveira LS, O'Leary HE, Nawaz S, Loureiro R, Davenport EC, Baxter P, Dando OR, Perkins E, Booker SA, Hardingham GE, Cousin MA, Chattarji S, Benke TA, Wyllie DJA, Kind PC. 2022. Enhanced hippocampal LTP but typical NMDA receptor and AMPA receptor function in a novel rat model of CDKL5 deficiency disorder. *bioRxiv* 2022.06.29.497927. doi:10.1101/2022.06.29.497927

Delarasse C, Daubas P, Mars LT, Vizler C, Litzenburger T, Iglesias A, Bauer J, Gaspera B Della, Schubart A, Decker L, Dimitri D, Roussel G, Dierich A, Amor S, Dautigny A, Liblau R, Pham-dinh D. 2003. Myelin / oligodendrocyte glycoprotein – deficient (MOG-deficient) mice reveal lack of immune tolerance to MOG in wild-type mice **112**. doi:10.1172/JCI200315861.Introduction

Demarest S, Pestana-Knight EM, Olson HE, Downs J, Marsh ED, Kaufmann WE, Partridge C-A, Leonard H, Gwadry-Sridhar F, Frame KE, Cross JH, Chin RFM, Parikh S, Panzer A, Weisenberg J, Utley K, Jaksha A, Amin S, Khwaja O, Devinsky O, Neul JL, Percy AK, Benke TA. 2019. Severity Assessment in CDKL5 Deficiency Disorder. *Pediatr Neurol* **97**:38–42. doi:10.1016/j.pediatrneurol.2019.03.017

Deoni SCL, Zinkstok JR, Daly E, Ecker C, Williams SCR, Murphy DGM. 2015. White-matter relaxation time and myelin water fraction differences in young adults with autism. *Psychol Med* **45**:795–805. doi:10.1017/S0033291714001858

Duncan GJ, Simkins TJ, Emery B, Duncan GJ. 2021. Neuron-Oligodendrocyte Interactions in the Structure and Integrity of Axons **9**. doi:10.3389/fcell.2021.653101

Durbagula S, Korlimarla A, Ravikumar G. 2022. Prenatal epigenetic factors are predisposing for neurodevelopmental disorders — Considering placenta as a model **114**:20–22. doi:10.1002/bdr2.2119

Edgar JM, Mclaughlin M, Werner HB, Mcculloch MC, Barrie JA, Brown A, Faichney AB, Snaidero N, Nave K, Griffiths IANR. 2009. Early Ultrastructural Defects of Axons and Axon – Glia Junctions in Mice Lacking Expression of Cnp1 **1824**:1815–1824. doi:10.1002/glia.20893

Emery B, Agalliu D, Cahoy JD, Watkins TA, Dugas JC, Mulinyawe SB, Ibrahim A, Ligon KL, Rowitch DH, Barres BA. 2009. Myelin Gene Regulatory Factor Is a Critical Transcriptional Regulator Required for CNS Myelination. *Cell* **138**:172–185. doi:10.1016/j.cell.2009.04.031

Fehr S, Wilson M, Downs J, Williams S, Murgia A, Sartori S, Vecchi M, Ho G, Polli R,

Psoni S, Bao X, de Klerk N, Leonard H, Christodoulou J. 2013. The CDKL5 disorder is an independent clinical entity associated with early-onset encephalopathy. *Eur J Hum Genet* **21**:266–273. doi:10.1038/ejhg.2012.156

Fichou Y, Nectoux J, Bahi-Buisson N, Chelly J, Bienvenu T. 2011. An isoform of the severe encephalopathy-related CDKL5 gene, including a novel exon with extremely high sequence conservation, is specifically expressed in brain. *J Hum Genet* **56**:52–57. doi:10.1038/jhg.2010.143

Fuchs C, Gennaccaro L, Trazzi S, Bastianini S, Bettini S, Lo Martire V, Ren E, Medici G, Zoccoli G, Rimondini R, Ciani E. 2018. Heterozygous CDKL5 Knockout Female Mice Are a Valuable Animal Model for CDKL5 Disorder. *Neural Plast* **2018**:9726950. doi:10.1155/2018/9726950

Fuchs C, Rimondini R, Viggiano R, Trazzi S, De Franceschi M, Bartesaghi R, Ciani E. 2015. Inhibition of GSK3β rescues hippocampal development and learning in a mouse model of CDKL5 disorder. *Neurobiol Dis* **82**:298–310. doi:10.1016/j.nbd.2015.06.018

Fuchs C, Trazzi S, Torricella R, Viggiano R, De Franceschi M, Amendola E, Gross C, Calzà L, Bartesaghi R, Ciani E. 2014a. Loss of CDKL5 impairs survival and dendritic growth of newborn neurons by altering AKT/GSK-3β signaling. *Neurobiol Dis* **70**:53–68. doi:10.1016/j.nbd.2014.06.006

Fuchs C, Trazzi S, Torricella R, Viggiano R, Franceschi M De, Amendola E, Gross C, Calzà L, Bartesaghi R, Ciani E. 2014b. Neurobiology of Disease Loss of CDKL5 impairs survival and dendritic growth of newborn neurons by altering AKT / GSK-3 β signaling. *Neurobiol Dis* **70**:53–68. doi:10.1016/j.nbd.2014.06.006

Fulton D, Paez PM, Campagnoni AT. 2010. The multiple roles of myelin protein genes during the development of the oligodendrocyte **2**:25–37. doi:10.1042/AN20090051

Gafson AR, Barthe NR, Bomont P, Carare RO, Durham HD, Julien J, Kuhle J, Leppert D. 2020. Neurofilaments : neurobiological foundations for biomarker applications. doi:10.1093/brain/awaa098

Galvani G, Mottolese N, Gennaccaro L, Loi M, Medici G, Tassinari M, Fuchs C, Ciani E, Trazzi S. 2021. Inhibition of microglia overactivation restores neuronal survival in a mouse model of CDKL5 deficiency disorder. *J Neuroinflammation* **18**:155. doi:10.1186/s12974-021-02204-0

Galvez-contreras AY, Zarate-lopez D, Torres-chavez AL. 2020. brain sciences Role of

Oligodendrocytes and Myelin in the Pathophysiology of Autism Spectrum Disorder.

Giulio Srubek T, Morello N, Eleonora C, Giustetto M. 2014. * Department of Neuroscience, University of Turin, Turin, Italy † National Institute of Neuroscience-Italy, Turin, Italy 115–127. doi:10.1111/jnc.12803

Grasso S, Chapelle J, Salemme V, Aramu S, Russo I, Vitale N, Di Cantogno LV, Dallaglio K, Castellano I, Amici A, Centonze G, Sharma N, Lunardi S, Cabodi S, Cavallo F, Lamolinara A, Stramucci L, Moiso E, Provero P, Albini A, Sapino A, Staaf J, Di Fiore PP, Bertalot G, Pece S, Tosoni D, Confalonieri S, Iezzi M, Di Stefano P, Turco E, Defilippi P. 2017. The scaffold protein p140Cap limits ERBB2-mediated breast cancer progression interfering with Rac GTPase-controlled circuitries. *Nat Commun* **8**. doi:10.1038/ncomms14797

Gudz TI, Komuro H, Macklin WB. 2006. Glutamate Stimulates Oligodendrocyte Progenitor Migration Mediated via an ␣ v Integrin / Myelin Proteolipid Protein Complex **26**:2458–2466. doi:10.1523/JNEUROSCI.4054-05.2006

Gurgone A, Pizzo R, Raspanti A, Chiantia G, Devi S, Comai D, Morello N, Pilotto F, Gnavi S, Lupori L, Mazziotti R, Sagona G, Putignano E, Nocentini A, Supuran CT, Marcantoni A, Pizzorusso T, Giustetto M. 2022. mGluR5 PAMs rescue cortical and behavioural defects in a mouse model of CDKL5 deficiency disorder. *Neuropsychopharmacology* 1–10. doi:10.1038/s41386-022-01412-3

Hagebeuk EEO, Marcelis CL, Alders M, Kaspers A, de Weerd AW. 2015. Two Siblings With a CDKL5 Mutation: Genotype and Phenotype Evaluation. *J Child Neurol* **30**:1515–1519. doi:10.1177/0883073815573317

Haigh SM, Eack SM, Keller T, Minshew NJ, Behrmann M. 2019. White matter structure in schizophrenia and autism: Abnormal diffusion across the brain in schizophrenia. *Neuropsychologia* **135**:107233. doi:10.1016/j.neuropsychologia.2019.107233

Hanefeld F. 1985. The clinical pattern of the Rett syndrome. *Brain Dev* **7**:320–325. doi:10.1016/s0387-7604(85)80037-1

Harauz G, Boggs JM. 2013. myelin basic protein isoforms **125**:334–361. doi:10.1111/jnc.12195.Myelin

Hardt R, Jordans S, Winter D, Gieselmann V, Wang-eckhardt L, Eckhardt M. 2020. Decreased turnover of the CNS myelin protein Opalin in a mouse model of

hereditary spastic paraplegia 35 **29**:3616–3630. doi:10.1093/hmg/ddaa246

Harlow DE, Saul KE, Komuro H, Macklin WB. 2015. Myelin Proteolipid Protein Complexes with ␣ v Integrin and AMPA Receptors In Vivo and Regulates AMPA-Dependent Oligodendrocyte Progenitor Cell Migration through the Modulation of Cell-Surface GluR2 Expression **35**:12018–12032. doi:10.1523/JNEUROSCI.5151-14.2015

Hartline DK. 2008. What is myelin? *Neuron Glia Biol* **4**:153–163. doi:10.1017/S1740925X09990263

Hector RD, Dando O, Landsberger N, Kilstrup-Nielsen C, Kind PC, Bailey MES, Cobb SR. 2016. Characterisation of CDKL5 Transcript Isoforms in Human and Mouse. *PLoS One* **11**:e0157758. doi:10.1371/journal.pone.0157758

Hedrick TL. n.d. Biomechanical Acclimation : Flying Axonal Domains : Role for Paranodal Junction in Node of Ranvier Assembly **18**:876–879. doi:10.1016/j.cub.2008.07.036

Hinman JD, Abraham ÆCR. 2007. What ' s Behind the Decline ? The Role of White Matter in Brain Aging 2023–2031. doi:10.1007/s11064-007-9341-x

Homberg JR, Kyzar EJ, Nguyen M, Norton WH, Pittman J, Poudel MK, Gaikwad S, Nakamura S, Koshiba M, Yamanouchi H, Scattoni ML, Ullman JFP, Diamond DM, Kaluyeva AA, Parker MO, Klimenko VM, Apryatin SA, Brown RE, Song C, Gainetdinov RR, Gottesman II, Kalueff A V. 2016. Understanding autism and other neurodevelopmental disorders through experimental translational neurobehavioral models. *Neurosci Biobehav Rev* **65**:292–312. doi:10.1016/j.neubiorev.2016.03.013

Hughes EG, Appel B. 2016. ScienceDirect The cell biology of CNS myelination. *Curr Opin Neurobiol* **39**:93–100. doi:10.1016/j.conb.2016.04.013

Huttner WB, Schiebler W, Greengard P, De Camilli P. 1983. Synapsin I (protein I), a nerve terminal-specific phosphoprotein. III. Its association with synaptic vesicles studied in a highly purified synaptic vesicle preparation. *J Cell Biol* **96**:1374–1388. doi:10.1083/jcb.96.5.1374

Ismail, Fatima Y, Shapiro BK. 2019. What are neurodevelopmental disorders ? : Current Opinion in Neurology 1–9. doi:10.1097/WCO.0000000000000710

Iwasato T, Nomura R, Ando R, Ikeda T, Tanaka M, Itohara S. 2004. Dorsal telencephalon-specific expression of Cre recombinase in PAC transgenic mice.

Genesis **38**:130–138. doi:10.1002/gene.20009

Jahn O, Tenzer S, Werner HB. 2009. Myelin Proteomics : Molecular Anatomy of an Insulating Sheath 55–72. doi:10.1007/s12035-009-8071-2

Jakimiec M, Paprocka J, Śmigiel R. 2020. CDKL5 Deficiency Disorder-A Complex Epileptic Encephalopathy. *Brain Sci* **10**. doi:10.3390/brainsci10020107

Jhang C-L, Huang T-N, Hsueh Y-P, Liao W. 2017. Mice lacking cyclin-dependent kinase-like 5 manifest autistic and ADHD-like behaviors. *Hum Mol Genet* **26**:3922–3934. doi:10.1093/hmg/ddx279

Jin X, Chen X, Xiao L, Chen X. 2017. MeCP2 Deficiency in Neuroglia : New Progress in the Pathogenesis of Rett Syndrome **10**:1–11. doi:10.3389/fnmol.2017.00316

Kammermeier PJ, Worley PF. 2007. Homer 1a uncouples metabotropic glutamate receptor 5 from postsynaptic effectors **104**:6055–6060. doi:10.1073/pnas.0608991104

Kandel ER, Schwartz JH, Thomas M, Siegelbaum SA, Hudspeth AJ, Editor A, Mack S, York N, Tibbetts PE. 2021. Principles of Neural Science . Fifth Edition . Edited by **88**:10–12. doi:10.1086/670559

Katayama S, Sueyoshi N, Inazu T, Kameshita I. 2020. Cyclin-Dependent Kinase-Like 5 (CDKL5): Possible Cellular Signalling Targets and Involvement in CDKL5 Deficiency Disorder. *Neural Plast* **2020**:6970190. doi:10.1155/2020/6970190

Kelly E, Schaeffer SM, Dhamne SC, Lipton JO, Lindemann L, Honer M, Jaeschke G, Super CE, Lammers SHT, Modi ME, Silverman JL, Dreier JR, Kwiatkowski DJ, Rotenberg A, Sahin M. 2018. mGluR5 Modulation of Behavioral and Epileptic Phenotypes in a Mouse Model of Tuberous Sclerosis Complex. *Nat Publ Gr* **43**:1457–1465. doi:10.1038/npp.2017.295

Kilstrup-Nielsen C, Rusconi L, La Montanara P, Ciceri D, Bergo A, Bedogni F, Landsberger N. 2012. What we know and would like to know about CDKL5 and its involvement in epileptic encephalopathy. *Neural Plast* **2012**. doi:10.1155/2012/728267

Kim K, Shin M, Cho H, Kim Y. 2014. Effects of endurance exercise on expressions of glial fibrillary acidic protein and myelin basic protein in developing rats with maternal infection-induced cerebral palsy **10**:9–14.

Koenning M, Jackson S, Hay CM, Faux C, Kilpatrick TJ, Willingham M, Emery B. 2012. Myelin Gene Regulatory Factor Is Required for Maintenance of Myelin and Mature Oligodendrocyte Identity in the Adult CNS **32**:12528–12542.

doi:10.1523/JNEUROSCI.1069-12.2012

Leonard H, Downs J, Benke TA, Swanson L, Olson H, Demarest S. 2022. CDKL5 deficiency disorder: clinical features, diagnosis, and management. *Lancet Neurol* **21**:563–576. doi:10.1016/S1474-4422(22)00035-7

Li P, Li H-X, Jiang H-Y, Zhu L, Wu H-Y, Li J-T, Lai J-H. 2017. Expression of NG2 and platelet-derived growth factor receptor alpha in the developing neonatal rat brain. *Neural Regen Res* **12**:1843–1852. doi:10.4103/1673-5374.219045

Lujan R, Somogyi P. 1996. Perisynaptic Location of Metabot ropic GI utamate Receptors mGluR1 and mGluR5 on Dendrites and Dendritic Spines in the Rat Hippocampus **8**:1488–1500.

Lupori L, Sagona G, Fuchs C, Mazziotti R, Stefanov A, Putignano E, Napoli D, Strettoi E, Ciani E, Pizzorusso T. 2019a. Site-specific abnormalities in the visual system of a mouse model of CDKL5 deficiency disorder. *Hum Mol Genet* **28**:2851–2861. doi:10.1093/hmg/ddz102

Lupori L, Sagona G, Fuchs C, Stefanov A, Putignano E, Napoli D, Strettoi E, Ciani E, Pizzorusso T. 2019b. Site-specific abnormalities in the visual system of a mouse model of CDKL5 deficiency disorder **28**:2851–2861. doi:10.1093/hmg/ddz102

Luyt K, Váradi A, Durant CF, Molnár E. 2006. Oligodendroglial metabotropic glutamate receptors are developmentally regulated and involved in the prevention of apoptosis. *J Neurochem* **99**:641–656. doi:10.1111/j.1471-4159.2006.04103.x

MacKay CI, Wong K, Demarest ST, Benke TA, Downs J, Leonard H. 2021. Exploring genotype-phenotype relationships in the CDKL5 deficiency disorder using an international dataset. *Clin Genet* **99**:157–165. doi:10.1111/cge.13862

Marcantoni A, Cerullo MS, Buxeda P, Tomagra G, Giustetto M, Chiantia G, Carabelli V, Carbone E. 2020. Amyloid Beta42 oligomers up-regulate the excitatory synapses by potentiating presynaptic release while impairing postsynaptic NMDA receptors **11**:2183–2197. doi:10.1113/JP279345

Mari F, Azimonti S, Bertani I, Bolognese F, Colombo E, Caselli R, Scala E, Longo I, Grosso S, Pescucci C, Ariani F, Hayek G, Balestri P, Bergo A, Badaracco G, Zappella M, Broccoli V, Renieri A, Kilstrup-Nielsen C, Landsberger N. 2005. CDKL5 belongs to the same molecular pathway of MeCP2 and it is responsible for the early-onset seizure variant of Rett syndrome. *Hum Mol Genet* **14**:1935–1946. doi:10.1093/hmg/ddi198

Marignier R, Hacohen Y, Cobo-calvo A, Pröbstel A, Aktas O, Alexopoulos H, Amato

M, Asgari N, Paul F, Petzold A, Pittock S, Reindl M, Sato DK, Selmaj K, Siva A, Stankoff B, Tintore M, Traboulsee A, Waters P, Waubant E, Weinshenker B, Derfuss T, Vukusic S, Hemmer B. 2021. Personal View disease **20**. doi:10.1016/S1474-4422(21)00218-0

Massa PT, Wu C, Fecenko-tacka K. 2004. Dysmyelination and Reduced Myelin Basic Protein Gene Expression by Oligodendrocytes of SHP-1-Deficient Mice. doi:10.1002/jnr.20155

Matsuoka T, Ahlberg PE, Kessaris N, Iannarelli P, Dennehy U, Richardson WD, McMahon AP, Koentges G. 2005. Neural crest origins of the neck and shoulder. *Nature* **436**:347–355. doi:10.1038/nature03837

Mazziotti R, Lupori L, Sagona G, Gennaro M, Sala G Della, Putignano E, Pizzorusso T. 2017. Searching for biomarkers of CDKL5 disorder : early-onset visual impairment in CDKL5 mutant mice **26**:2290–2298. doi:10.1093/hmg/ddx119

Me C. 2012. Successful Cognitive Aging in Rats : A Role for mGluR5 Glutamate Receptors , Homer 1 Proteins and Downstream Signaling Pathways **7**. doi:10.1371/journal.pone.0028666

Meschkat M, Steyer AM, Weil MT, Kusch K, Jahn O, Piepkorn L, Agüi-Gonzalez P, Phan NTN, Ruhwedel T, Sadowski B, Rizzoli SO, Werner HB, Ehrenreich H, Nave KA, Möbius W. 2022. White matter integrity in mice requires continuous myelin synthesis at the inner tongue. *Nat Commun* **13**. doi:10.1038/s41467-022-28720-y

Montague P, Mccallion S, Davies RW, Griffi R. 2006. Myelin-Associated Oligodendrocytic Basic Protein : A Family of Abundant CNS Myelin Proteins in Search of a Function 479–487. doi:10.1159/000095110

Montini E, Andolfi G, Caruso A, Buchner G, Walpole SM, Mariani M, Consalez G, Trump D, Ballabio A, Franco B. 1998. Identification and characterization of a novel serine-threonine kinase gene from the Xp22 region. *Genomics* **51**:427–433. doi:10.1006/geno.1998.5391

Morelli A, Ravera S, Panfoli I. 2011. Hypothesis of an Energetic Function for Myelin 179–187. doi:10.1007/s12013-011-9174-8

Morello N, Schina R, Pilotto F, Phillips M, Melani R, Pizzorusso T, Pozzo-miller L, Giustetto M. 2018. Loss of Mecp2 Causes Atypical Synaptic and Molecular Plasticity of Parvalbumin-Expressing Interneurons Reflecting Rett Syndrome – Like Sensorimotor Defects **5**.

Morrison-Levy N, Borlot F, Jain P, Whitney R. 2021. Early-Onset Developmental and Epileptic Encephalopathies of Infancy: An Overview of the Genetic Basis and Clinical Features. *Pediatr Neurol* **116**:85–94. doi:10.1016/j.pediatrneurol.2020.12.001

Moult PR, Gladding CM, Sanderson TM, Fitzjohn SM, Bashir ZI, Molnar E, Collingridge GL. 2006. during Metabotropic Glutamate Receptor-Mediated Long-Term Depression **26**:2544–2554. doi:10.1523/JNEUROSCI.4322-05.2006

Nature LTO. 1994. Initial events of myelination involve Fyn tyrosine kinase signalling **367**:572–576.

Nave K, Werner HB. n.d. Myelination of the Nervous System : Mechanisms and Functions. doi:10.1146/annurev-cellbio-100913-013101

Okuda K, Kobayashi S, Fukaya M, Watanabe A, Murakami T, Hagiwara M, Sato T, Ueno H, Ogonuki N, Komano-Inoue S, Manabe H, Yamaguchi M, Ogura A, Asahara H, Sakagami H, Mizuguchi M, Manabe T, Tanaka T. 2017. CDKL5 controls postsynaptic localization of GluN2B-containing NMDA receptors in the hippocampus and regulates seizure susceptibility. *Neurobiol Dis* **106**:158–170. doi:10.1016/j.nbd.2017.07.002

Okuda K, Takao K, Watanabe A, Miyakawa T, Mizuguchi M, Tanaka T. 2018. Comprehensive behavioral analysis of the Cdkl5 knockout mice revealed significant enhancement in anxiety- and fear-related behaviors and impairment in both acquisition and long-term retention of spatial reference memory. *PLoS One* **13**:e0196587. doi:10.1371/journal.pone.0196587

Olga K, Yulia B, Vassilios P. 2020. The Functions of Mitochondrial 2 , 3 -Cyclic Nucleotide-3 -Phosphodiesterase and Prospects for Its Future.

Olson HE, Demarest ST, Pestana-Knight EM, Swanson LC, Iqbal S, Lal D, Leonard H, Cross JH, Devinsky O, Benke TA. 2019. Cyclin-Dependent Kinase-Like 5 Deficiency Disorder: Clinical Review. *Pediatr Neurol* **97**:18–25. doi:10.1016/j.pediatrneurol.2019.02.015

Pavlowsky A, Zanchi A, Pallotto M, Giustetto M, Chelly J, Sala C, Billuart P. 2010. Neuronal JNK pathway activation by IL-1 is mediated through IL1RAPL1, a protein required for development of cognitive functions. *Commun Integr Biol* **3**:245–247. doi:10.4161/cib.3.3.11414

Pérez-cerdá F, Sánchez-gómez MV, Matute C. 2015. Pío del Río Hortega and the discovery of the oligodendrocytes **9**:7–12. doi:10.3389/fnana.2015.00092

Pirko I. 2012. Biogenesis and Signi fi cance of Central Nervous System Myelin.

Pizzo R, Gurgone A, Castroflorio E, Amendola E, Gross C, Sassoè-pognetto M, Giustetto M. 2016. Lack of Cdkl5 Disrupts the Organization of Excitatory and Inhibitory Synapses and Parvalbumin Interneurons in the Primary Visual Cortex **10**:1–16. doi:10.3389/fncel.2016.00261

Poitelon Y, Kopec AM, Belin S. 2020. Myelin Fat Facts: An Overview of Lipids and Fatty Acid Metabolism. *Cells* **9**. doi:10.3390/cells9040812

Pronker MF, Lemstra S, Snijder J, Heck AJR, Thies-weesie DME, Pasterkamp RJ, Janssen BJC. 2016. adhesion and signalling. *Nat Commun* **7**:1–13. doi:10.1038/ncomms13584

Raasakka A, Kursula P. 2014. 3 ′ -phosphodiesterase : on a highway to structure and function **30**:956–966. doi:10.1007/s12264-013-1437-5

Raskind WH, Williams CA, Hudson LD, Bird TD. 1991. Complete deletion of the proteolipid protein gene (PLP) in a family with X-linked Pelizaeus-Merzbacher disease. *Am J Hum Genet* **49**:1355–1360.

Ricciardi S, Ungaro F, Hambrock M, Rademacher N, Stefanelli G, Brambilla D, Sessa A, Magagnotti C, Bachi A, Giarda E, Verpelli C, Kilstrup-Nielsen C, Sala C, Kalscheuer VM, Broccoli V. 2012. CDKL5 ensures excitatory synapse stability by reinforcing NGL-1-PSD95 interaction in the postsynaptic compartment and is impaired in patient iPSC-derived neurons. *Nat Cell Biol* **14**:911–923. doi:10.1038/ncb2566

Roberts RC, Mccollum LA, Schoonover KE, Mabry SJ, Roche JK, Lahti AC. 2022. Ultrastructural evidence for glutamatergic dysregulation in schizophrenia. *Schizophr Res* **249**:4–15. doi:10.1016/j.schres.2020.01.016

Rusconi L, Salvatoni L, Giudici L, Bertani I, Kilstrup-Nielsen C, Broccoli V, Landsberger N. 2008. CDKL5 expression is modulated during neuronal development and its subcellular distribution is tightly regulated by the C-terminal tail. *J Biol Chem* **283**:30101–30111. doi:10.1074/jbc.M804613200

Ruskamo S, Raasakka A, Pedersen JS, Martel A, Škubník K, Darwish T, Porcar L, Kursula P. 2022. Human myelin proteolipid protein structure and lipid bilayer stacking. *Cell Mol Life Sci* **79**:419. doi:10.1007/s00018-022-04428-6

Ryan M, Ibrahim M, Parmar HA. 2014. Secondary Demyelination D i s o rde r s an d D e s t r u c t i o n o f White Matter Secondary demyelinating disorders White matter Destruction Central nervous system **52**:48105.

Sala G Della, Putignano E, Chelini G, Melani R, Calcagno E, Ratto GM, Amendola E, Gross CT, Giustetto M. 2016. Archival Report Dendritic Spine Instability in a Mouse Model of CDKL5 Disorder Is Rescued by Insulin-like Growth Factor 1. *Biol Psychiatry* **80**:302–311. doi:10.1016/j.biopsych.2015.08.028

Schnaar RL, Lopez PHH. 2009. Myelin-associated glycoprotein and its axonal receptors 1–2. doi:10.1002/jnr.21992

Sehmbi M, Cd R, Minuzzi L, Kapczinski F, Steiner M, Rb S. 2018. Association of intracortical myelin and cognitive function in bipolar I disorder 62–72. doi:10.1111/acps.12875

Sherafat A, Pfeiffer F, Reiss AM, Wood WM. 2021. Microglial Neuropilin-1 trans-regulates oligodendrocyte expansion during development and remyelination.

Sherman DL, Brophy PJ. 2005. MECHANISMS OF AXON ENSHEATHMENT AND MYELIN GROWTH **6**:683–690. doi:10.1038/nrn1743

Simons M, Lyons DA. 2013. Axonal selection and myelin sheath generation in the central nervous system. *Curr Opin Cell Biol* **25**:512–519. doi:10.1016/j.ceb.2013.04.007

Sivilia S, Mangano C, Beggiato S, Giuliani A, Torricella R, Baldassarro VA, Fernandez M, Lorenzini L, Giardino L, Borelli AC, Ferraro L, Calzà L. 2016. CDKL5 knockout leads to altered inhibitory transmission in the cerebellum of adult mice. *Genes Brain Behav* **15**:491–502. doi:10.1111/gbb.12292

Skoff RP, Bessert DA, Cerghet M, Franklin MJ, Rout UK, Nave K, Carlock L, Ghandour MS. 2004. The myelin proteolipid protein gene modulates apoptosis in neural and non-neural tissues 1247–1257. doi:10.1038/sj.cdd.4401498

Snaidero N, Simons M. 2014. Myelination at a glance 2999–3004. doi:10.1242/jcs.151043

Sock E, Wegner M. 2019. Transcriptional control of myelination and remyelination. *Glia* **67**:2153–2165. doi:10.1002/glia.23636

Spampinato SF, Copani A, Nicoletti F, Sortino MA, Caraci F. 2018. Metabotropic glutamate receptors in glial cells: A new potential target for neuroprotection? *Front Mol Neurosci* **11**:1–13. doi:10.3389/fnmol.2018.00414

Stadelmann C, Timmler S, Barrantes-freer A, Simons M. 2022. MYELIN IN THE CENTRAL NERVOUS SYSTEM : STRUCTURE , FUNCTION , AND PATHOLOGY 1381–1431. doi:10.1152/physrev.00031.2018

Tang S, Terzic B, Wang I-TJ, Sarmiento N, Sizov K, Cui Y, Takano H, Marsh ED,

Zhou Z, Coulter DA. 2019. Altered NMDAR signaling underlies autistic-like features in mouse models of CDKL5 deficiency disorder. *Nat Commun* **10**:2655. doi:10.1038/s41467-019-10689-w

Tang S, Wang I-TJ, Yue C, Takano H, Terzic B, Pance K, Lee JY, Cui Y, Coulter DA, Zhou Z. 2017. Loss of CDKL5 in Glutamatergic Neurons Disrupts Hippocampal Microcircuitry and Leads to Memory Impairment in Mice. *J Neurosci Off J Soc Neurosci* **37**:7420–7437. doi:10.1523/JNEUROSCI.0539-17.2017

Tang Y, Wang ZI, Sarwar S, Choi JY, Wang S, Zhang X, Parikh S, Moosa AN, Pestana-Knight E. 2021. Brain morphological abnormalities in children with cyclin-dependent kinase-like 5 deficiency disorder. *Eur J Paediatr Neurol EJPN Off J Eur Paediatr Neurol Soc* **31**:46–53. doi:10.1016/j.ejpn.2021.02.004

Terzic B, Fuccillo M V, Zhou Z, Terzic B, Davatolhagh MF, Ho Y, Tang S, Liu Y, Xia Z, Cui Y, Fuccillo M V. 2021. Temporal manipulation of Cdkl5 reveals essential postdevelopmental functions and reversible CDKL5 deficiency disorder – related deficits Temporal manipulation of Cdkl5 reveals essential postdevelopmental functions and reversible CDKL5 deficiency disorder – related deficits **131**.

Thornton MA, Hughes EG. 2020. Neuron-oligodendroglia interactions: Activity-dependent regulation of cellular signaling. *Neurosci Lett* **727**:134916. doi:10.1016/j.neulet.2020.134916

Trazzi S, Fuchs C, Viggiano R, De Franceschi M, Valli E, Jedynak P, Hansen FK, Perini G, Rimondini R, Kurz T, Bartesaghi R, Ciani E. 2016. HDAC4: a key factor underlying brain developmental alterations in CDKL5 disorder. *Hum Mol Genet* **25**:3887–3907. doi:10.1093/hmg/ddw231

Urdinguio RG, Lopez-serra L, Lopez-nieva P, Alaminos M, Diaz-uriarte R, Fernandez AF, Esteller M. 2008. Mecp2-Null Mice Provide New Neuronal Targets for Rett Syndrome **3**. doi:10.1371/journal.pone.0003669

Valli E, Trazzi S, Fuchs C, Erriquez D, Bartesaghi R, Perini G, Ciani E. 2012. CDKL5, a novel MYCN-repressed gene, blocks cell cycle and promotes differentiation of neuronal cells. *Biochim Biophys Acta* **1819**:1173–1185. doi:10.1016/j.bbagrm.2012.08.001

Van Bergen NJ, Massey S, Quigley A, Rollo B, Harris AR, Kapsa RMI, Christodoulou J. 2022. CDKL5 deficiency disorder: molecular insights and mechanisms of pathogenicity to fast-track therapeutic development. *Biochem Soc Trans* **50**:1207–1224. doi:10.1042/BST20220791

Verpelli C, Dvoretskova E, Vicidomini C, Rossi F, Chiappalone M, Schoen M, Stefano B Di, Mantegazza R, Broccoli V, Bo TM, Dityatev A, Sala C. 2011. Importance of Shank3 Protein in Regulating Metabotropic Glutamate Receptor 5 (mGluR5) Expression and Signaling at. *J Biol Chem* **286**:34839–34850. doi:10.1074/jbc.M111.258384

Vicidomini C, Ponzoni L, Lim D, Schmeisser MJ, Reim D, Morello N, Orellana D, Tozzi A, Durante V, Scalmani P. 2017. Pharmacological enhancement of mGlu5 receptors rescues behavioral de fi cits in SHANK3 knock-out mice. *Nat Publ Gr* 689–702. doi:10.1038/mp.2016.30

Vigli D, Rusconi L, Valenti D, La Montanara P, Cosentino L, Lacivita E, Leopoldo M, Amendola E, Gross C, Landsberger N, Laviola G, Kilstrup-Nielsen C, Vacca RA, De Filippis B. 2019. Rescue of prepulse inhibition deficit and brain mitochondrial dysfunction by pharmacological stimulation of the central serotonin receptor 7 in a mouse model of CDKL5 Deficiency Disorder. *Neuropharmacology* **144**:104–114. doi:10.1016/j.neuropharm.2018.10.018

Vlkolinsky R, Cairns N, Fountoulakis M, Lubec G. 2001. Decreased brain levels of 2 J , 3 J -cyclic nucleotide-3 J -phosphodiesterase in Down syndrome and Alzheimer ' s disease **22**:547–553.

Vora P, Mina R, Namaka M, Frost EE. 2010. A novel transcriptional regulator of myelin gene expression : implications for neurodevelopmental disorders : NeuroReport 1–10. doi:10.1097/WNR.0b013e32833da500

Wang D, Sinn K, Arias-moreno X, Tan W, Cheng G. 2021. Biochemical and Biophysical Research Communications Sirt3 increases CNPase enzymatic activity through deacetylation and facilitating substrate accessibility. *Biochem Biophys Res Commun* **571**:181–187. doi:10.1016/j.bbrc.2021.07.079

Wang H, Zhuo M. 2012. Group I metabotropic glutamate receptor-mediated gene transcription and implications for synaptic plasticity and diseases **3**:1–8. doi:10.3389/fphar.2012.00189

Wang I-TJ, Allen M, Goffin D, Zhu X, Fairless AH, Brodkin ES, Siegel SJ, Marsh ED, Blendy JA, Zhou Z. 2012. Loss of CDKL5 disrupts kinome profile and event-related potentials leading to autistic-like phenotypes in mice. *Proc Natl Acad Sci U S A* **109**:21516–21521. doi:10.1073/pnas.1216988110

Weaving LS, Christodoulou J, Williamson SL, Friend KL, McKenzie OLD, Archer H, Evans J, Clarke A, Pelka GJ, Tam PPL, Watson C, Lahooti H, Ellaway CJ,

Bennetts B, Leonard H, Gécz J. 2004. Mutations of CDKL5 cause a severe neurodevelopmental disorder with infantile spasms and mental retardation. *Am J Hum Genet* **75**:1079–1093. doi:10.1086/426462

Werner HB, Amer-albers EKR, Tenzer S, Ohno-iwashita Y, Monasterio-schrader PDE. 2013. A Critical Role for the Cholesterol-Associated Proteolipids PLP and M6B in Myelination of the Central Nervous System **586**:567–586. doi:10.1002/glia.22456

Williamson SL, Giudici L, Kilstrup-Nielsen C, Gold W, Pelka GJ, Tam PPL, Grimm A, Prodi D, Landsberger N, Christodoulou J. 2012. A novel transcript of cyclin-dependent kinase-like 5 (CDKL5) has an alternative C-terminus and is the predominant transcript in brain. *Hum Genet* **131**:187–200. doi:10.1007/s00439-011-1058-x

Wolf NI. 2021. Hypomyelinating leukodystrophies — unravelling myelin biology. *Nat Rev Neurol* **17**. doi:10.1038/s41582-020-00432-1

Yool D, Montague P, McLaughlin M, McCulloch MC, Edgar JM, Nave K-A, Davies RW, Griffiths IR, McCallion AS. 2002. Phenotypic analysis of mice deficient in the major myelin protein MOBP, and evidence for a novel Mobp isoform. *Glia* **39**:256–267. doi:10.1002/glia.10103

Yoshikawa F, Sato Y, Tohyama K, Akagi T, Furuse T, Sadakata T, Tanaka M, Shinoda Y, Hashikawa T, Furuichi T. 2016. Mammalian-Specific Central Myelin Protein Opalin Is Redundant for Normal Myelination : Structural and Behavioral Assessments 1–18. doi:10.1371/journal.pone.0166732

Yuan A, Rao M V., Veeranna, Nixon RA. 2017. Neurofilaments and neurofilament proteins in health and disease. *Cold Spring Harb Perspect Biol* **9**. doi:10.1101/cshperspect.a018309

Zhang Ye, Chen K, Sloan SA, Bennett ML, Scholze AR, O'Keeffe S, Phatnani HP, Guarnieri P, Caneda C, Ruderisch N, Deng S, Liddelow SA, Zhang C, Daneman R, Maniatis T, Barres BA, Wu JQ. 2014. An RNA-sequencing transcriptome and splicing database of glia, neurons, and vascular cells of the cerebral cortex. *J Neurosci* **34**:11929–11947. doi:10.1523/JNEUROSCI.1860-14.2014

Zhang Yonghong, Matt L, Patriarchi T, Malik ZA, Chowdhury D, Park DK, Renieri A, Ames JB, Hell JW. 2014. Capping of the N-terminus of PSD-95 by calmodulin triggers its postsynaptic release. *EMBO J* **33**:1341–1353. doi:10.1002/embj.201488126

Zhang Y, Sloan SA, Clarke LE, Caneda C, Plaza CA, Blumenthal PD, Vogel H,

Steinberg GK, Edwards MSB, Iii JAD, Cheshier SH, Shuer LM, Chang EF, Grant GA, Gephart MGH, Barres BA. 2016. Differences With Mouse. *Neuron* **89**:37–53. doi:10.1016/j.neuron.2015.11.013.Purification

Zhao C, Dong C, Frah M, Deng Y, Marie C, Zhang F, Xu L, Ma Z, Dong X, Lin Y, Koenig S, Nait-Oumesmar B, Martin DM, Wu LN, Xin M, Zhou W, Parras C, Lu QR. 2018. Dual Requirement of CHD8 for Chromatin Landscape Establishment and Histone Methyltransferase Recruitment to Promote CNS Myelination and Repair. *Dev Cell* **45**:753-768.e8. doi:10.1016/j.devcel.2018.05.022

Zhu Y-C, Li D, Wang L, Lu B, Zheng J, Zhao S-L, Zeng R, Xiong Z-Q. 2013. Palmitoylation-dependent CDKL5-PSD-95 interaction regulates synaptic targeting of CDKL5 and dendritic spine development. *Proc Natl Acad Sci U S A* **110**:9118–9123. doi:10.1073/pnas.1300003110

Zhu Y-C, Xiong Z-Q. 2019. Molecular and Synaptic Bases of CDKL5 Disorder. *Dev Neurobiol* **79**:8–19. doi:10.1002/dneu.22639

ANNEXURE:

American College of Neuropsychopharmacology

www.nature.com/npp

ARTICLE

Check for updates

mGluR5 PAMs rescue cortical and behavioural defects in a mouse model of CDKL5 deficiency disorder

Antonia Gurgone[1], Riccardo Pizzo[1], Alessandra Raspanti[1], Giuseppe Chiantia[1], Sunaina Devi[1], Debora Comai[1], Noemi Morello[1], Federica Pilotto[1], Sara Gnavi[1], Leonardo Lupori[2], Raffaele Mazziotti[3], Giulia Sagona[4], Elena Putignano[5], Alessio Nocentini[6], Claudiu T. Supuran[6], Andrea Marcantoni[7], Tommaso Pizzorusso[2,5] and Maurizio Giustetto[1]✉

Cyclin-dependent kinase-like 5 (CDKL5) deficiency disorder (CDD) is a devastating rare neurodevelopmental disease without a cure, caused by mutations of the serine/threonine kinase CDKL5 highly expressed in the forebrain. CDD is characterized by early-onset seizures, severe intellectual disabilities, autistic-like traits, sensorimotor and cortical visual impairments (CVI). The lack of an effective therapeutic strategy for CDD urgently demands the identification of novel druggable targets potentially relevant for CDD pathophysiology. To this aim, we studied Class I metabotropic glutamate receptors 5 (mGluR5) because of their important role in the neuropathological signs produced by the lack of CDKL5 in-vivo, such as defective synaptogenesis, dendritic spines formation/maturation, synaptic transmission and plasticity. Importantly, mGluR5 function strictly depends on the correct expression of the postsynaptic protein Homer1bc that we previously found atypical in the cerebral cortex of Cdkl5$^{-/y}$ mice. In this study, we reveal that CDKL5 loss tampers with (i) the binding strength of Homer1bc-mGluR5 complexes, (ii) the synaptic localization of mGluR5 and (iii) the mGluR5-mediated enhancement of NMDA-induced neuronal responses. Importantly, we showed that the stimulation of mGluR5 activity by administering in mice specific positive-allosteric-modulators (PAMs), i.e., 3-Cyano-N-(1,3-diphenyl-1H-pyrazol-5-yl)benzamide (CDPPB) or RO6807794, corrected the synaptic, functional and behavioral defects shown by Cdkl5$^{-/y}$ mice. Notably, in the visual cortex of 2 CDD patients we found changes in synaptic organization that recapitulate those of mutant CDKL5 mice, including the reduced expression of mGluR5, suggesting that these receptors represent a promising therapeutic target for CDD.

Neuropsychopharmacology; https://doi.org/10.1038/s41386-022-01412-3

INTRODUCTION

CDKL5 is a serine/threonine kinase highly expressed in the forebrain during the peak of synaptogenesis [1]. CDKL5 phosphorylates several substrates and is involved in a broad variety of cellular processes such as gene expression, neuronal migration, axon outgrowth, dendritic morphogenesis, synapses development and function [2–5]. In the nucleus CDKL5 has been shown to interact with epigenetic factors, such as methyl-CpG-binding protein 2 (MeCP2) and DNA Methyltransferase 1 (DNMT1) [6, 7], nevertheless the role of CDKL5 in regulating gene expression is still not fully understood. Recently, several cytoplasmic targets of CDKL5 phosphorylation, including MAP1S, EB2 and ARHGEF2, have been identified pointing to a major role of this kinase in the control of cytoskeletal function. Moreover, CDKL5 has been found to accumulate at synapses where it can interact with the palmitoylated form of postsynaptic density protein-95 (PSD-95) [8]. The interaction with PSD-95 facilitates the phosphorylation of the adhesion molecule netrin-G1 ligand (NGL-1) [9] promoting the maturation of dendritic spines, i.e., the vast majority of glutamatergic postsynaptic sites in the forebrain, as well as the formation and function of excitatory connections. In addition, Barbiero et al. (2017) [10] showed that IQ motif containing GTPase activating protein 1 (IQGAP1) can interact with CDKL5 and thus mediate the formation of complexes with post-synaptic proteins such as PSD-95 or both AMPA- and NMDA-glutamatergic receptors. Interestingly, shRNA-mediated knockdown of CDKL5 can influence the synaptic expression of the GluA2 subunit [11] further highlighting that the involvement of CDKL5 in glutamatergic neurotransmission is yet to be unfolded.

To study the consequences of the lack of CDKL5 in-vivo, different CDKL5$^{-/y}$ mouse lines have been recently generated [12–14]. These mutants display a broad spectrum of behavioral abnormalities, including hind-limb clasping, motor hyperactivity, abnormal eye tracking, learning and memory deficits, and autistic–like phenotypes [13] closely modeling human CDD [15]. Despite epileptic seizures have so far been reported exclusively in aging heterozygous female mice [16], CDKL5$^{-/y}$ mice exhibit multiple defects recapitulating the disease, such as sensorimotor, visual and auditory impairments [14, 17, 18]. For example, cortical visual impairment (CVI), that is correlated with developmental delay in CDD patients [15], is found in CDKL5 mutant mice starting from P27-P28 both in heterozygous and homozygous animals [14, 17]. Aberrant sensory processing in mice

[1]"Rita Levi-Montalcini" Department of Neuroscience, University of Turin, Turin, Italy. [2]BIO@SNS lab, Scuola Normale Superiore, 56124 Pisa, Italy. [3]Department of Developmental Neuroscience, IRCCS Stella Maris Foundation, 56128 Pisa, Italy. [4]NEUROFARBA, Department of Neuroscience, Psychology, Drug Research and Child Health, University of Florence, 50135 Florence, Italy. [5]Institute of Neuroscience, CNR, 56124 Pisa, Italy. [6]NEUROFARBA Department, Section of Pharmaceutical and Nutraceutical Sciences, University of Florence, 50019 Sesto Fiorentino, Florence, Italy. [7]Department of Drug Science, University of Turin, Turin, Italy. ✉email: maurizio.giustetto@unito.it

Received: 4 February 2022 Revised: 4 July 2022 Accepted: 19 July 2022
Published online: 09 August 2022

SPRINGER NATURE

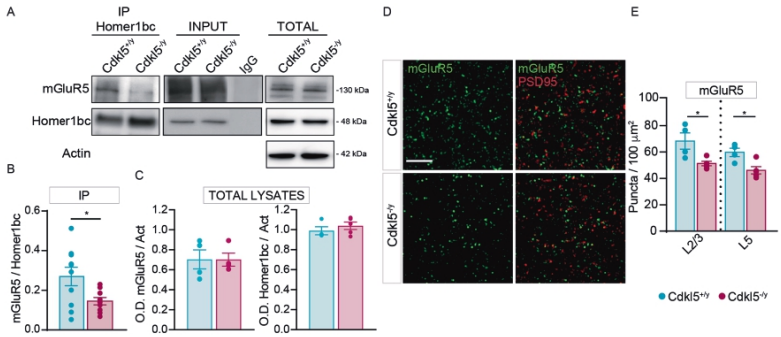

Fig. 1 CDKL5 loss is responsible for both the disruption of mGluR5-Homer1bc interaction and the reduction of mGluR5 localization in the cortical neuropil. A Co-IP of cortical synaptosomal fraction (P2) from P56 mice by using anti-Homer1bc. IgG: control lane in the absence of antibodies. Immunoprecipitates, inputs (P2) and total cortical lysates were analyzed by immunoblotting for mGluR5 and Homer1bc. **B**, **C** Bar graphs showing Co-IP (**B**) and total cortical lysates (**C**) quantitation expressed as optical density (O.D.). **D** Confocal microscopy images showing mGluR5^{+} (green) and PSD-95^{+} (red) immunopuncta in layers II/III of S1 cortex (scale bar: 5 µm). **E** Bar graphs displaying the density of mGluR5^{+} puncta. Student T test *$p < 0.05$ (Co-IP: $n = 8$; WB: $n = 4$ IFL: $n = 4$).

lacking CDKL5 is associated with severe abnormalities of the cerebral cortex, including altered dendritic arborization of pyramidal neurons, the downregulation of the postsynaptic scaffolding proteins PSD-95 and Homer, and the disruption of AKT-mTOR signaling [12, 14, 19–21]. Moreover, we previously reported that CDKL5 plays a key role in the dynamic of dendritic spines turn-over in the primary somatosensory (S1) cortex [19] by promoting their stabilization. In addition, S1 cortex of CDKL5$^{-/y}$ mice show impaired excitatory synaptic transmission and maintenance of long-term potentiation induced by theta-burst stimulation, emphasizing the role of CDKL5 in excitatory cortical connectivity [18, 19].

Given all the above, we reasoned that identifying druggable targets with relevant synaptic function will speed up the discovery of novel therapeutic options for CDD. Here we report that both the expression and function of a member of group I metabotropic glutamate receptors, mGluR5, are abnormal in Cdkl5$^{-/y}$ mice cerebral cortex and that the administration of selective mGluR5 positive allosteric modulators (PAMs) can rescue synaptic, cellular, functional and behavioural defects shown by mutant mice.

MATERIALS AND METHODS

All procedures were performed in accordance with the European Community Council Directive 2010/63/UE for care and use of experimental animals with protocols approved by the Italian Minister for Scientific Research (Authorization number 175/2015-PR) and the Bioethics Committee of the University of Torino, Italy. Complete methods, experimental procedures and statistics are reported in the Supplementary Materials section.

All data values are reported in Table S1. Statistical analysis and the n for each experimental group are reported in figure legends.

RESULTS

Altered mGluR5/Homer1bc organization in the cerebral cortex of Cdkl5$^{-/y}$ mice

We focused on mGluR5 because of their role in mechanisms involved in CDD such as synaptogenesis, dendritic spines formation/maturation and synaptic plasticity [22–25]. Moreover, mGluR5 must interact with Homer1bc, that is downregulated in the cortex of Cdkl5$^{-/y}$ mice [17, 20], to exert signaling functions within the PSD [26–29]. First, we evaluated the strength of mGluR5-Homer1bc binding in mutant mice. Intriguingly, co-immunoprecipitation (co-IP) assays of cortical synaptosomal fraction (Fig. 1A) revealed that the amount of mGluR5 immunoprecipitated with Homer1bc was significantly reduced in Cdkl5$^{-/y}$ mice compared to Cdkl5$^{+/y}$ animals (O.D mGluR5/Homer1bc *$p < 0.05$; Fig. 1B), while the total amount of both Homer1bc and mGluR5 did not change between genotypes (O.D mGluR5/Act and O.D Homer1b/Act $p > 0.05$; Fig. 1C).

We next assessed mGluR5 expression in the neuropil by performing immunofluorescence experiments on S1 cortices from Cdkl5$^{-/y}$ and Cdkl5$^{+/y}$ mice (Fig. 1D). By using a fixation/staining protocol improved for postsynaptic protein localization [21, 30], mGluR5 immunofluorescence (Fig. 1D) resulted in discrete puncta that were found closely localized, but only rarely overlapping, with PSD-95^{+} puncta in agreement with previously reported perisynaptic localization of mGluR5 [31]. Interestingly, the density of mGluR5-puncta was strongly reduced in layers II-III and V of S1cortex in Cdkl5$^{-/y}$ mice compared to controls (layers II-III and V *$p < 0.05$; Fig. 1D, E). These data indicate that Cdkl5 loss interferes with Homer1bc-dependent insertion/stabilization of mGluR5 in the postsynaptic membrane.

Excitatory neurotransmission and mGluR5-mediated signaling are severely disrupted in Cdkl5$^{-/y}$ cortical neurons

Our data suggest that mGluR5 function might be compromised in the absence of CDKL5 [32, 33]. To test this idea, we recorded spontaneous miniature excitatory postsynaptic currents (mEPSCs) in neuronal cultures of the S1 cortex from both Cdkl5$^{+/y}$ and Cdkl5$^{-/y}$ mice (Fig. 2A–D, upper part), before and after mGluR5 activation. As we reported previously in acute cortical slices [19], mEPSCs recorded from CDKL5-null neurons showed an increased inter-event interval (IEI) (Cdkl5$^{+/y}$ vs Cdkl5$^{-/y}$ *$p < 0.05$; Fig. 2D) while the mean peak amplitude was similar between genotypes (Cdkl5$^{+/y}$ vs Cdkl5$^{-/y}$ $p > 0.05$; Fig. 2C). Intriguingly, 2-minutes stimulation with the selective mGluR5 agonist DHPG (100 µM) produced a significant increase in the IEI of mEPSCs in Cdkl5$^{+/y}$ cultures [34, 35] but not in Cdkl5$^{-/y}$ neurons (Fig. 2E).

Next, we tested NMDA-mediated responses because these receptors activity can be modulated by mGluR5 [36]. When NMDA currents were elicited by the application of NMDA (50 µM) [37], Cdkl5$^{-/y}$ cultures showed a significant reduction of I_{NMDA} compared to Cdkl5$^{+/y}$ neurons (Cdkl5$^{+/y}$ vs Cdkl5$^{-/y}$ **$p < 0.01$; Fig. 2F). Intriguingly, the application of NMDA together with DHPG

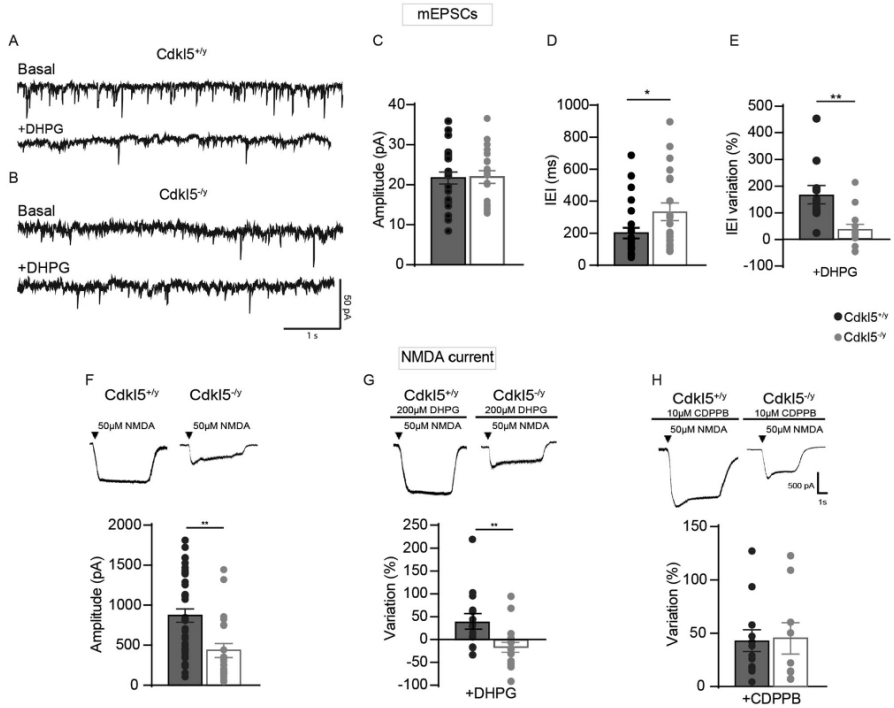

Fig. 2 CDKL5 loss tampers with both mEPSCs and NMDA current. A Sample traces of miniature excitatory postsynaptic current (mEPSC) recorded from Cdkl5$^{+/y}$ neurons (**A**, upper part) and Cdkl5$^{-/y}$ neurons (**B**, upper part) and after the application of DHPG (**A**, **B** lower part). **C**, **D** Bar graphs showing the mean average amplitude (**C**) and the inter-event interval (IEI) of mEPSCs (**D**). **E** Bar graphs displaying the % of IEI variation IEI after the application of DHPG (100 μM). **F** Representative traces of currents obtained with patch-clamp recordings on S1 neurons cultures from Cdkl5$^{+/y}$ and Cdkl5$^{-/y}$ embryos after NMDA (50 μM) application (upper part), bar graphs showing differences of I_{NMDA} current between genotypes (lower part). **G** Representative traces of NMDA currents on S1 neurons after 2-min application of DHPG (100 μM-upper part); bar graphs showing the % change of I_{NMDA} after the application of DHPG (lower part). **H** Representative traces of NMDA after 2-min CDPPB + NMDA application (upper part), bar graphs showing the % change of I_{NMDA} current after the application of CDPPB (lower part). Student's t-test, chi-square, two-way ANOVA followed by Fisher's multiple comparison test, *$p < 0.05$, **$p < 0.01$, ***$p < 0.001$ (mEPSC Cdkl5$^{+/y}$ $n = 22$ cells, Cdkl5$^{-/y}$ $n = 28$; minis+DHPG Cdkl5$^{+/y}$: $n = 12$ cells; minis+DHPG Cdkl5$^{-/y}$: $n = 13$ cells. NMDA: Cdkl5$^{+/y}$ $n = 36$ cells, Cdkl5$^{-/y}$ $n = 23$ cells; NMDA + DHPG Cdkl5$^{+/y}$ $n = 15$ cells and NMDA + DHPG Cdkl5$^{-/y}$ $n = 14$ cells; NMDA + CDPPB Cdkl5$^{+/y}$ $n = 12$ cells; NMDA + CDPPB Cdkl5$^{-/y}$ $n = 9$ cells).

(100 μm) increased I_{NMDA} in Cdkl5$^{+/y}$ cells, (Fig. 2G; see also [38]) while it produced a small decrease in Cdkl5$^{-/y}$ neurons, as illustrated by the sharp difference in the percentage of I_{NMDA} variation between genotypes (DHPG-Cdkl5$^{+/y}$ vs DHPG-Cdkl5$^{-/y}$ *$p < 0.05$; Fig. 2G). Strikingly, while 73% of Cdkl5$^{+/y}$ cortical neurons (11/15 cells) showed potentiated I_{NMDA} after the application of DHPG, most of Cdkl5$^{-/y}$ neurons did not respond to DHPG (10/14; 71%) as shown by plotted data (Fig. 2G). These results disclose that loss of CDKL5 disrupts excitatory neurotransmission at multiple sites and severely affects mGluR5 normal function.

CDPPB potentiates NMDAR current in cortical neurons lacking CDKL5

We and others have previously shown that in conditions where I_{NMDA} is not sensitive to DHPG, the application of selective mGluR5 PAMs can instead elicit the strengthening of this current [38, 39]. Among these, 3-Cyano-N-(1,3-diphenyl-1H-pyrazol-5-yl)benzamide (CDPPB) offers several advantages compared to agonist drugs such as higher subtype selectivity, reduced desensitization, and more subtle modulatory effects on receptor function [40]. Thus, we examined the effect produced by CDPPB on cortical neurons by measuring NMDA current. Intriguingly, 2 min bath application of CDPPB (10 μM) preceding NMDA (50 μM) administration produced a comparable increase of I_{NMDA} (Fig. 2F, lower part) in both genotypes (CDPPB-Cdkl5$^{+/y}$ vs CDPPB-Cdkl5$^{-/y}$ $p > 0.05$; Fig. 2H) when compared to the average amplitude of I_{NMDA} measured after administration of NMDA alone. Consistently, in the case of CDPPB application, the majority of both Cdkl5$^{-/y}$ and Cdkl5$^{+/y}$ neurons showed potentiated I_{NMDA} (Cdkl5$^{+/y}$: 13/18, 78%; Cdkl5$^{-/y}$ 10/12, 83%) resulting in a significantly increase compared to DHPG-treated Cdkl5$^{-/y}$ neurons (chi-square DHPG-Cdkl5$^{-/y}$: 29% vs CDPPB-Cdkl5$^{-/y}$: 83% ****$p < 0.0001$). These results show that positive allosteric modulation can rescue mGluR5-

dependent strengthening of NMDA-mediated activation in Cdkl5$^{-/y}$ neurons.

CDPPB treatment ameliorates visual, sensorimotor and memory functions in Cdkl5$^{-/y}$ mice

Encouraged by the positive effects we obtained on synaptic currents, we evaluated the therapeutic potential of CDPPB by treating mice with one intraperitoneal injection (i.p.) of CDPPB (3 mg/Kg), as in Vicidomini et al. (2017) [38], that were subsequently exposed to a battery of tests.

We investigated cortical visual responses by transcranial intrinsic optical signal (IOS) imaging before and after CDPPB administration in the same animals. As expected from our previous data [17, 20], baseline response amplitude of Cdkl5$^{-/y}$ mice was strongly decreased compared to Cdkl5$^{+/y}$ littermates (Cdkl5$^{+/y}$ vs vehicle-Cdkl5$^{-/y}$ / CDPPB-Cdkl5$^{-/y}$ $^{**}p < 0.01$, Fig. 3A, B). After CDPPB treatment, visual responses approached Cdkl5$^{+/y}$ levels (Cdkl5$^{+/y}$ vs CDPPB-Cdkl5$^{-/y}$ post-injection $p = 0.6$; Cdkl5$^{+/y}$ vs vehicle-Cdkl5$^{-/y}$ post-injection $^{*}p < 0.05$) significantly increasing from their baseline values (vehicle-Cdkl5$^{-/y}$ post-injection vs CDPPB-Cdkl5$^{-/y}$ post-injection $^{*}p < 0.05$; CDPPB-Cdkl5$^{-/y}$ baseline vs CDPPB-Cdkl5$^{-/y}$ post-injection $^{*}p < 0.05$; vehicle-Cdkl5$^{-/y}$ baseline vs vehicle-Cdkl5$^{-/y}$ post-injection $p = 0.90$). By contrast, visual response remained impaired in vehicle-treated mutants. These experiments indicate that cortical response to visual stimulation is ameliorated by CDPPB treatment in Cdkl5$^{-/y}$ mice.

When assessed for sensorimotor responses in the adhesive tape-removal test [41, 42], Cdkl5$^{-/y}$ mice displayed a significant increase in time-to-contact the tape compared to Cdkl5$^{+/y}$ mice (vehicle-Cdkl5$^{+/y}$ vs vehicle-Cdkl5$^{-/y}$ $^{**}p < 0.01$; Fig. 3C). Importantly, a single CDPPB injection produced a reduction of the latency exclusively in mutant mice whose performance became similar to controls (vehicle-Cdkl5$^{+/y}$ vs CDPPB-Cdkl5$^{-/y}$ $p > 0.4$; Fig. 3C). Moreover, the number of correct spontaneous alternations in the Y-maze paradigm for working memory was decreased in Cdkl5$^{-/y}$ mice compared to Cdkl5$^{+/y}$ animals (vehicle-Cdkl5$^{+/y}$ vs vehicle-Cdkl5$^{-/y}$ $^{**}p < 0.01$; Fig. 3D), confirming previous observations [43]. Intriguingly, working memory was rescued in Cdkl5$^{-/y}$ mice by CDPPB (vehicle-Cdkl5$^{+/y}$ vs CDPPB-Cdkl5$^{-/y}$ $p > 0.4$; Fig. 3D), while it did not affect memory in Cdkl5$^{+/y}$ mice. Also, total number of arms entries did not change between genotypes under either treated or untreated conditions (Fig. 3E). To assess locomotor activity, we used the open-field test. As previously reported [44], Cdkl5$^{-/y}$ mice showed an increase in both total distance traveled (vehicle-Cdkl5$^{+/y}$ vs vehicle-Cdkl5$^{-/y}$ $^{*}p < 0.05$; Fig. 3F) and speed (vehicle-Cdkl5$^{+/y}$ vs vehicle-Cdkl5$^{-/y}$ $^{*}p < 0.05$; Fig. 3G) that was not changed by CDPPB treatment (vehicle-Cdkl5$^{-/y}$ vs CDPPB-Cdkl5$^{-/y}$ $p > 0.4$; Fig. 3F, G). These data indicate that the action of CDPPB can reverse atypical visual cortical response, sensorimotor and short-term memory impairments in Cdkl5$^{-/y}$ mice, but not locomotor activity.

mGluR5 PAMs rescue both synaptic and activity defects in Cdkl5$^{-/y}$ cerebral cortex

In parallel with the observed behavioral and functional rescues, acute CDPPB treatment normalized both number and organization of postsynaptic sites as well as neuronal activity in primary cortices of Cdkl5$^{-/y}$ mice. CDPPB increased the density of Homer1bc^{+} puncta in both S1 and V1 cortices of Cdkl5$^{-/y}$ mice (S1: layers II-III and V vehicle-Cdkl5$^{-/y}$ vs CDPPB-Cdkl5$^{-/y}$ $^{**}p < 0.01$. V1: layers II-III and V vehicle-Cdkl5$^{-/y}$ vs CDPPB-Cdkl5$^{-/y}$ $^{*}p < 0.05$; Fig. 4A, B), reproducing Cdkl5$^{+/y}$ mice conditions (S1 and V1: layers II-III and V: vehicle-Cdkl5$^{+/y}$ vs CDPPB-Cdkl5$^{-/y}$ $p > 0.3$; Fig. 4A, B). Intriguingly, CDPPB treatment also normalized mGluR5^{+} puncta density in both S1 and V1 cortices of Cdkl5$^{-/y}$ mice (S1: layers II-III and V: vehicle-Cdkl5$^{-/y}$ vs CDPPB-Cdkl5$^{-/y}$ $^{***}p < 0.001$; vehicle-Cdkl5$^{+/y}$ vs CDPPB-Cdkl5$^{-/y}$ $p > 0.3$. V1: layers II-III and V: vehicle-Cdkl5$^{-/y}$ vs CDPPB-Cdkl5$^{-/y}$ $^{*}p < 0.05$. S1 and V1: vehicle-Cdkl5$^{+/y}$ vs CDPPB-Cdkl5$^{-/y}$ $p > 0.3$; Fig. 4C, D). Finally, the density of cells expressing ARC, an immediate-early gene (IEG) induced by mGluR5 activation [45, 46], was restored in the V1 cortex of CDKL5-mutants after a single CDPPB administration (layers I-VI: vehicle-Cdkl5$^{+/y}$ vs vehicle-Cdkl5$^{-/y}$ $^{**}p < 0.01$; vehicle-Cdkl5$^{-/y}$ vs CDPPB-Cdkl5$^{-/y}$ $^{***}p < 0.001$; Fig. 4E, F).

To increase the reproducibility of our study, we treated another group of Cdkl5$^{-/y}$ and Cdkl5$^{+/y}$ animals with a different mGluR5 PAM, the RO6807794 (RO68) compound [47]. Two hours after an i.p. injection with RO68 (0.3 mg/kg as in [45]), the density of Homer1bc^{+} puncta in S1 cortex of Cdkl5$^{-/y}$ mice was increased (S1: layers II-III and V vehicle-Cdkl5$^{-/y}$ vs CDPPB-Cdkl5$^{-/y}$ $^{*}p < 0.05$. V1: layers II-III and V vehicle-Cdkl5$^{-/y}$ vs CDPPB-Cdkl5$^{-/y}$ $^{*}p < 0.05$; Fig. S1A, B) reproducing Cdkl5$^{+/y}$ mice conditions (S1 layers II-III and V: vehicle-Cdkl5$^{+/y}$ vs CDPPB-Cdkl5$^{-/y}$ $p > 0.3$; Fig. S1A, B). Intriguingly, RO68 was also able to restore neuronal activity in S1 cortex in Cdkl5$^{-/y}$ mice (Fig. S1C) throughout cortical layers (vehicle-Cdkl5$^{+/y}$ vs vehicle-Cdkl5$^{-/y}$ $^{***}p < 0.001$; vehicle-Cdkl5$^{-/y}$ vs RO68-Cdkl5$^{-/y}$ $^{***}p < 0.001$), as indicated by c-Fos^{+} cell density (Fig. S1D; see also [21]), that reached the magnitude of Cdkl5$^{+/y}$ mice (vehicle-Cdkl5$^{+/y}$ vs CDPPB-Cdkl5$^{-/y}$ $p > 0.05$). These results strongly support the idea that the atypical circuit organization, both structural and molecular, shown by the cerebral cortex of Cdkl5$^{-/y}$ mice can be rescued by activating mGluR5-mediated signaling.

A protracted treatment with CDPPB effectively restores Cdkl5$^{-/y}$ mice deficits

To assess the therapeutic potential of mGluR5 activation, we treated animals for five consecutive days with CDPPB that 24 h after the last injection were behaviourally tested and then sacrificed for brain analyses. The density of Homer1bc^{+} puncta was restored in both upper and deeper layers of the S1 cortex in treated mutant mice (layers II-III and V: vehicle-Cdkl5$^{-/y}$ vs CDPPB-Cdkl5$^{-/y}$ $^{**}p < 0.01$; Fig. S2A, B), while protracted CDPPB had no effect on Homer1bc expression in Cdkl5$^{+/y}$ animals (layers II-III and V: vehicle-Cdkl5$^{+/y}$ vs CDPPB-Cdkl5$^{+/y}$ $p = 0.9$; Fig. S2B, C). Next, we analysed hind-limb clasping, a sign displayed by Cdkl5$^{-/y}$ mice [5, 12, 46]. In line with previous studies, vehicle-treated mutants showed increased hind-limb clasping compared to controls (vehicle-Cdkl5$^{+/y}$ vs vehicle-Cdkl5$^{-/y}$ $^{***}p < 0.001$; Fig. S2C and [12]) whereas after CDPPB treatment Cdkl5$^{-/y}$ mice spent significantly less time clasping their hind paws (vehicle-Cdkl5$^{-/y}$ vs CDPPB-Cdkl5$^{-/y}$ $^{**}p < 0.01$; Fig. S2C). Moreover, the differences shown by the two genotypes in the adhesive tape-removal test were abolished by 5-days CDPPB treatment (vehicle-Cdkl5$^{+/y}$ vs. CDPPB-Cdkl5$^{-/y}$ $p > 0.7$; Fig. S2D). Intriguingly, visual response was also significantly improved after the prolonged CDPPB treatment. While the baseline response amplitude was strongly reduced in Cdkl5$^{-/y}$ mice compared to Cdkl5$^{+/y}$ littermates (Cdkl5$^{+/y}$ vs vehicle-Cdkl5$^{-/y}$ $^{**}p < 0.01$; Cdkl5$^{+/y}$ vs CDPPB-Cdkl5$^{-/y}$ $^{*}p < 0.05$, fig S2F, G), no differences were shown by the two Cdkl5$^{-/y}$ groups (vehicle-Cdkl5$^{-/y}$ vs pre-CDPPB-Cdkl5$^{-/y}$ $p > 0.3$; Fig. S2F). After CDPPB treatment, mutants showed robust changes in response amplitude (pre-CDPPB-Cdkl5$^{-/y}$ vs post-CDPPB-Cdkl5$^{-/y}$ $^{**}p < 0.01$) highlighting a substantial effect of treatment during time. Importantly, after CDPPB-treatment, Cdkl5$^{-/y}$ mice reached amplitude values significantly different from vehicle-treated mutants (CDPPB-Cdkl5$^{-/y}$ vs vehicle-Cdkl5$^{-/y}$ post-injection $^{**}p < 0.01$).

Finally, we evaluated the effects of sub-chronic CDPPB treatment on cortical activation assessing both c-Fos and ARC expression. Intriguingly, the reduction of IEGs expression shown by mutant mice (c-FOS: vehicle-Cdkl5$^{+/y}$ vs vehicle-Cdkl5$^{-/y}$ $^{**}p < 0.01$ Fig. S2H, I; ARC: vehicle-Cdkl5$^{+/y}$ vs vehicle-Cdkl5$^{-/y}$ $^{**}p < 0.01$; Fig. S2J, K) was abolished by the treatment (c-FOS and ARC vehicle-Cdkl5$^{+/y}$ vs CDPPB-Cdkl5$^{-/y}$ $p > 0.05$; Fig. S2I, K).

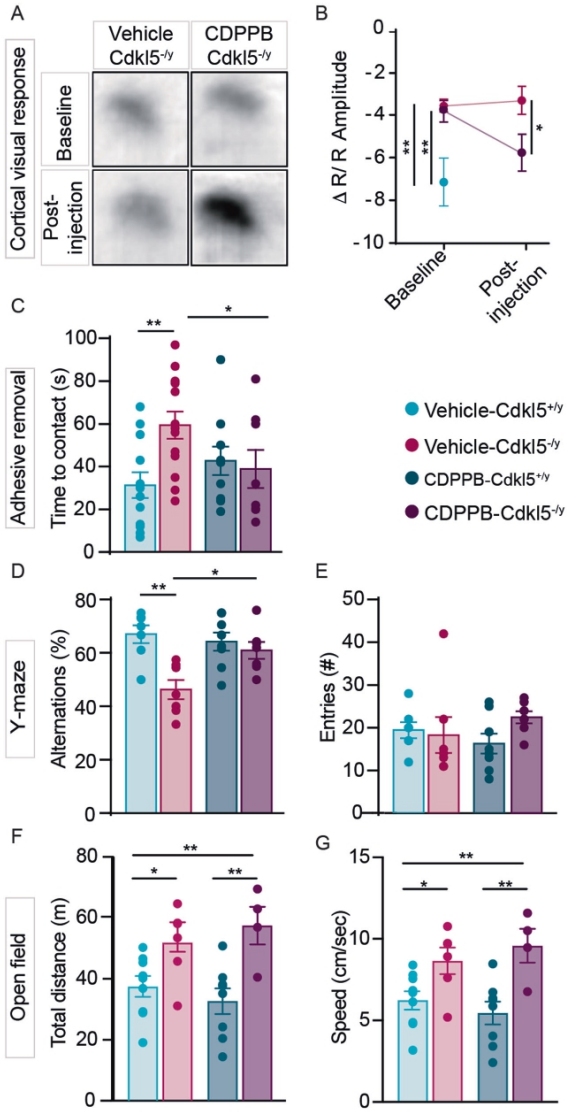

Fig. 3 Acute CDPPB treatment rescues visual response, sensorimotor and memory deficits in Cdkl5-/y mice. A Samples images showing differences of IOS evoked responses in vehicle- and CDPPB-treated Cdkl5$^{-/y}$ mice. **B** Trajectory of the IOS amplitude in vehicle-Cdkl5$^{+/y}$, vehicle-Cdkl5$^{+/y}$ and CDPPB-Cdkl5$^{-/y}$ treated mice. **C** Bar graphs showing contact latency with the tape placed under mice's forepaw. **D**, **E** Bar graphs showing the percentage of the correct alternations (**D**) and the number of entries (**E**) made by Cdkl5$^{+/y}$ and Cdkl5$^{-/y}$ mice, treated with either vehicle or CDPPB, in the Y-maze. **F**, **G** Bar graphs showing the total distance traveled (**F**) and the mean speed (**G**) in the open field arena of mice treated with either vehicle or CDPPB. One-way ANOVA followed by Tukey's multiple comparison; two-way ANOVA followed by Sidak or Bonferroni's multiple comparison test, $*p < 0.05$, $**p < 0.01$ (IOS: vehicle-Cdkl5$^{+/y}$ $n = 3$, vehicle-Cdkl5$^{-/y}$ $n = 8$, CDPPB-Cdkl5$^{-/y}$ $n = 6$; behavioural tests: vehicle-Cdkl5$^{+/y}$ $n = 12$, vehicle-Cdkl5$^{-/y}$ $n = 13$, CDPPB-Cdkl5$^{+/y}$ $n = 8$, CDPPB-Cdkl5$^{-/y}$ $n = 7$).

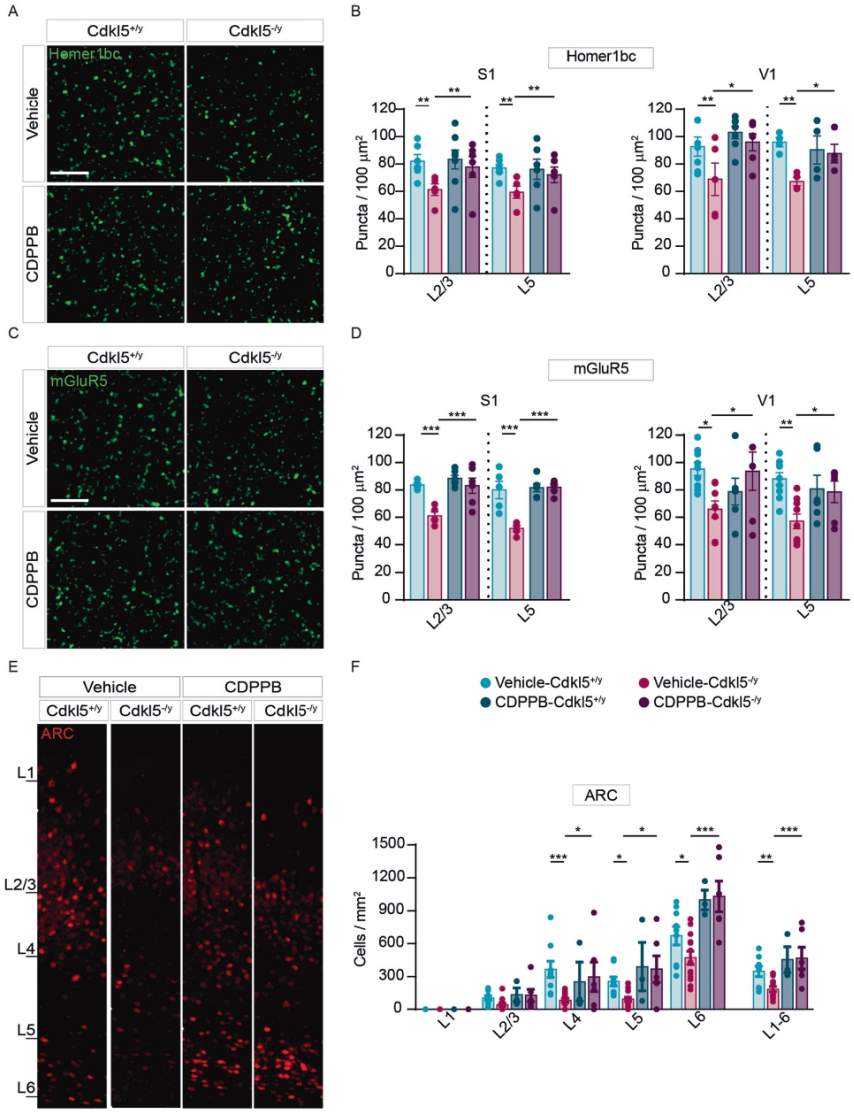

Fig. 4 Structural defects exhibited by Cdkl5-/y mice cortices are rescued by an acute CDPPB injection. A, C Representative confocal images showing Homer1bc^{+} and mGluR5^{+} puncta in layer II-III of S1 cortex from either vehicle- or CDPPB-treated mice (scale bar: 5 µm). **B, D** Bar graphs showing both Homer1bc^{+} (**B**) and mGluR5^{+} (**D**) immunopuncta density in layers II-III and V of both S1 and V1 cortices in either vehicle- or CDPPB-treated mice. **E** Confocal images of ARC immunostaining on coronal sections of the V1 cortex from mice treated with vehicle or CDPPB (scale bar: 25 µm), and relative ARC^{+} cells density quantitation (**F**) throughout the cortical layers. Two-way ANOVA followed by Fisher's multiple comparison test, $*p < 0.05$, $**p < 0.01$, $***p < 0.001$; ($n = 6$ animals for each genotype).

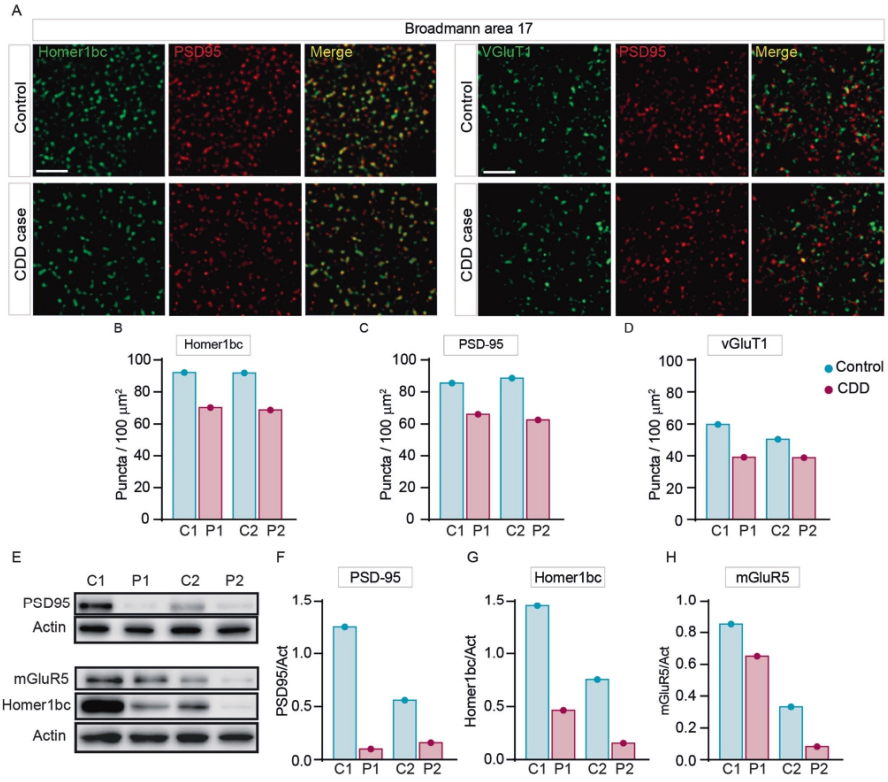

Fig. 5 Aberrant expression of excitatory synaptic proteins in the BA17 cortex of CDD patients. A Illustrative confocal images taken from layers II-III of the BA17 cortex. (**A**) PSD-95^{+}(red), Homer1bc^{+}(green), VGluT1^{+}(green) immunofluorescence puncta. Note the virtually complete overlapping of PSD-95 and Homer1bc immunofluorescence (scale bar: 5 µm). **B**–**D** Bar graphs showing the analysis of puncta density in layers II-III of BA17 cortices. **E** Western blotting showing the expression of PSD-95, Homer1bc and mGluR5 in lysates from BA17 cortices. **F**–**H** Bar graphs displaying the optical density (O.D.) analysis of PSD-95 (**F**), Homer1bc (**G**) and mGluR5 (**H**) expression. Student's t-test, $*p < 0.05$, $**p < 0.01$ (C1 = F, 4 years old; P1 = F, 5.7 years old; C2 = F, 29 years old; P2 = F, 30 years old).

The BA17 cortex of CDD patients recapitulates the synaptic defects shown by Cdkl5$^{-/y}$ mice

To assess the translational potential of our findings, we examined excitatory synaptic structures in the 2 postmortem CDD patient brains available worldwide that were obtained from the Harvard Brain Tissue Resource Center (Belmont; USA). These experiments were performed on sections from the primary visual cortex (BA17) of CDD cases and age/sex-matched neurotypical controls. Intriguingly, the results showed a clear reduction of both postsynaptic proteins PSD-95^{+} and Homer1bc^{+} as well as of the presynaptic marker VGluT1^{+}, irrespective of case age (5 and 30 years old), compared to NTs (Fig. 5A). Moreover, although a statistical comparison was not performed with only 2 cases, the analysis of immunopuncta revealed a reduction in the cortices of CDD patients with respect to controls (Fig. 5A–D), indicative of an overall reduction of glutamatergic synapses. We next evaluated Homer1bc, PSD-95 and mGluR5 expression by western blotting on BA17 cortical lysates. Intriguingly, as shown in Fig. 5E–H, the BA17 area from CDD samples showed a robust reduction of their expression compared to controls. Although derived from a limited dataset, these results suggest that both structural and molecular signatures of CDKL5 loss in the cerebral cortex largely overlap between mice and humans and support the translational potential of a mGluR5-directed therapeutic strategy.

DISCUSSION

It is urgent to find therapeutic targets that shall be rapidly translated into treatments for CDD, a devastating condition without corrective options. In this study, we focus our attention on mGluR5, a group I metabotropic glutamate receptor highly expressed in the cerebral cortex of both mice and humans [48]. To properly function, mGluR5 requires binding with Homer1bc [32], a scaffolding protein that is severely downregulated in the cerebral cortex of both Cdkl5$^{-/y}$ mice and CDD patients [18, 21]; Fig. 5A] as well as in iPSCs-derived neurons from CDD patients [49].

We show for the first time that CDKL5 plays a role in the expression of mGluR5 in the cerebral cortex of both CDD patients and CDKL5 mutant mice, an effect likely produced by the defective formation of mGluR5-Homer1bc complexes at synapses as indicated by our data. Moreover, we revealed that synaptic transmission, both basal and NMDA-mediated, is altered in S1 neurons lacking CDKL5 and that it is unresponsive to the modulation normally produced by the selective mGluR5 agonist DHPG. Because Shank1, by forming complexes with Homer1bc, PSD-95 and NMDAR, promotes the cooperation between NMDAR and mGluR5 signaling machineries [29, 50, 51], our electrophysiological evidence strongly suggest that CDKL5 loss tampers with the synergistic cooperation between these glutamatergic receptors. This effect is likely produced by a reduced amount of Homer1bc recruited in the postsynaptic density in the absence of CDKL5 which, in turn, results in an atypical postsynaptic localization/stabilization of mGluR5. Interestingly, aberrant NMDARs signaling have been previously reported by Okuda and colleagues [13] in the hippocampus of a different CDKL5 mutant mouse line showing severe NMDA-dependent epileptic seizures due to the incorrect postsynaptic accumulation of GluN2B-containing NMDARs [13]. Similar results have been obtained in the hippocampus of the $Cdkl5^{R59X}$ knock-in CDD mouse model [52]. Altogether, although with some differences, these findings further support the idea that CDKL5 plays a crucial role in the correct localization/function of glutamate receptors, both ionotropic and metabotropic, at the synapse. Remarkably, an aberrant expression and function of mGluR5 has been reported in several neurodevelopmental diseases such as Fragile X, Phelan McDermid syndrome, Tuberous sclerosis (TSC) and Rett syndrome [32, 38, 39, 53] further supporting the primary role of mGluR5 signaling as a common deranged pathway in monogenic neurodevelopmental disorders.

The reduced expression/function of mGluR5, combined with relevant synaptic and behavioral signs shown by CDKL5 mutants, provided us with solid bases for attempting the first preclinical assessment of mGluR5 PAMs efficiency for treating CDD that we report in this study. Intriguingly, our results revealed that an acute treatment with CDPPB is effective in restoring several endophenotypes and behavioral signs produced by CDKL5 loss. Our data show that in primary cortical neuronal cultures, CDPPB can restore mGluR5-mediated potentiation of NMDA currents in $Cdkl5^{-/y}$ pyramidal neurons. Considering the negative response of NMDA current to DHPG treatment that we report in mutant neurons, the effect of CDPPB is surprising and still without a clear pharmacological explanation, although it closely replicates what has been found previously in Shank3-KO neurons [38]. Furthermore, the present findings suggest that CDPPB treatment can facilitate the functional maturation of excitatory contacts in the absence of CDKL5. The effect of CDPPB is likely due to the following mechanisms: (i) increased synaptic expression of both Homer1bc and mGluR5, two essential molecular determinants of dendritic spine formation and stabilization [54, 55], as revealed by our immunofluorescence experiments; (ii) restored mGluR5-Homer1bc interaction, a crucial mechanism for the normal activity of mGluR5 [27, 32], as suggested by our electrophysiology results.

Interestingly, as shown by our results, these synaptic effects are reflected by beneficial outcomes in terms of cortical activation and behavioral response in mutant animals. Indeed, the results showing that cortical activation in response to visual stimulation can be rescued by CDPPB treatment in $Cdkl5^{-/y}$ mice, strengthens the translational value of our preclinical results, confirming that CVI can be used in the clinic as a solid biomarker for CDD [5, 17].

Interestingly, our findings indicate that mGluR5 signaling greatly suffers from the lack of CDKL5, but it does not become completely non-functional. In support of this idea, our data show that a 5-days treatment with CDPPB in CDKL5-null mice produces an effect on both the density of $Homer1bc^{+}$ excitatory synapses and cortical IEG expression (i.e.: c-Fos and ARC) in the cerebral cortex as well as on behavioral/visual defects. Thus, although further studies are needed to dissect out the mechanisms of CDPPB action on excitatory synapse signaling, our results encourage further testing of mGluR5 PAMs in CDD models and offer hope for a future use of these compounds in the clinic. Our data set obtained with another mGluR5 PAM, the RO68 compound, further strengthens this idea. Considerably, RO68 has the clinically relevant advantage that it can be dissolved in salina with an extremely low percentage of detergent (i.e.,: Tween-80) and has a higher potency compared to other mGluR5 PAMs. Remarkably, RO68 is efficacious even at very low concentrations (i.e., 0.3 mg/kg), thus reducing the risk of toxicity, as we show in this study where this compound was able to rescue neuroanatomical and functional signs of CDKL5 mutants, and as it was previously shown in a TSC mouse model [47].

The positive action of mGluR5 PAMs on the molecular organization of postsynaptic structures is encouraging in view of the data we have obtained from two post-mortem CDD brains. Remarkably, we show for the first time that CDKL5 mutation robustly affects the excitatory synaptic compartment in the human BA17 cortex. Our data show that both the localization and the expression of several synaptic molecules (i.e., VGluT1, Homer1bc, PSD-95 and mGluR5) could be negatively affected, as we and others previously reported in CDKL5-null mice [5, 12, 18]. These results, when confirmed on a larger group CDD brains, shall contribute to disclose connectivity impairments of the primary visual cortex underlying CVI in these patients [15] and, consequently, strengthen the face-validity of $Cdkl5^{-/y}$ mice in modeling CDD. Importantly, our data indicate that the synaptic abnormalities and mGluR5 downregulation occurring in human CDD patients are potentially rescuable by positive allosteric modulation of mGluR5. Positively, we did not detect the insurgence of any spontaneous seizures in our study using two different drugs, thus heightening our confidence about the safety of mGluR5-PAM treatment for CDD. Importantly, previous studies reported that mGluR5 positive modulation does not exacerbate seizure incidence under both acute and subchronic treatment regimens [56, 57]. Nevertheless, it is known that the modulation of the NMDARs by the activation of the mGluR5 might be associated with epileptic phenotypes [58] thus prompting us to further explore this issue.

In further support of our findings, Negraes et al. (2021) have found similar synaptic defects in iPSCs-derived cortical neurons from CDD patients [49]. In apparent contrast from our observation, they disclosed an increased mGluR5-PanHomer association in CDD human organoids [49] while we revealed that mGluR5-Homer1bc binding, an association crucial for this receptor function, is decreased in CDKL5 mutant mice. The most parsimonious explanation of this discrepancy arises primarily either the different technical approaches or the experimental models used (i.e., mice brain vs CDD human organoids). Moreover, no discrimination between different Homer isoforms was attempted by Negraes et al. although it is known that the binding between mGluR5 and Homer1bc or Homer1a produces opposite effects on mGluR5 membrane expression and function [44, 59, 60]. Hence, the enhanced mGluR5-PanHomer interaction could be produced by an increased association with Homer1a, thus not ruling out a decrease of mGluR5-Homer1bc binding as revealed by our study.

In conclusion, we believe that our findings on the efficacy of mGluR5 activation pave the way for including these receptors as a promising therapeutic target for CDD. Our results also suggest that an early-onset and prolonged regime of mGluR5 activation has the potential to stably revert the morphofunctional defects shown by adult CDKL5 mutants, without inducing epileptic seizures. Finally, this study further supports previous indications that abnormalities of mGluR5 signaling represents a convergent pathway for multiple neurodevelopmental diseases, a solid hallmark now including CDD.

REFERENCES

1. Rusconi L, Salvatoni L, Giudici L, Bertani I, Kilstrup-Nielsen C, Broccoli V, et al. CDKL5 expression is modulated during neuronal development and its subcellular distribution is tightly regulated by the C-terminal tail. J Biol Chem. 2008;283:30101–11.
2. Baltussen LL, Negraes PD, Silvestre M, Claxton S, Moeskops M, Christodoulou E, et al. Chemical genetic identification of CDKL5 substrates reveals its role in neuronal microtubule dynamics. EMBO J. 2018;37:e99763.
3. Muñoz IM, Morgan ME, Peltier J, Weiland F, Gregorczyk M, Cm Brown F, et al. Phosphoproteomic screening identifies physiological substrates of the CDKL5 kinase. EMBO J. 2018;37:e99559.
4. Nawaz MS, Giarda E, Bedogni F, La Montanara P, Ricciardi S, Ciceri D, et al. CDKL5 and Shootin1 interact and concur in regulating neuronal polarization. PLoS One. 2016;11:e0148634.
5. Trazzi S, De Franceschi M, Fuchs C, Bastianini S, Viggiano R, Lupori L, et al. CDKL5 protein substitution therapy rescues neurological phenotypes of a mouse model of CDKL5 disorder. Hum Mol Genet. 2018;27:1572–92.
6. Kameshita I, Sekiguchi M, Hamasaki D, Sugiyama Y, Hatano N, Suetake I, et al. Cyclin-dependent kinase-like 5 binds and phosphorylates DNA methyltransferase 1. Biochem Biophys Res Commun. 2008;377:1162–7.
7. Mari F, Azimonti S, Bertani I, Bolognese F, Colombo E, Caselli R, et al. CDKL5 belongs to the same molecular pathway of MeCP2 and it is responsible for the early-onset seizure variant of Rett syndrome. Hum Mol Genet. 2005;14:1935–46.
8. Zhu Y-C, Li D, Wang L, Lu B, Zheng J, Zhao S-L, et al. Palmitoylation-dependent CDKL5-PSD-95 interaction regulates synaptic targeting of CDKL5 and dendritic spine development. Proc Natl Acad Sci USA. 2013;110:9118–23.
9. Ricciardi S, Ungaro F, Hambrock M, Rademacher N, Stefanelli G, Brambilla D, et al. CDKL5 ensures excitatory synapse stability by reinforcing NGL-1-PSD95 interaction in the postsynaptic compartment and is impaired in patient iPSC-derived neurons. Nat Cell Biol. 2012;14:911–23.
10. Barbiero I, Peroni D, Tramarin M, Chandola C, Rusconi L, Landsberger N, et al. The neurosteroid pregnenolone reverts microtubule derangement induced by the loss of a functional CDKL5-IQGAP1 complex. Hum Mol Genet. 2017;26:3520–30.
11. Tramarin M, Rusconi L, Pizzamiglio L, Barbiero I, Peroni D, Scaramuzza L, et al. The antidepressant tianeptine reverts synaptic AMPA receptor defects caused by deficiency of CDKL5. Hum Mol Genet. 2018;27:2052–63.
12. Amendola E, Zhan Y, Mattucci C, Castroflorio E, Calcagno E, Fuchs C, et al. Mapping pathological phenotypes in a mouse model of CDKL5 disorder. PLoS One. 2014;9:5–16.
13. Okuda K, Kobayashi S, Fukaya M, Watanabe A, Murakami T, Hagiwara M, et al. CDKL5 controls postsynaptic localization of GluN2B-containing NMDA receptors in the hippocampus and regulates seizure susceptibility. Neurobiol Dis. 2017;106:157–70.
14. Wang I-TJ, Allen M, Goffin D, Zhu X, Fairless AH, Brodkin ES, et al. Loss of CDKL5 disrupts kinome profile and event-related potentials leading to autistic-like phenotypes in mice. Proc Natl Acad Sci USA. 2012;109:21516–21.
15. Demarest ST, Olson HE, Moss A, Pestana-Knight E, Zhang X, Parikh S, et al. CDKL5 deficiency disorder: Relationship between genotype, epilepsy, cortical visual impairment, and development. Epilepsia. 2019;60:1733–42.
16. Wang HT, Zhu ZA, Li YY, Lou SS, Yang G, Feng X, et al. CDKL5 deficiency in forebrain glutamatergic neurons results in recurrent spontaneous seizures. Epilepsia. 2021;62:517–28.
17. Mazziotti R, Lupori L, Sagona G, Gennaro M, Sala GD, Putignano E, et al. Searching for biomarkers of CDKL5 disorder: early-onset visual impairment in CDKL5 mutant mice. Hum Mol Genet. 2017;26:2290–8.
18. Pizzo R, Lamarca A, Sassoè-Pognetto M, Giustetto M. Structural Bases of Atypical Whisker Responses in a Mouse Model of CDKL5 Deficiency Disorder. Neuroscience. 2020;445:130–43.
19. Della Sala G, Putignano E, Chelini G, Melani R, Calcagno E, Michele Ratto G, et al. Dendritic spine instability in a mouse model of CDKL5 disorder is rescued by insulin-like growth factor 1. Biol Psychiatry. 2016;80:302–11.
20. Lupori L, Sagona G, Fuchs C, Mazziotti R, Stefanov A, Putignano E, et al. Site-specific abnormalities in the visual system of a mouse model of CDKL5 deficiency disorder. Hum Mol Genet. 2019;28:2851–61.
21. Pizzo R, Gurgone A, Castroflorio E, Amendola E, Gross C, Sassoè-Pognetto M, et al. Lack of Cdkl5 disrupts the organization of excitatory and inhibitory synapses and parvalbumin interneurons in the primary visual cortex. Front Cell Neurosci. 2016;10:261.
22. Ballester-Rosado CJ, Sun H, Huang JY, Lu HC. mGluR5 exerts cell-autonomous influences on the functional and anatomical development of layer IV cortical neurons in the mouse primary somatosensory cortex. J Neurosci. 2016;36:8802–14.
23. Chen C-C, Lu H-C, Brumberg JC. mGluR5 knockout mice display increased dendritic spine densities. Neurosci Lett. 2012;524:65–68.
24. Edfawy M, Guedes JR, Pereira MI, Laranjo M, Carvalho MJ, Gao X, et al. Abnormal mGluR-mediated synaptic plasticity and autism-like behaviours in Gprasp2 mutant mice. Nat Commun. 2019;10:1431.
25. Piers TM, Kim DH, Kim BC, Regan P, Whitcomb DJ, Cho K. Translational concepts of mglur5 in synaptic diseases of the brain. Front Pharm. 2012;3:1–7.
26. Giuffrida R, Musumeci S, D'Antoni S, Bonaccorso CM, Giuffrida-Stella AM, Oostra BA, et al. A reduced number of metabotropic glutamate subtype 5 receptors are associated with constitutive Homer proteins in a mouse model of fragile X syndrome. J Neurosci. 2005;25:8908–16.
27. Ronesi JA, Collins KA, Hays SA, Tsai N-P, Guo W, Birnbaum SG, et al. Disrupted Homer scaffolds mediate abnormal mGluR5 function in a mouse model of fragile X syndrome. Nat Neurosci. 2012;15:431–40, S1.
28. Scheefhals N, MacGillavry HD. Functional organization of postsynaptic glutamate receptors. Mol Cell Neurosci. 2018;91:82–94.
29. Tu JC, Xiao B, Naisbitt S, Yuan JP, Petralia RS, Brakeman P, et al. Coupling of mGluR/Homer and PSD-95 complexes by the shank family of postsynaptic density proteins. Neuron. 1999;23:583–92.
30. Morello N, Schina R, Pilotto F, Phillips M, Melani R, Plicato O, et al. Loss of Mecp2 causes atypical synaptic and molecular plasticity of parvalbumin-expressing interneurons reflecting rett syndrome-like sensorimotor defects. eNeuro. 2018;5:ENEURO.0086–18.2018.
31. Lujan R, Nusser Z, Roberts JD, Shigemoto R, Somogyi P. Perisynaptic location of metabotropic glutamate receptors mGluR1 and mGluR5 on dendrites and dendritic spines in the rat hippocampus. Eur J Neurosci. 1996;8:1488–1500.
32. Aloisi E, Le Corf K, Dupuis J, Zhang P, Ginger M, Labrousse V, et al. Altered surface mGluR5 dynamics provoke synaptic NMDAR dysfunction and cognitive defects in Fmr1 knockout mice. Nat Commun. 2017;8:1103.
33. Kammermeier PJ, Worley PF. Homer 1a uncouples metabotropic glutamate receptor 5 from postsynaptic effectors. Proc Natl Acad Sci USA. 2007;104:6055–60.
34. Moult PR, Gladding CM, Sanderson TM, Fitzjohn SM, Bashir ZI, Molnar E, et al. Tyrosine phosphatases regulate AMPA receptor trafficking during metabotropic glutamate receptor-mediated long-term depression. J Neurosci. 2006;26:2544–54.
35. Verpelli C, Dvoretskova E, Vicidomini C, Rossi F, Chiappalone M, Schoen M, et al. Importance of Shank3 protein in regulating metabotropic glutamate receptor 5 (mGluR5) expression and signaling at synapses. J Biol Chem. 2011;286:34839–50.
36. Reiner A, Levitz J. Glutamatergic signaling in the central nervous system: Ionotropic and metabotropic receptors in concert. Neuron. 2018;98:1080–98.
37. Marcantoni A, Cerullo MS, Buxeda P, Tomagra G, Giustetto M, Chiantia G, et al. Amyloid Beta42 oligomers up-regulate the excitatory synapses by potentiating presynaptic release while impairing postsynaptic NMDA receptors. J Physiol. 2020;598:2183–97.
38. Vicidomini C, Ponzoni L, Lim D, Schmeisser M, Reim D, Morello N, et al. Pharmacological enhancement of mGlu5 receptors rescues behavioral deficits in SHANK3 knock-out mice Europe PMC Funders Group. Mol Psychiatry. 2017;22:689–702.
39. Auerbach BD, Osterweil EK, Bear MF. Mutations causing syndromic autism define an axis of synaptic pathophysiology. Nature. 2011;480:63–8.
40. Chen Y, Goudet C, Pin J-P, Conn PJ. N-{4-Chloro-2-[(1,3-dioxo-1,3-dihydro-2H-isoindol-2-yl)methyl]phenyl}-2-hydroxybenzamide (CPPHA) acts through a novel site as a positive allosteric modulator of group 1 metabotropic glutamate receptors. Mol Pharmacol.2008;73:909–18.
41. Bouet V, Boulouard M, Toutain J, Divoux D, Bernaudin M, Schumann-Bard P, et al. The adhesive removal test: A sensitive method to assess sensorimotor deficits in mice. Nat Protoc. 2009;4:1560–4.
42. Komotar RJ, Kim GH, Sughrue ME, Otten ML, Rynkowski MA, Kellner CP, et al. Neurologic assessment of somatosensory dysfunction following an experimental rodent model of cerebral ischemia. Nat Protoc. 2007;2:2345–7.
43. Fuchs C, Trazzi S, Torricella R, Viggiano R, De Franceschi M, Amendola E, et al. Loss of CDKL5 impairs survival and dendritic growth of newborn neurons by altering AKT/GSK-3beta signaling. Neurobiol Dis. 2014;70:53–68.
44. Terzic B, Davatolhagh MF, Ho Y, Tang S, Liu YT, Xia Z, et al. Temporal manipulation of Cdkl5 reveals essential postdevelopmental functions and reversible CDKL5 deficiency disorder-related deficits. J Clin Invest. 2021;131:e143655.
45. Ménard C, Quirion R. Successful cognitive aging in rats: A role for mGluR5 glutamate receptors, homer 1 proteins and downstream signaling pathways. PLoS One. 2012;7:e28666.
46. Wang H, Zhuo M. Group I metabotropic glutamate receptor-mediated gene transcription and implications for synaptic plasticity and diseases. Front Pharm. 2012;3:189.
47. Kelly E, Schaeffer SM, Dhamne SC, Lipton JO, Lindemann L, Honer M, et al. MGluR5 modulation of behavioral and epileptic phenotypes in a mouse model of tuberous sclerosis complex. Neuropsychopharmacology. 2018;43:1457–65.
48. Ferraguti F, Shigemoto R. Metabotropic glutamate receptors. Cell Tissue Res. 2006;326:483–504.

49. Negraes PD, Trujillo CA, Yu N-K, Wu W, Yao H, Liang N, et al. Altered network and rescue of human neurons derived from individuals with early-onset genetic epilepsy. Mol Psychiatry. 2021;26:7047–68.
50. Ango F, Pin JP, Tu JC, Xiao B, Worley PF, Bockaert J, et al. Dendritic and axonal targeting of type 5 metabotropic glutamate receptor is regulated by Homer1 proteins and neuronal excitation. J Neurosci. 2000;20:8710–6.
51. Hering H, Sheng M. Dendritic spines: Structure, dynamics and regulation. Nat Rev Neurosci. 2001;2:880–8.
52. Yennawar M, White RS, Jensen FE. AMPA receptor dysregulation and therapeutic interventions in a mouse model of CDKL5 deficiency disorder. J Neurosci. 2019;39:4814–28.
53. Gogliotti RG, Senter RK, Rook JM, Ghoshal A, Zamorano R, Malosh C, et al. $mGlu_5$ positive allosteric modulation normalizes synaptic plasticity defects and motor phenotypes in a mouse model of Rett syndrome. Hum Mol Genet. 2016;25:1990–2004.
54. Oh WC, Hill TC, Zito K. Synapse-specific and size-dependent mechanisms of spine structural plasticity accompanying synaptic weakening. Proc Natl Acad Sci USA. 2013;110:E305–12.
55. Sala C, Futai K, Yamamoto K, Worley PF, Hayashi Y, Sheng M. Inhibition of dendritic spine morphogenesis and synaptic transmission by activity-inducible protein Homer1a. J Neurosci. 2003;23:6327–37.
56. Pacey LK, Tharmalingam S, Hampson DR. Subchronic administration and combination metabotropic glutamate and GABAB receptor drug therapy in fragile X syndrome. J Pharm Exp Ther. 2011;338:897–905.
57. Hanak TJ, Libbey JE, Doty DJ, Sim JT, DePaula-Silva AB, Fujinami RS. Positive modulation of mGluR5 attenuates seizures and reduces TNF-α+ macrophages and microglia in the brain in a murine model of virus-induced temporal lobe epilepsy. Exp Neurol. 2019;311:194–204.
58. Hanada T. Ionotropic glutamate receptors in epilepsy: A review focusing on AMPA and NMDA receptors. Biomolecules 2020;10:464.
59. Shiraishi-Yamaguchi Y, Furuichi T. The Homer family proteins. Genome Biol. 2007;8:206.
60. Bertaso F, Roussignol G, Worley P, Bockaert J, Fagni L, Ango F. Homer1a-dependent crosstalk between NMDA and metabotropic glutamate receptors in mouse neurons. PLoS ONE. 2010;5:e9755.

AUTHOR CONTRIBUTIONS

AG and MG conceived and designed the study. AG performed biochemical experiments. LL, GS, RM, and EP performed IOS experiments. SG performed experiments on human tissues, AG, RP, NM, and FP performed behavioural experiments, AG, RP, SD and DC performed immunofluorescence experiments. AM and GC performed electrophysiological experiments. CS, AN synthesized and provided RO6807794; AG, RP, AR, SD, TP, AM, and MG analyzed the data. AG and MG wrote the manuscript.

FUNDING

This work was supported by research grants from: University of Pennsylvania Orphan Disease Center on behalf of LouLou Foundation (CDKL5 PILOT GRANT PROGRAM n. CDKL5 - 17 - 106 – 01) and from Associazione CDKL5 Insieme verso la cura (Italy) to MG and TP; The International Foundation for CDKL5 Research, Associazione Albero di Greta and Fondazione CRT (n. 2018.0889) and by Fondazione Telethon-Italy (Grants nn. GGP15098 and GGP19045) to MG.

COMPETING INTERESTS

The authors declare no competing interests.

ETHICAL APPROVAL

The study was conducted in accordance with European Community Council Directive 2010/63/UE for care and use of experimental animals with protocols approved by the Italian Minister for Scientific Research (Authorization number 38/2020-PR) and the Bioethics Committee of the University of Torino, Italy.

ADDITIONAL INFORMATION

Supplementary information The online version contains supplementary material available at https://doi.org/10.1038/s41386-022-01412-3.

Correspondence and requests for materials should be addressed to Maurizio Giustetto.

Reprints and permission information is available at http://www.nature.com/reprints

Publisher's note Springer Nature remains neutral with regard to jurisdictional claims in published maps and institutional affiliations.

Acknowledgment

Research is a task, which despite of consistent and dedicated mind with regards to strenuous and hard labor also requires patience. First of all, I want to present my sagacious sense of gratitude and admiration towards my mentor Prof. Maurizio Giustetto, for welcoming me into the laboratory even when I was an immigrant newcomer coming from another world. I am grateful of you that you were always ready to guide and support me in both my research and personal life, for settling me down in a new country. Your encouragement, illuminating guidance, unflinching support, and incredible suggestions during these four long years have been invaluable. I sincerely feel fortunate and honored to work under your guidance. I am truly grateful for the opportunity to learn from you and for the impact I have had on my scientific and professional development.

I want to take a moment to thank our collaborators who have been critical to the success of this project. I want to name Prof. Annalisa Buffo and Dr. Martina Lorenzati for their valuable suggestions, and experimental support, especially for the OPCs isolation by MACs technique and oligodendroglial experiments. I also want to thank Prof. Chiara Salio and Dr. Patrizia Aimar who devoted a lot of their time to the sample preparation and image acquisition procedures of TEM experiments.

I want to express gratitude to my seniors Dr.Antonia Gurgone, and Dr. Riccardo Pizzo for their guidance and valuable suggestions to develop independent thinking in me. I deeply acknowledge their time, support, inspiration, and untiring efforts. I want to say a big special thanks to Anto who never said no and was always ready to listen to my problems and help me out with them at any time, late evenings, weekends. I am also thankful to Debora Comai, and Giuseppe Chiantia for the companionship, encouragement, and tremendous support that enabled me to take this research and feel relaxed in hard times. I would like to extend my heartfelt thanks to all the students specially Agnese and other members of the lab.

A special mention to my parents and my beautiful sister Shweta who have supported me in countless ways throughout my academic journey. Your love, encouragement, and belief in me have been the driving force behind my success. I cannot thank you enough for being my rock and providing me with the strength to persevere through the obstacles I faced. I am here today all because of you, your hard work, and your sacrifice. I have achieved this goal because of your moral

and financial investments in me. Also, a big thanks to my best friend Poonam, my gossip partner for inseparable support, unconditional love, and enormous patience. I express my heartfelt gratitude to my better half, my beloved husband who has been my constant source of love, support, and encouragement throughout this journey. You stay stood for me, maintained a healthy work-life balance, and handled all household chores so that I can work for deadlines and focus solely on my studies. I am eternally grateful for everything you have done for me.

Last but the most important I pay homage to those experimental animals who have sacrificed their lives in making a success of this research work.